FEMTOSECOND LASERS FOR DATACOMMUNICATIONS APPLICATIONS

Christopher Gilmour Leburn

A Thesis Submitted for the Degree of PhD
at the
University of St Andrews

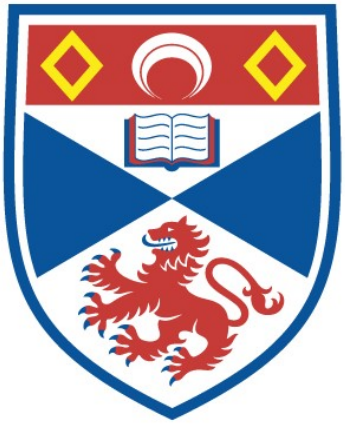

2005

Femtosecond Lasers for Datacommunications Applications

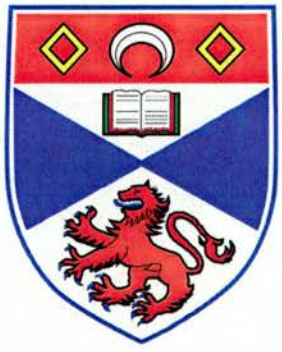

Thesis presented for the degree of

Doctor of Philosophy

to the University of St Andrews

by

Christopher Gilmour Leburn, MSc.

The J. F. Allen Physics Research Laboratories
School of Physics and Astronomy
University of St. Andrews
North Haugh
St. Andrews
Scotland KY16 9SS

May, 2005

Declarations

I, Christopher Gilmour Leburn, hereby certify that this thesis, which is approximately thirty thousand words in length, has been written by me, that it is a record of the work carried out by me and that it has not been submitted in any previous application for a higher degree.

Signature of candidate: Date: 01-09-05

I was admitted as a research student and as a candidate for the degree of Doctor of Philosophy in October, 2001; the higher study for which this is a record was carried out at the University of St Andrews between 2001 and 2005.

Signature of candidate: Date: 01-09-05

I hereby certify that the candidate has fulfilled the conditions of the Resolution and Regulations appropriate for the degree of Doctor of Philosophy in the University of St Andrews and that the candidate is qualified to submit this thesis in application for that degree.

Signature of supervisor: Date: 01-09-05

In submitting this thesis to the University of St Andrews I understand that I am giving permission for it to be made available for use in accordance with the regulations of the University Library for the time being in force, subject to any copyright vested in the work not being affected thereby. I also understand that the title and abstract will be published, and that a copy of the work may be made and supplied to any *bona fide* library or research worker.

Signature of candidate: Date: 01-09-05

for

Mum, Dad,

Joppy, Pete

&

Ruth

Abstract

The work presented in this thesis details the development of all-solid-state ultrashort pulsed lasers suitable for datacommunications applications at either 1300nm or 1550nm. This is achieved through the design and construction of three different types of laser system based on the gain materials Cr^{4+}:forsterite (chromium-doped magnesium iron silicate) and Cr^{4+}:YAG (chromium-doped yttrium aluminium garnet).

A Cr^{4+}:forsterite based system is the first laser that is presented. This configuration utilises a relatively novel GaInNAs semiconductor device to initiate the generation of 130fs pulses around 1300nm. Although GaInNAs devices have previously been used to generate pulses of light in the picosecond domain, this is the first time ultrashort pulses have been achieved in the femtosecond domain. As such, it has been possible to use the results from this laser system to further the understanding of various dynamics of GaInNAs devices.

An SBR mode-locked Cr^{4+}:YAG laser system introduces the concept of femtosecond pulse generation around 1550nm. This is done in order to lay the necessary foundations for understanding the motivation and physics behind high pulse repetition frequency (prf) all-solid state femtosecond lasers suitable for datacommunications applications. Details are then given for the construction and operation of a simple 3-element Cr^{4+}:YAG laser that generates 70fs pulses at a prf greater than 4GHz. The success of this system leads to the development of a compact and robust engineered prototype with a footprint of $215\times106mm^2$.

Integration of the high prf laser systems into novel optical time division multiplexing/wavelength division multiplexing (OTDM/WDM) based assessments prove successful with the demonstration of a datacommunications system capable of generating 1.36Tb/s. This still remains to be the only system capable of achieving such a high capacity from a single source and demonstrates the ongoing success of femtosecond lasers through continued research and development.

Contents

Chapter 1 – Ultrashort Laser Pulse Generation and Characterisation

1.1 Introduction

There is now a wide range of different types of lasers in the world. A ubiquitous category of laser is incorporated in CD players and DVD players. In contrast to comments made following its initial conception in 1958[1], when the laser was referred to as "the solution looking for a problem"[2], the laser is now being used in applications in industrial processing, engineering, metrology, scientific research, communications, holography, medicine and also for some military purposes. Almost every day our lives are being influenced in some way by lasers.

The research undertaken in this project has resulted from earlier scientific investigations that were carried out by the ultrashort-pulse laser research group at the University of St Andrews. This group is involved in the generation, measurement and characterisation of ultrashort pulses from a variety of laser-based sources. The work contained in this thesis focuses on the development of compact ultrashort-pulse lasers for telecommunication and medical applications, particularly in the 1300nm and 1550nm wavelength regions.

By way of introduction, we might ask, what is an ultrashort pulse? In the laser physics community an ultrashort pulse is considered to one having a duration in the picosecond domain (10^{-12}s) or more usually in the femtosecond domain (10^{-15}s). That is to say,

$$1\text{fs} = 0.000000000000001\text{s}$$

Understandably, this can be hard to visualise. Due to this difficulty there have been several "real-life" analogies that have been thought up to compare a second with a femtosecond. For example, if the width of a golf ball represented one femtosecond then

one second's worth of golf balls would line up to give a length of over 400 trips from Earth to Mars and back again!

So, what is so special about ultrashort pulses? Why are they so useful? Well, there are four main features of ultrashort pulses that make them attractive for so many applications. These are their ultrashort pulse duration, high pulse repetition rate, broad spectrum and high peak intensity. The ultrashort pulse duration gives a very fast temporal resolution, much like a strobe light or the slow-motion cameras we see at Wimbledon. The beautiful nature of the femtosecond time domain allows us to take 'snapshots' of atomic and molecular processes. This is invaluable in the field of spectroscopy where scientists are able to measure the relaxation processes of carriers in semiconductors[3] and chemical reaction dynamics[4]. The repetition rate of a laser is the frequency of the pulse train. It is inversely proportional to the length of the laser cavity. The shorter the length of a laser cavity, the higher the repetition rate. This has obvious implications in the telecommunications industry, which requires multi-gigahertz repetition rate sources for high-capacity systems and photonic switching devices[5, 6]. One of the misconceptions about lasers is that they all produce light at very discrete, "monochromatic" wavelengths. This is not the case for ultrashort pulse laser sources. Due to their short pulse durations they can support bandwidths of many tens of nanometres. This has advantages in such areas as optical coherence tomography[7] (a non-invasive imaging technique used in biological systems) and again in the telecommunications industry where these sources can be used in dense wavelength-division-multiplexing (DWDM) applications[8]. The high peak powers generated from ultrashort pulses can be used to alter materials by a technique known as 'cold' ablation[9]. If the pulses are powerful enough they can cause a solid to change directly to a gas, which means that there is much less heat generated around the selected

area. This becomes important in areas such as micro-machining and also in surgery, particularly in corneal surgery and brain tumour removal[10, 11]. These high peak powers can also lead to various nonlinear effects, which can be harnessed to generate other wavelengths via frequency conversion processes. These nonlinear effects also have implications in telecommunication systems and can determine the range and information-carrying capacity of optical fibres.

There are, of course, many more applications that can benefit from ultrafast lasers, and only a few brief applications have been outlined in this section to highlight the various features of a femtosecond pulse train. These applications are possible due to the development of femtosecond solid-state lasers, and their mode-locking techniques, particularly Kerr-lens mode locking and saturable absorber mode locking.

1.2 Why 1300nm and 1550nm lasers?

Before taking a deeper look at the physics of ultrashort pulse generation, it is worth considering some of the applications for which the lasers described in this thesis were designed. This project was funded through a £12 million interdisciplinary research programme known as the Ultrafast Photonics Collaboration (UPC). The main aim of this collaboration was to focus research on ultrafast data communications, with the ultimate objective of generating the technology that will be required for the development of the next generation of photonics and allow data transfer at speeds in excess of 100Tb/s. The collaboration involves researchers from 6 leading UK universities and 5 industrial companies. This project related to the development of ultrashort-pulse laser sources for use in datacommunication systems or datacommunication systems based experiments. This involved developing femtosecond lasers operating at wavelengths around either 1300nm or 1550nm.

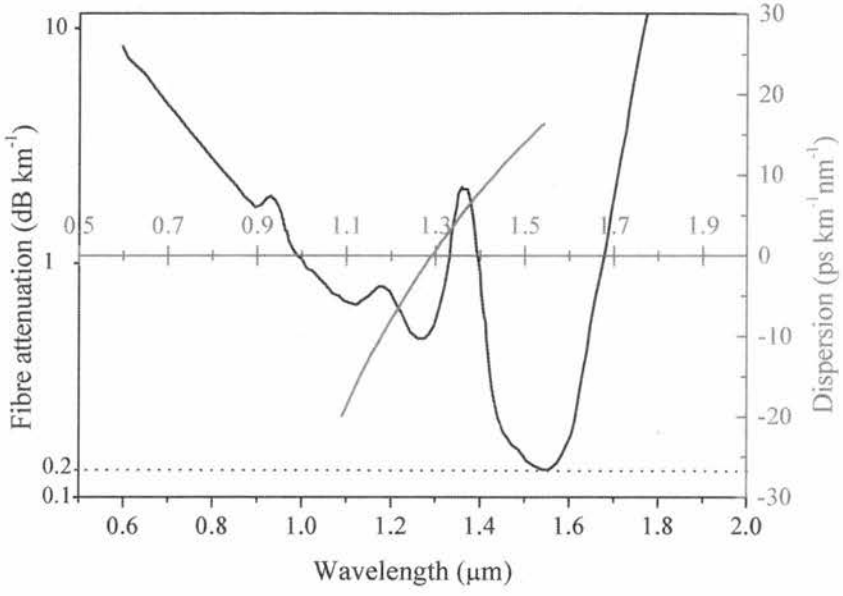

Fig 1.1 *Graph of attenuation and dispersion properties of optical fibre.*

Fig. 1.1 shows the attenuation and dispersion properties for a typical optical fibre that is used in telecommunication systems. There is a reduced attenuation around 1300nm and a principal minimum around 1550nm. Most long-range telecommunication systems use the 1550nm spectral region because it benefits from having the lowest losses and suitable amplifiers are already well developed. It follows, therefore, that there is a requirement to develop 1550nm laser sources with broad spectral bandwidths (WDM) and high repetition rates (OTDM).

In addition, there are important benefits from using communication systems based around the 1300nm spectral region. Fig. 1.1 also shows that at around 1300nm optical fibre has zero dispersion losses. This means that a signal around 1300nm travelling down a fibre will not spectrally disperse significantly over long lengths. This has important ramifications in WDM systems[12], were the wavelength components of an optical signal must propagate in a fibre at the same relative speed. The 1300nm

spectral region also has greater potential for medical photonics where the operating wavelength is well matched to an attenuation minimum in human skin[13].

1.3 Pulse propagation within a dielectric medium

In this section the various aspects of laser physics that underlie the generation of femtosecond pulses through a process known as mode locking are outlined. The reader will first be introduced to the mathematical description of a pulse and how low intensity light interacts with dielectric materials through pulse propagation in a linear regime. There is then a natural progression towards high intensity pulses and how they give rise to various nonlinear effects, some of which are exploitable in ultrashort pulse generation.

1.3.1 Mathematical description of an optical pulse

To discuss what happens when a pulse of light interacts with a dielectric material, within a laser system, we must first be able to describe mathematically the characteristics of this incident pulse. The time dependent electric field, $E(t)$, associated with an optical pulse can be described as

$$E(t) = \varepsilon(t)e^{i\phi(t)}e^{-i\omega_0 t} \qquad 1.1$$

where ω_0 is the optical carrier frequency, $\varepsilon(t)$ is the time varying electric field envelope and $\phi(t)$ is the temporal phase variation across the pulse[14]. The pulse shaping that takes place in the laser systems that have been used throughout this project result in a pulse amplitude that has a temporal envelope which can be represented as a hyperbolic secant function and is expressed as

$$\varepsilon(t) = \varepsilon_0 \operatorname{sech}\left(\frac{1.763t}{\Delta\tau_p}\right) \qquad 1.2$$

where ε_0 is the real electric field amplitude and $\Delta\tau_p$ is the full width half maximum duration of a pulse. This pulse shape is also referred to as a sech^2 pulse, as the intensity $I(t)$ takes the form

$$I(t) \approx |\varepsilon(t)|^2 = \varepsilon_0^2 \sec h^2\left(\frac{1.763t}{\Delta\tau_p}\right) \qquad 1.3$$

The requirement to know the shape of laser pulses that have been generated is crucial when measuring the pulse duration and this will be described in more detail in section 1.5. The spectral field amplitude of a pulse can be obtained by taking the Fourier transform of the temporal field amplitude[15]. If the temporal characteristics of a pulse change over time (i.e. intensity or phase) this will be evidenced in the spectral characteristics. This dependence gives a mathematical relationship known as the bandwidth theorem, which states that there is a minimum time-bandwidth product (*TBP*) given by

$$\Delta\nu\Delta\tau_p \geq TBP \qquad 1.4$$

where $\Delta\nu$ is the full width half maximum spectral bandwidth of a given pulse. The minimum value for the *TBP* is produced when a pulse is said to be "transform limited" i.e. the temporal phase variation across the pulse, $\phi(t) = 0$. This value depends on the shape of the pulse. For a sech^2 pulse profile the minimum *TBP* is 0.315. If $\phi(t) \neq 0$ then the pulse is said to be frequency chirped. Fig. 1.2 illustrates the difference between frequency-chirped and transform-limited pulses.

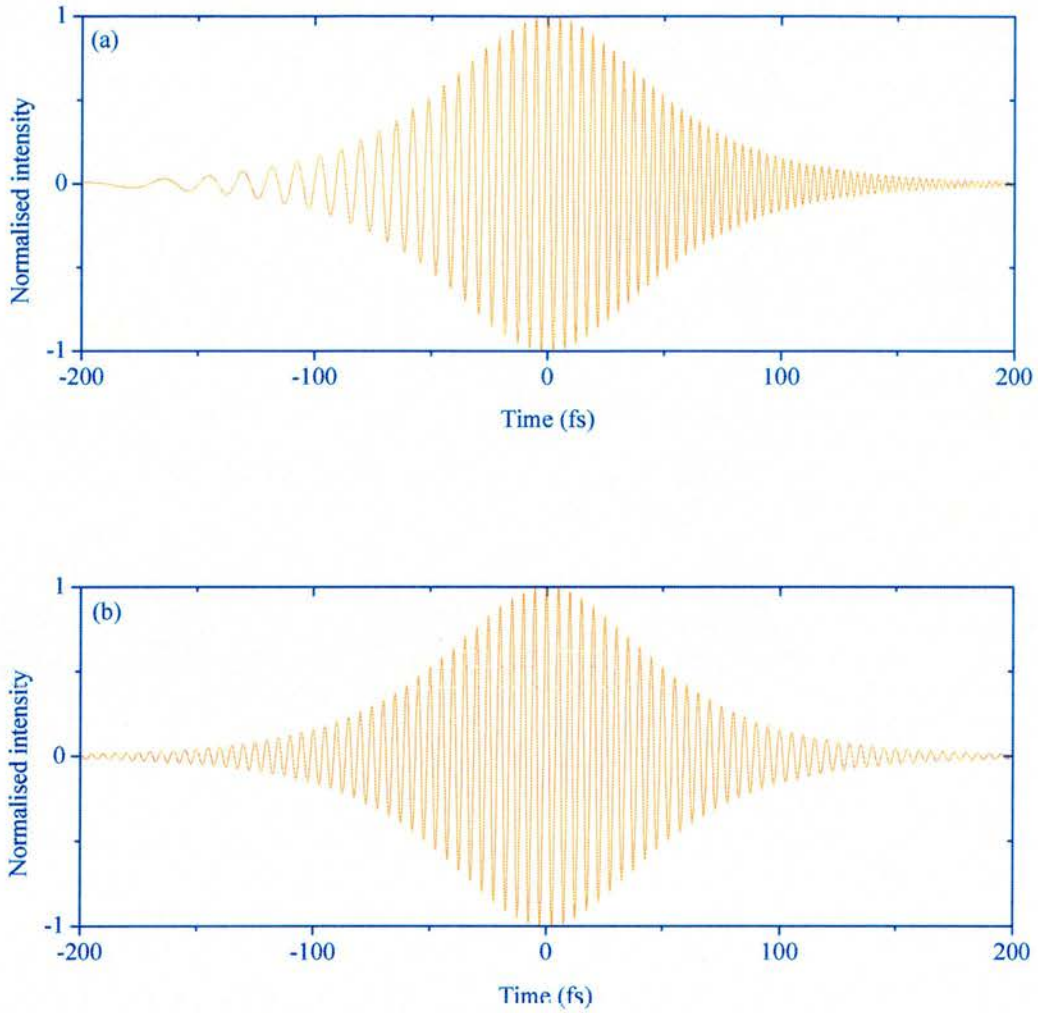

***Fig. 1.2** a) A 70 fs pulse at 1500nm that has a degree of positive chirp and b) its transform-limited counterpart.*

A positively chirped pulse passing through a dielectric medium will have longer wavelength components emerging from the medium earlier than the shorter wavelength components. Owing to the fact that the spectral content of a chirped pulse remains the same, the pulse duration will increase as dictated by the bandwidth theorem. This leads to an increase in value of the time-bandwidth product. Being able to control the degree of frequency chirp in a pulse is vital if ultrashort pulses are desired. The sub-sections

below detail how chirp arises within a laser and how it can be controlled accurately so that the desired transform-limited pulses can be obtained.

For the generation, control and measurement of ultrashort pulses it is imperative that there is an understanding of how these pulses interact with dielectric media as they propagate in a laser resonator. By definition, a dielectric medium under irradiation by an electromagnetic field will produce an intensity-dependent polarisation response given by

$$P = \varepsilon_0 \chi_1 E + \varepsilon_0 \chi_2 E^2 + \varepsilon_0 \chi_3 E^3 + ... \qquad 1.5$$

where ε_0 is the permittivity of free space, E is the applied electric field and χ_n is the n^{th} order susceptibility of the material. When dealing with low intensity electric fields, only the linear susceptibility term, χ_1, is significant. This term is responsible for the effects of refraction and dispersion within a material. Higher orders of susceptibility only become significant when high peak power laser pulses are of sufficient strength to generate the extremely high electric fields necessary to access these nonlinear effects. The second order term, χ_2, is responsible for the nonlinear effects such as second-harmonic generation and sum-frequency mixing while the third-order term, χ_3, is responsible for third-harmonic generation and the optical Kerr effect. [The significance of nonlinear pulse propagation will be discussed in section 1.3.4.] Linear pulse propagation through a dielectric medium is the first step that must be considered in understanding pulse propagation as a whole.

1.3.2 Linear pulse propagation

When an optical pulse passes through a linear dielectric medium it will experience a frequency-dependent phase change, $\phi(\omega)$, which is defined to be

$$\phi(\omega) = \frac{\omega}{c} L n_0(\omega) = L n_0(\lambda) \frac{2\pi}{\lambda} = \beta(\omega) L \qquad 1.6$$

where ω is the angular frequency, λ is the wavelength, c is the speed of light, L is the length and $n_0(\lambda)$ is the wavelength-dependent refractive index of the dielectric material[16]. $\beta(\omega)$ is defined as the propagation constant. The definition of this wavelength dependent refractive index is given by

$$n_0(\lambda) = 1 + \frac{1}{2}\mathrm{Re}[\chi_1(\lambda)] \qquad 1.7$$

Equation 1.7 shows that the first-order susceptibility is directly related to the wavelength of the optical pulse. This dependence on the wavelength of the light is a manifestation of dispersion within dielectric media. If the propagation constant, $\beta(\omega)$, is expanded as a Taylor series, centred around ω_0, then it is possible to understand which dispersive effects can be related to the first susceptibility term. This is shown below in equation 1.8

$$\beta(\omega) = \beta(\omega_0) + \beta'(\omega - \omega_0) + \frac{1}{2!}\beta''(\omega - \omega_0)^2 + \frac{1}{3!}\beta'''(\omega - \omega_0)^3 + \ldots.. \qquad 1.8$$

The β coefficients in the above expansion describe the various different physical effects governing the propagation of a pulse through a medium. $\beta(\omega_0)$ relates to the phase velocity, v_ϕ, of a pulse and can be written as

$$\beta(\omega_0) = \frac{\omega_0}{v_\phi} \qquad 1.9$$

The phase velocity is the velocity at which the central carrier frequency, ω_0, propagates. The second term in the expansion is related to the group velocity, v_g, of the pulse. It is the velocity that the pulse envelope propagates inside a dielectric medium, and is given by

$$\beta' = \frac{d\beta}{d\omega} = \frac{1}{c}\left(n + \omega_0 \frac{dn}{d\omega}\right) = \frac{1}{v_g} \qquad 1.10$$

β'' describes the change of the shape of the carrier envelope of a propagating pulse. It is given by

$$\beta'' = \frac{d\beta'}{d\omega} = \frac{d^2\beta}{d\omega^2} = \frac{1}{c}\left(2\frac{dn}{d\omega} + \omega_0 \frac{d^2n}{d\omega^2}\right) \qquad 1.11$$

This term describes the group velocity dispersion (GVD). It is the most significant pulse broadening effect. In most dielectric materials, the value of the group velocity dispersion is positive. This means that longer wavelength components of a pulse will travel faster than the shorter wavelength components. So, if transform-limited pulses pass through a dielectric material they will experience a frequency-dependent phase change, which gives rise to some positive value of GVD. In doing so, the temporal envelope will broaden and the pulse will become positively frequency chirped. The fourth term from equation 1.8, β''', is know as the third order dispersion (TOD) of a material and is given by

$$\beta''' = \frac{d\beta''}{d\omega} = \frac{1}{c}\left(3\frac{d^2n}{d\omega^2} + \omega\frac{d^3n}{d\omega^3}\right) \qquad 1.12$$

Third-order dispersion effects can usually be neglected because they only become more prevalent when very short (<20 fs) pulses are being generated[17, 18].

1.3.3 Dispersion compensation

To obtain the desired transform-limited pulses illustrated in Fig. 1.2(b) it is necessary to compensate for the positive dispersion produced by the frequency-dependent phase change, $\phi(\omega)$, of the various elements in a laser. As a pulse of light propagates within a laser cavity, different wavelength components of that pulse will experience different cavity periods. Suitable optical components need to be introduced into the resonator to

provide a net negative GVD to compensate for this positive chirp. A number of techniques have been devised to provide this net negative dispersion. One of the first techniques involved using pairs of diffraction gratings to allow shorter wavelength components to travel around a laser cavity with a reduced optical path length with respect to the longer wavelength components[19]. There are several other techniques in use today, which provide the necessary negative GVD. These include Gires-Tournois interferometers (GTIs)[20], chirped mirrors[17], and the more common approach involving the use of prism pairs within a laser system. This last method was described by Fork *et al.* in 1984[21-23] and it is one of the methods that was used to provide the necessary negative GVD in the various laser systems that were designed in this project. A typical 4-prism layout used to compensate for positive GVD is shown in Fig. 1.3.

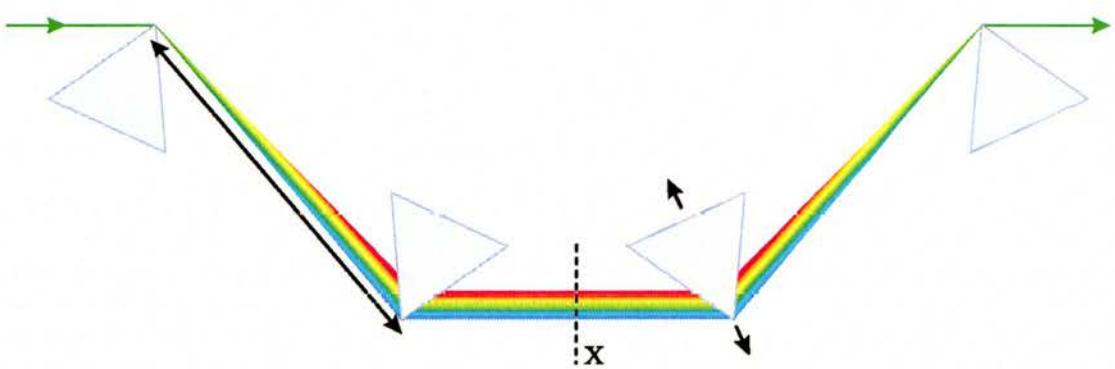

Fig. 1.3 *A two-prism pair arrangement that can be used to generate negative GVD.*

The four identical prisms are cut so that the minimum deviation angle coincides with the Brewster angle. This minimises the propagation losses through the prisms when they are inserted into a laser system. This low-loss technique is vital when trying to compensate for dispersion in low threshold or low gain laser systems, and explains why prisms are often preferred over the grating alternatives, which impose larger insertion losses. The exit angle from the first prism is dependent on the wavelength component of

the incident light. The shorter the wavelength component, the more acute the exit angle from the prism. This allows the shorter wavelength components to pass through less of the second prism which gives rise to a shorter dispersive optical path length for these shorter wavelength components. One point to note is that, in most cases, the prism material will have positive material dispersion properties that must be accounted for when setting up this type of arrangement. There are a few exceptions to this case and they will be discussed later. Fig. 1.3 illustrates that the two prism pairs are symmetric about the position X. If a mirror is placed at position X it can be seen that a double-pass through a single prism pair will achieve the same result as a single pass through two prism pairs. A single prism pair is often implemented when dispersion compensation is required within a laser cavity. In mathematical terms, the total dispersion, D, of a prism sequence can be written as

$$D = \left(\frac{\lambda}{cL}\right)\frac{d^2p}{d\lambda^2} \tag{1.13}$$

where L is the physical length of the light path and p is the optical path length. The derivative $d^2p/d\lambda^2$ is a function of the angular divergence of the laser light from the prism, θ, the refractive index of the prism material, n, and the tip-to-tip separation, l, of the prisms in the cavity.

$$\frac{d^2p}{d\lambda^2} = 4l\left\{\left[\frac{d^2n}{d\lambda^2} + \left(2n - \frac{1}{n^3}\right)\left(\frac{dn}{d\lambda}\right)^2\right]\sin(\theta) - 2\left(\frac{dn}{d\lambda}\right)^2\cos(\theta)\right\} \tag{1.14}$$

It can be shown that for sufficiently large values of l the overall dispersion becomes negative. Therefore, by changing the prism tip-to-tip separation it is possible to vary the total dispersion of the cavity from positive to negative. This can give rise to the required negative GVD necessary for the generation of transform-limited pulses.

An alternative and simplified approach that was used to provide the necessary negative GVD relied on the same physics as described above, but required just one prism to be inserted into the laser cavity. This second method is described in some detail in Chapter 4.

1.3.4 Nonlinear pulse propagation

The high peak powers associated with ultrashort pulses give rise to nonlinear responses from dielectric media. These responses are generated by the higher-order susceptibilities χ_2, and χ_3, which are contained in equation 1.5. Second-order nonlinear effects only occur in non-centrosymmetric materials[24] (i.e. materials with low symmetry). As previously mentioned, they are responsible for second harmonic generation and sum-frequency mixing. The effects of χ_2 will not be discussed in this work because the materials used in this project were centrosymmetric in nature. Third-order nonlinear effects occur in all optical materials. So, for a centrosymmetric material, χ_3 is the first nonlinear term that needs to be considered. This term is responsible for a number of important phenomena involved in the generation of ultrashort pluses. They include the optical Kerr effect, which gives rise to self-phase modulation and self-focusing and these will now be described in detail.

1.3.5 The optical Kerr effect

A transparent dielectric material will experience a χ_3 induced change in refractive index, Δn, in the presence of a strong electromagnetic field, $E(t)$. The refractive index of this material can be broken up into two terms; one for the linear refractive index, n_0, and the other for the nonlinear refractive index, n_{2E}.

$$n = n_0 + n_{2E}\left|E(t)\right|^2 \qquad 1.15$$

where the nonlinear refractive index, n_{2E}, is given by,

$$n_{2E} = \frac{3\chi_3}{8n_0} \tag{1.16}$$

In the case of ultrashort pulse generation, the electric field is associated with the intensity of an optical pulse by

$$I(t) \sim cn\left|E(t)\right|^2 \tag{1.17}$$

This means that equation 1.15 can be re-written in terms of intensity, *I(t)*.

$$n = n_0 + n_{2I} I(t) \tag{1.18}$$

n_{2I} is the related nonlinear refractive index coefficient and is, for nearly all materials, positive. It is given by

$$n_{2I} = \frac{2n_{2E}}{\varepsilon_0 c n_0} \tag{1.19}$$

From the above equations it can be seen that a sufficiently intense pulse can give rise to an increase of the refractive index of a dielectric material. This phenomenon is known as the optical Kerr effect, which is responsible for self-focusing and self-phase modulation.

1.3.6 Self-focusing

To understand self-focusing we need to consider an optical pulse passing through a Kerr medium. This pulse will have an intensity distribution that is Gaussian-like in its spatial beam cross-section. There is a higher intensity in the centre of the pulse compared to the intensity in the wings of the pulse. Due to this non-uniform intensity distribution, there is a non-uniform response of the refractive index across the beam, as implied in equation 1.18.

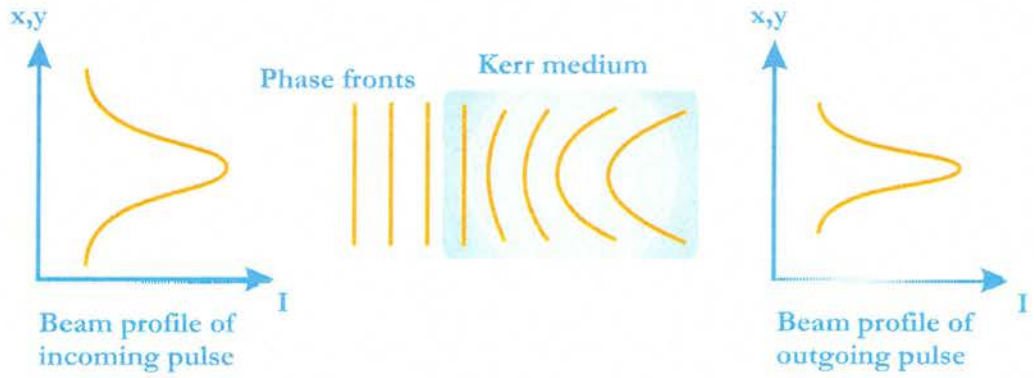

***Fig. 1.4** Self-focusing.*

Fig. 1.4 illustrates how the phase fronts in the centre of the beam will consequently experience a larger phase shift and become retarded with respect to those in the wings of the beam. This results in the beam becoming focused, much as it would if it was passing through a simple lens. This lensing action gives rise to the term known as the "Kerr-lens effect". This effect is exploited in the technique known as Kerr-lens mode locking, which will be described in section 1.4.3.

1.3.7 Self-phase modulation

Even if pulse durations reach the sub-picosecond regime the effects of the optical Kerr effect can still be said to be instantaneous. The change in refractive index, Δn, corresponding to the changing intensity of a pulse profile will reach a maximum at the peak of the pulse profile. For materials with a positive nonlinear refractive index coefficient, n_{2I}, there will also be a resulting phase shift, $\Delta\phi(t)$, and therefore a change in frequency, $\Delta\nu$, as described by

$$\Delta\nu = \frac{d}{dt}.(\Delta\phi(t)) = \frac{d}{dt}.\left(\frac{2\pi}{\lambda}Ln_{2I}I(t)\right) \qquad 1.20$$

where L is the propagation length of the material and $I(t)$ is the pulse intensity. As the leading edge of the pulse rises in intensity, the refractive index of the localised dielectric

medium increases. As a result, the velocity of the pulse decreases such that these frequency components of the pulse undergo a red-shift. At the trailing edge of the pulse the opposite effect is seen and a blue-shift is observed. These effects are illustrated in Fig. 1.5.

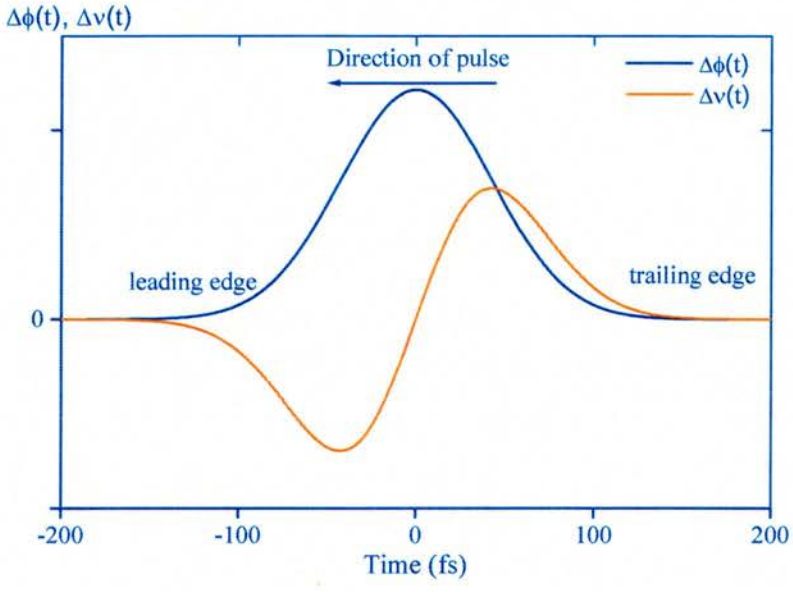

Fig. 1.5 *Self- phase modulation – Phase shift of the pulse is indicated in blue and the instantaneous frequency shift is in orange.*

Self-phase modulation (SPM) is vital in the generation of ultrashort pulses. This is because the effect gives rise to a broadening of the spectral bandwidth by distributing the intracavity power over more oscillating modes. In turn, the generation of shorter pulses are allowed as described by equation 1.4. The effects of SPM are often approximated to be another form of linear dispersion, which can be compensated using the techniques described earlier.

1.4 Ultrashort pulse generation

There are a number of techniques that can be implemented to force a laser oscillator to produce a periodic sequence of pulses. These include Q-switching[25], cavity dumping[26] and gain switching[15]. The technique which allows the generation of pulses in the femtosecond regime, is known as mode locking[27, 28].

There are several ways and means to mode lock a laser, however, only two techniques will be described, as they are the two that relate to the laser systems discussed in later chapters. One technique involves the insertion of a semiconductor saturable absorber, which relies on having an intensity-dependent saturable absorber mechanism. The other relies on an intensity dependent and dynamic loss mechanism, which manifests itself as a loss or gain modulation through utilisation of the Kerr effect. Both of these techniques involve some or all of the physics that has been described in section 1.3.

1.4.1 Mode locking

An explanation of mode locking can be given by looking at a simple two-mirror laser cavity in which only certain frequencies are allowed to oscillate. These frequencies are determined by the separation of the mirrors. There must be an integral number of half wavelengths between the two mirrors in order to set up a standing wave. This is shown in the figure below.

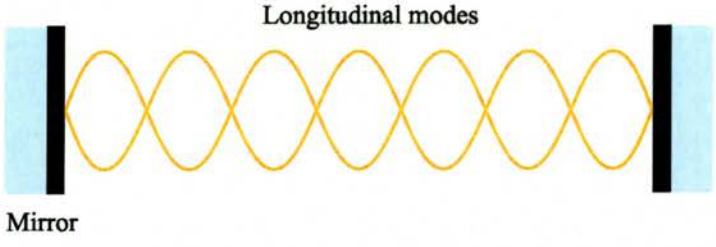

Fig. 1.6 *Standing wave set up in a two-mirror cavity.*

These standing waves are usually known as the longitudinal modes and are separated in frequency by

$$\Delta\nu = \frac{c}{2nl} \tag{1.21}$$

where c is the speed of light and $2nl$ is the round-trip optical length of the cavity. From this equation it follows that the optical length of the cavity, along with the bandwidth of the gain material, determine the oscillation frequencies allowed in any laser system. The output from a laser system as a function of time will depend on the relative phases, frequencies and amplitudes of these longitudinal modes. The total electric field for the output of a laser can be written as

$$E(t) = \sum_{n=0}^{N-1} (E_0)_n \exp[i(\omega_n t + \delta_n)] \tag{1.22}$$

where $(E_0)_n$, ω_n, and δ_n are the amplitude, angular frequency and phase of the n^{th} mode respectively.

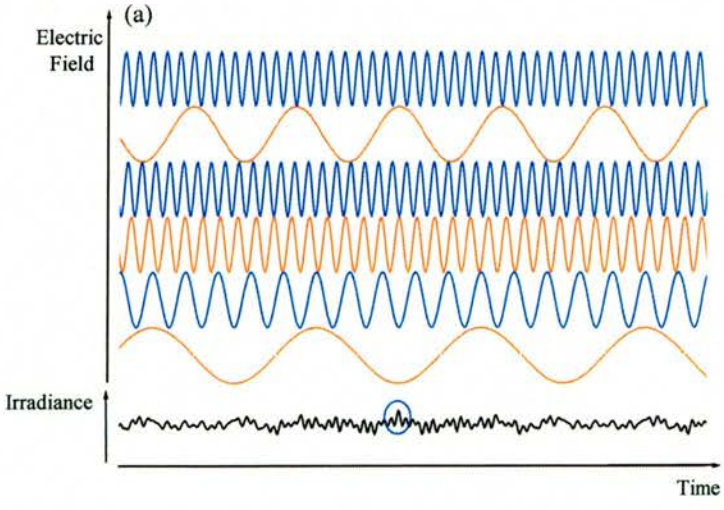

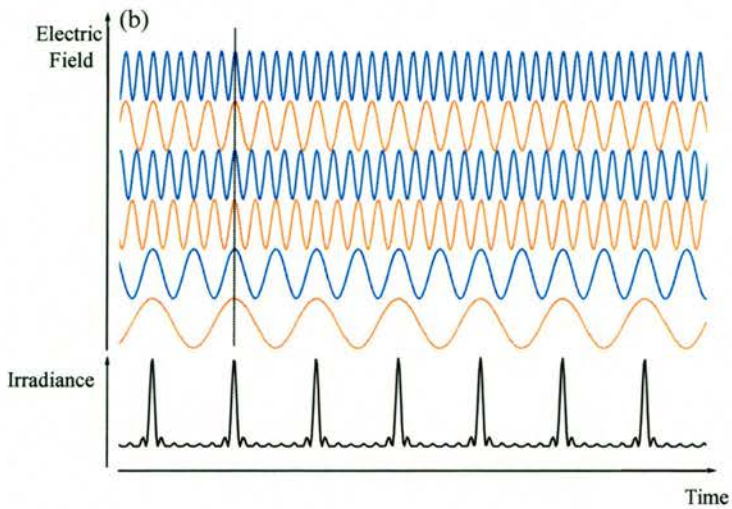

Fig. 1.7 *Comparison of cw and mode-locked laser outputs. (a) shows a cw output with random fluctuations of the irradiance and (b) shows phase- locked modes adding up constructively to give a series of narrow intense pulses.*

These parameters usually vary independently of each other, such that all the longitudinal modes are incoherent and the total irradiance of the system is simply the sum of irradiances of the individual modes. This is illustrated in Fig. 1.7(a). If a few modes happen to be in phase at a particular time then the irradiance exhibits small fluctuations at that given time, as shown by the blue circle.

If all the modes are forced to maintain the same relative phase (i.e. $\delta_n=\delta=0$) then the laser becomes mode locked as illustrated in Fig. 1.7(b). Now the total irradiance can only be determined by adding the individual electric fields rather than irradiances. So now the resultant electric field is written as

$$E(t) = E_0 \exp(i\delta)\sum_{n=0}^{N-1}\exp(i\omega_n t) \qquad 1.23$$

The greater the number of modes that can be mode locked together the shorter the pulse duration becomes. The temporal spacing of this regular sequence of intense pulses is equal to the round-trip time of the laser cavity, τ_{prf}, given by

$$\tau_{prf} = \frac{2nl}{c} \qquad 1.24$$

Mode locking is achieved by introducing a modulation to the system usually in the form of an amplitude or frequency modulation within the cavity. There are many ways of generating this necessary modulation and much literature has been written on each different technique. However, in the subject matter of this thesis, just two techniques were used to generate femtosecond pulses, and these were passive mode locking by use of a saturable absorber in the form of a semiconductor saturable absorber or Kerr-lens mode-locking. Both of these techniques are classed as passive mode locking techniques that rely on mode locking that is brought about by an amplitude modulation.

In passive mode locking, a non-linear intracavity element, which exhibits an intensity dependent loss, is present in the system to allow the circulating radiation to modulate and subsequently mode lock itself in a process known as self-amplitude modulation (SAM)[29-31]. The phases of the modes in the cavity self-adjust to produce a field that exhibits the least loss as it propagates round the cavity. This is known as the maximum emission principle[32] and ensures that given the suitable circumstances, a pulsed laser field will build up from amplitude noise.

1.4.2 Passive mode locking with saturable absorbers[33-35]

Passive mode locking utilises nonlinear effects to induce the necessary modulation that initiates the mode-locking process. This modulation can be thought of as a shutter, which has been placed close to one of the end mirrors of the laser cavity. When the shutter is closed there is a loss in the system and there is no laser output. If the shutter is opened briefly every *2nl/c* seconds the phase relationships of the oscillating modes become fixed and a train of pulses are generated. In passive mode locking this periodic 'shutter' modulation of the gain (or loss) is created by an intracavity element, which has

some appropriate non-linear intensity-dependent characteristic and is known as a saturable absorber.

If the recovery time of the saturable absorber is long compared to the duration of the pulse, the front edge of the pulse becomes suppressed while the tail of the pulse passes through without being attenuated. This effect is called slow saturable absorption (SSA) as illustrated in Fig. 1.8(a).

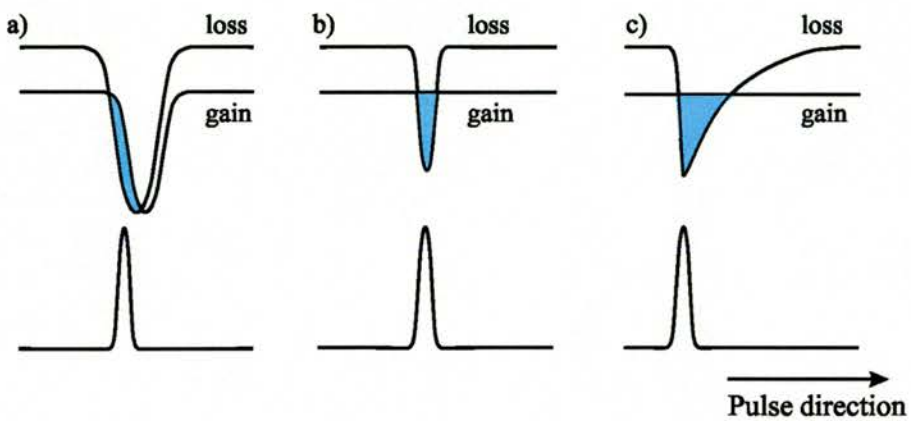

Fig. 1.8 *Passively mode-locked pulse shaping mechanisms due to gain and loss dynamics of: (a) a slow saturable absorber, (b) a fast saturable absorber and, (c) solitonic mode locking with a slow saturable absorber.*

This mechanism relies on the presence of 'dynamic gain saturation', which describes the rapid recovery of the gain saturation between pulses. This gain saturation, along with the long recovery time of the absorber, produces the necessary short net gain window. Unfortunately, solid-state lasers do not have significant gain saturation because they have upper-state lifetimes that are typically much longer than the pulse repetition period. The solution comes in the form of two other mechanisms, which are capable of producing the required short net gain window in the absence of gain saturation. These are fast saturable absorber mode locking (Fig. 1.8(b)) and solitonic mode locking (Fig. 1.8(c)).

Fast saturable absorber (FSA) mode locking requires a saturable absorber with a fast recovery time so that a suitable short net gain window can be created. For solid-state laser systems, the most successful FSA-based mode-locking mechanism has been Kerr-lens mode locking (KLM), whereby the laser crystal itself is encouraged to act like a fast saturable absorber.

1.4.3 Kerr-lens mode locking

Kerr-lens mode locking (KLM), or 'self-mode locking', relies on the intensity dependent nature of the refractive index of the gain material.

A high intensity pulse with a Gaussian radially-varying intensity profile passing through the gain will induce a Kerr-lens through self-focusing (section 1.3.6) and the beam will become focused (and spectrally broader due to SPM). In the continuous wave (cw) regime the beam does not have sufficiently high enough intensity to create a Kerr-lens and therefore no focussing takes place. A pulsed laser field that builds up from an amplitude noise spike can have sufficient intensity to induce the Kerr-lens effect.

By introducing a slit into the cavity (hard-aperture KLM), high intensity pulses focus the laser beam through the slit therefore introducing less loss at high intensity and more loss at low intensity. As such, the laser prefers to operate in the low-loss, high intensity, pulsed regime. Soft-aperture KLM is similar to hard-aperture KLM. Instead of using an intracavity slit the cavity is designed so that the pump-beam geometry allows access to more gain for intracavity beams that are focused through the self-focusing mechanism (i.e. more favourable regime for high intensity pulses). It is this process that acts as an intensity dependent and dynamic loss mechanism, which manifests itself as a loss or gain modulation akin to the FSA mechanism (Fig. 1.8(b)).

One important feature of KLM is that it is inherently broadband. This is because self-phase modulation (section 1.3.7) comes into play by accessing more of the available gain (and therefore reducing the pulse duration). In fact, the dynamics of KLM have allowed for the generation of pulses as short as 5fs from Ti:Sapphire lasers[9].

Although KLM has been extremely successful in generating ultrashort pulses, the process does have some significant drawbacks. KLM lasers are not usually self-starting. They require a noise perturbation to build up amplitude noise into a stable pulse. This perturbation can be brought about by physically tapping an element of the cavity. Some cavities can be self-starting, but these usually require micron precision alignment of the cavity. In addition, KLM operation has to usually take place near one end of the laser cavities stability regions, where the self-focusing of the beam is large enough to sustain mode locking.

Although KLM is able to produce the shortest ultrashort pulses from vibronic laser systems, it is not the only way to generate pulses in the femtosecond domain.

1.4.4 Soliton mode locking

There is another mechanism known as soliton mode locking, which can also be used to generate ultrashort pulses. In soliton mode locking, the pulse shaping that leads to mode-locked operation relies on the formation and propagation of soliton-like pulses by exactly balancing the group velocity dispersion (GVD) against the self-phase modulation (that is brought about by the optical Kerr effect) within the cavity. In solitonic mode locking an additional loss mechanism (typically a saturable absorber) is required to initiate the formation of solitonic pulses from background noise spikes, and to stabilise the solitonic pulses once they are formed. Fig. 1.8 shows that the short net-gain windows that are achieved through SSA and FSA are not necessary for solitonic

mode locking because the soliton formation is the dominant pulse shaping mechanism. This de-couples the saturable absorber from the cavity and relaxes the constraints of the saturable absorber, thus allowing for a much longer net-gain window (Fig. 1.8(c)) than its SSA and FSA counterparts. This greatly relaxes the limitations of the saturable absorber used to initiate the mode locking. The relaxation time of the saturable absorber can be up to 10 times longer than the pulse duration of the laser. This makes semiconductor saturable absorbers ideal candidates as mode-locking devices.

1.4.5 Semiconductor saturable absorbers

Semiconductor saturable absorber mirrors (SESAMs) and saturable Bragg reflectors (SBRs) both have an intensity dependent reflectivity. This allows for favoured operation of pulses over the continuous wave regime. Although some sources claim that SBRs and SESAMs should be classed as separate devices, they are in fact very similar in structure and in the way they operate. Differences between the two types of devices are usually attributable to the way they are grown and processed.

The first semiconductor devices used to mode lock solid-state lasers date back to 1992[36]. Since then, they have become very popular intracavity devices that can be exploited in lasers to generate picosecond and femtosecond pulses. Epitaxial growth techniques such as molecular beam epitaxy (MBE) and metal-organic chemical vapour deposition (MOCVD) can be used to produce devices with very well defined parameters. Being able to grow devices that have specific and pre-determined properties makes them very attractive as modelocking elements. These devices consist typically of alternate layers of high and low index semiconductor materials, which act as a Bragg reflector with a thin saturable absorber layer near the top of the device. The modulation

that is necessary for mode locking to take place is brought about via bleaching of the absorber layer when sufficiently intense intracavity pulses are incident on the device.

A semiconductor saturable absorber has five important macroscopic properties that determine its performance within a laser system. These are: the impulse recovery time, τ_A, modulation depth, ΔR, the non-saturable loss, ΔR_{NS}, saturation fluence, F_{sat}, and spectral bandwidth, $\Delta\lambda$.

The first of these properties is the impulse recovery time of the device. Essentially, this is the time it takes for the device to recover after a suitably intense pulse has bleached the absorber. When FSA mode locking is the dominant mechanism within the cavity, the recovery time needs to be very fast (around that of the pulse being generated). When solitonic mode locking is the dominant mechanism then the recovery time does not have to be as fast. In fact, it can be up to 10 times larger than the pulse duration.

The modulation depth, ΔR, is the maximum nonlinear change in reflectivity between a low intensity pulse and a high intensity pulse, which will bleach the absorber. A large value for this property will allow of the generation of very short pulses and increase the chances of self-starting operation, however it also increases the potential for unwanted Q-switching instabilities within solid-state lasers, therefore a balance must be found. Typically, ΔR is in the range of 1-2%. This value can be altered by changing the reflectivity of the front surface of the absorber or by changing the absorber thickness.

Once an intense pulse has bleached the absorber, any remaining loss of the device is known as the non-saturable loss, ΔR_{NS}. These include reflectivity of the Bragg stack (which will be <100%), scattering losses within the material and excited state absorption. The design and growth characteristics of the device strongly affect this

parameter. For low gain laser systems, such as those discussed in this work, it is imperative to have intracavity losses that are as low as possible. Ideally, the non-saturable losses should be as low as possible.

The saturation fluence is defined as the pulse fluence (energy density per unit area) required to saturate the absorption of a device. The value for the saturation fluence should be kept relatively small so that the incident fluence needed to saturate the device does not damage the structure.

The shortest pulse durations that can be generated from a SBR mode locked laser system are limited by two factors. One is the bandwidth of the gain material and the other is the spectral bandwidth of the Bragg mirror of the device. The bandwidth of the devices is determined by the index contrast of the layers and the thickness of the layers in the Bragg stack.

1.5 Ultrashort pulse measurement

There are four main features of a pulse train that need to be measured in order to gain a good characterisation of the laser system. These are: the average power output, the repetition rate of the system, the spectral bandwidth and the pulse duration of the pulses. The first three of these parameters are all relatively trivial to determine. A suitable power meter can be used to make power measurements of the laser. A fast detector connected to a suitable oscilloscope can be used to measure the repetition rate of the laser system. Passing the pulses through a spectrometer allows the recording of the spectrum of the laser. There is a significant problem when it comes to measuring the duration of an ultrashort pulse. The solution involves comparing the pulses against themselves through a process known as autocorrelation[37]. As mentioned earlier, it is

crucial to know the pulse shape of pulses that are being measured. Fig. 1.9 illustrates the differences between a sech^2 pulse profile and a Gaussian pulse profile.

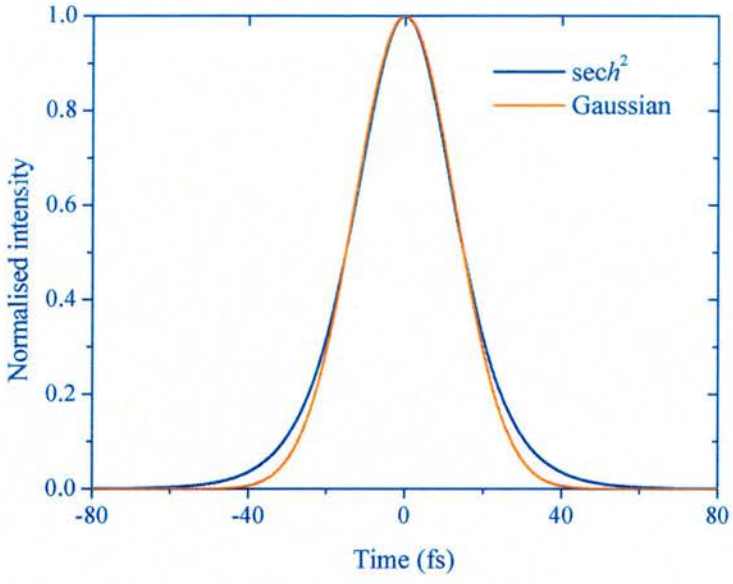

Fig. 1.9 *Comparision of Gausian and sech^2 pulse profiles.*

At first glance it appears that the two profiles are almost identical, but this is not the case. The transform-limited time-bandwidth product (*TBP*) for a Gaussian pulse and a sech^2 pulse are very different. For a Gaussian pulse the transform-limited *TBP* is 0.44. The sech^2 equivalent is 0.32. This is why it is important to know the pulse shape when making measurements, especially on pulses that might have some degree of chirp associated with them.

1.5.1 Two-photon absorption autocorrelator

There are a wide variety of different autocorrelation techniques[24, 38, 39]. The autocorrelator described here is probably the least expensive and simplest to construct, as well as being the easiest to use. Fig. 1.10 shows the basic setup of the two-photon absorption autocorrelator.

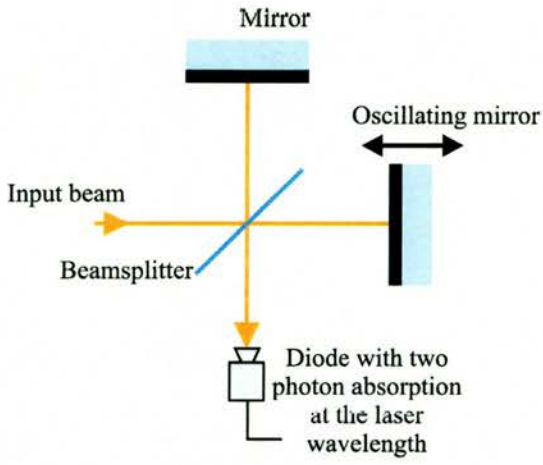

Fig. 1.10 *Representative autocorrelator setup.*

The incoming laser pulse is split into two by the beam splitter. One of these pulses is reflected off a static mirror onto the detector. The other pulse is reflected off an oscillating mirror onto the detector. This oscillating mirror causes the pulses to temporally scan over one another at the detector. The detector must have a quadratic response to the incident intensity. These detectors take two basic forms. One involves using a second harmonic crystal to generate the desired quadratic response. However, these can be expensive and require a suitable phasematching bandwidth. The other simply involves a photodiode that gives a non-linear response through two-photon absorption. This can be achieved by using a semiconductor devices such as a LED or diode laser[37, 40]. Photons with energy larger than the semiconductor bandgap energy, E_g, will be absorbed linearly with respect to the incident power. If a high intensity, high energy pulse of photons is high enough then less energetic photons, of energy $\frac{1}{2}E_g<E<E_g$, will undergo efficient two-photon absorption. The photocurrent created by this process has the quadratic response that is desired. At 1300nm and 1550nm this can be achieved by using inexpensive silicon diodes.

The oscillation provided by one of the mirrors varies the relative delay between the two pulses. The two pulses from each arm must overlap perfectly on the detector.

The two-photon detector will measure the combined signal of the two pulses, which is proportional to the degree of overlap and can be described by

$$G(\tau)=\int_{-\infty}^{\infty}\left|\left[E(t)+E(t-\tau)\right]^2\right|^2 d\tau \qquad 1.25$$

If the two-photon detector is calibrated for a relatively slow frequency response, the autocorrelator will record the time-averaged intensity autocorrelation. This intensity autocorrelation can be described as

$$g(\tau)=1+\frac{2\int_{-\infty}^{\infty} I(t)I(t-\tau)dt}{\int_{-\infty}^{\infty} I(t)^2 dt} \qquad 1.26$$

When $\tau=0$ and $\pm\infty$ equation 1.26 produces values of 3 and 1 respectively hence for an intensity autocorrelation a contrast ratio of 3:1 is expected as illustrated in Fig. 1.11(a). The FWHM of an autocorrelation trace, Δt, is related to the pulse duration, $\Delta\tau_p$, by the expression

$$\Delta\tau_p=\frac{\Delta t}{k} \qquad 1.27$$

where k is a conversion factor[24]. The value of the conversion factor depends on the shape of the pulse. If a Gaussian pulse shape is assumed then $k=1.414$. For a sech^2 pulse shape $k=1.543$.

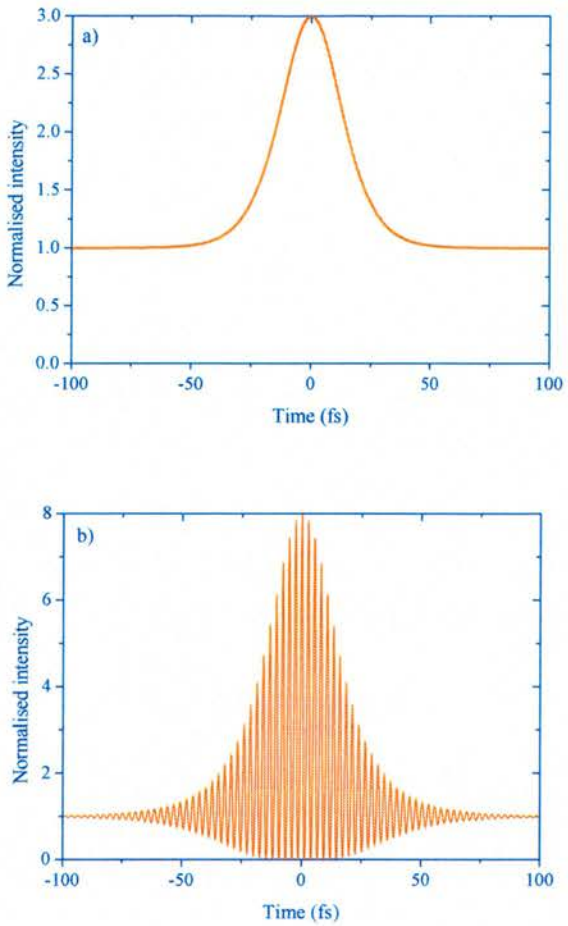

Fig. 1.11 *a) Typical intensity autocorrelation trace and b) interferometric autocorrelation trace.*

The other type of autocorrelation is known as a fringe-resolved or interferometric autocorrelation (Fig. 1.11(b)). The difference between intensity autocorrelation and interferometric autocorrelation depends on the response time of the detector used and the speed of oscillation of the moving mirror. An interferometric autocorrelation scans in such a way so that the fringes created on the beamsplitter can be individually resolved. For a transform-limited pulse the value of each fringe period corresponds to a change of delay of $\Delta\tau = \pm\pi/\omega$. This technique can provide limited information about the chirp of a pulse. The intensity autocorrelation is a relatively easy way to determine the duration of a pulse therefore it was intensity autocorrelation that was utilised throughout this project to determine the pulse durations of the various pulsed laser systems.

1.6 Conclusions

In this chapter, the various benefits of ultrashort optical pulses in a range of applications have been discussed. Particular attention has been given to pulse generation and characterisation. I also discussed the relevant features of the propagation of these ultrashort pulses through dispersive materials. These give rise to various nonlinear effects and exploitable mode-locking techniques, which can be harnessed to generate femtosecond pulses. The autocorrelation measurement technique was described to give an understanding of how the ultrashort pulses could be characterised temporally. The content of the chapters that follow will build on the physics that has been covered in this chapter.

1.7 References

1. A.L. Schawlow and C.H. Townes, "Infrared and Optical Masers", *Physical Review*, vol. 112, (6), p. 1940-1949, 1958.
2. C.H. Townes, "The first laser", in *A Century of Nature: Twenty-One Discoveries that Changed Science and the World*, L. Garwin and T. Lincoln, Editors, The University of Chicago Press. p. 107-112, 2003.
3. S. Link, H.A. Durr, and W. Eberhardt, "Femtosecond spectroscopy", *Journal of Physics-Condensed Matter*, vol. 13, (34), p. 7873-7884, 2001.
4. A.H. Zewail, "Femtochemistry: Atomic-scale dynamics of the chemical bond", *Journal of Physical Chemistry A*, vol. 104, (24), p. 5660-5694, 2000.
5. S. Nakamura, Y. Ueno, and K. Tajima, "Ultrafast (200-fs Switching, 1.5-Tb/s Demultiplexing) and High-Repetition (10 GHz) Operations of a Polarization-Discriminating Symmetric Mach–Zehnder All-Optical Switch", *IEEE Photonics technology letters*, vol. 10, (11), p. 1575-1577, 1998.
6. R.P. Schreieck, M.H. Kwakernaak, H. Jackel, and H. Melchior, "All-optical switching at multi-100-Gb/s data rates with Mach- Zehnder interferometer switches", *IEEE Journal of Quantum Electronics*, vol. 38, (8), p. 1053-1061, 2002.
7. J. Lu, J. Cheng, and B.D. Cameron. "Low sidelobe limited diffraction optical coherence tomography", in *Clinical Diagnostic Systems: Technologies and Instrumentation, Proceedings of SPIE*, 2002.
8. L.F. Mollenauer, P.V. Mamyshev, J. Gripp, M.J. Neubelt, N. Mamysheva, L. Gruner-Nielsen, and T. Veng, "Demonstration of massive wavelength-division multiplexing over transoceanic distances by use of dispersion-managed solitons", *Optics Letters*, vol. 25, (10), p. 704-706, 2000.
9. U. Keller, "Recent developments in compact ultrafast lasers", *Nature*, vol. 424, (6950), p. 831-838, 2003.
10. F.H. Loesel, M.H. Niemz, J.F. Bille, and T. Juhasz, "Laser-induced optical breakdown on hard and soft tissues and its dependence on the pulse duration: Experiment and model", *IEEE Journal of Quantum Electronics*, vol. 32, (10), p. 1717-1722, 1996.
11. D.X. Hammer, R.J. Thomas, G.D. Noojin, B.A. Rockwell, P.K. Kennedy, and W.P. Roach, "Experimental investigation of ultrashort pulse laser-induced breakdown thresholds in aqueous media", *IEEE Journal of Quantum Electronics*, vol. 32, (4), p. 670-678, 1996.
12. T. Dennis, Curtis, E.A., Oates, C.W., Hollberg, L., Gilbert S.L., "Wavelength References for 1300-nm Wavelength-Division Multiplexing", *Journal of Lightwave Technology*, vol. 20, (5), p. 776-782, 2002.
13. C.K. Sun, C.C. Chen, S.W. Chu, T.H. Tsai, Y.C. Chen, and B.L. Lin, "Multiharmonic-generation biopsy of skin", *Optics Letters*, vol. 28, (24), p. 2488-2490, 2003.
14. J. Wilson and J. Hawkes, "Optelectronics - An introduction", 3rd ed. London: Prentice Hall, 1998.

15. A.E. Siegman, "Lasers". Calafornia: University Science Books, 1986.

16. I. Walmsley, L. Waxer, and C. Dorrer, "The role of dispersion in ultrafast optics", *Review of Scientific Instruments*, vol. 72, (1), p. 1-29, 2001.

17. D.J. Ripin, C. Chudoba, J.T. Gopinath, J.G. Fujimoto, E.P. Ippen, U. Morgner, F.X. Kartner, V. Scheuer, G. Angelow, and T. Tschudi, "Generation of 20-fs pulses by a prismless Cr4+: YAG laser", *Optics Letters*, vol. 27, (1), p. 61-63, 2002.

18. C. Chudoba, J.G. Fujimoto, E.P. Ippen, H.A. Haus, U. Morgner, F.X. Kartner, V. Scheuer, G. Angelow, and T. Tschudi, "All-solid-state Cr:forsterite laser generating 14-fs pulses at 1.3 μm", *Optics Letters*, vol. 26, (5), p. 292-294, 2001.

19. E.B. Treacy, "Optical Pulse Compression with Diffration Gratings", *Ieee Journal of Quantum Electronics*, vol. 5, (9), p. 454-458, 1969.

20. R. Szipocs, A. Kohazi-Kis, S. Lako, P. Apai, A.P. Kovacs, G. DeBell, L. Mott, A.W. Louderback, A.V. Tikhonravov, and M.K. Trubetskov, "Negative dispersion mirrors for dispersion control in femtosecond lasers: chirped dielectric mirrors and multi-cavity Gires-Tournois interferometers", *Applied Physics B: Lasers and Optics*, vol. 70, p. S51-S57, 2000.

21. R.L. Fork, O.E. Martinez, and J.P. Gordon, "Negative Dispersion Using Pairs of Prisms", *Optics Letters*, vol. 9, (5), p. 150-152, 1984.

22. J.P. Gordon and R.L. Fork, "Optical-Resonator with Negative Dispersion", *Optics Letters*, vol. 9, (5), p. 153-155, 1984.

23. O.E. Martinez, R.L. Fork, and J.P. Gordon, "Theory of Passively Mode-Locked Lasers Including Self-Phase Modulation and Group-Velocity Dispersion", *Optics Letters*, vol. 9, (5), p. 156-158, 1984.

24. I.G. Cormack, "Rapid techniques for ultrashort optical pulse characterisation", PhD thesis: School of Physics and Astronomy, University of St Andrews: St Andrews, 2001.

25. R. Paschotta, R. Haring, E. Gini, H. Melchior, U. Keller, H.L. Offerhaus, and D.J. Richardson, "Passively Q-switched 0.1-mJ fiber laser system at 1.53 μm", *Optics Letters*, vol. 24, (6), p. 388-390, 1999.

26. M.H. Dunn, "Lasers 2", in *MSc. Lecture course*. 2001, School of Physics and Astronomy, University of St Andrews,2001.

27. H.A. Haus, "Mode-locking of lasers", *IEEE Journal of Selected Topics in Quantum Electronics*, vol. 6, (6), p. 1173-1185, 2000.

28. U. Keller. "Advances in Lasers and Applications: Ultrashort pulse generation", in *Proceedings of the 52nd Scottish Universities Summer School in Physics*, St Andrews, Scotland, 1998.

29. M. DiDomenico, Jr., J.E. Geusic, H.M. Marcos, and R.G. Smith, "Generation of ultrashort optical pulses by mode locking the YAIG: Nd laser", *Applied Physics Letters*, vol. 8, (7), p. 180-183, 1966.

30. H.W. Mocker and R.J. Collins, "Mode competition and self-modelocking effects in a Q-switched ruby laser", *Applied Physics Letters*, vol. 7, (10), p. 270-273, 1965.

31. A.J. DeMaria, D.A. Stetser, and H. Heynau, "Self mode-locking of lasers with saturable absorbers", *Applied Physics Letters*, vol. 8, (7), p. 174-176, 1966.

32. H. Statz and C.L. Tang, "Phase Locking of Modes in Lasers", *Journal of Applied Physics*, vol. 36, (12), p. 3923-3927, 1965.

33. S. Tsuda, W.H. Knox, S.T. Cundiff, W.Y. Jan, and J.E. Cunningham, "Mode-locking ultrafast solid-state lasers with saturable Bragg reflectors", *IEEE Journal of Selected Topics in Quantum Electronics*, vol. 2, (3), p. 454-464, 1996.

34. U. Keller, K.J. Weingarten, F.X. Kartner, D. Kopf, B. Braun, I.D. Jung, R. Fluck, C. Honninger, N. Matuschek, and J.A. derAu, "Semiconductor saturable absorber mirrors (SESAM's) for femtosecond to nanosecond pulse generation in solid-state lasers", *IEEE Journal of Selected Topics in Quantum Electronics*, vol. 2, (3), p. 435-453, 1996.

35. B. Craig and A. Krueger, "Saturable Bragg reflectors simplify modelocking", *Laser Focus World*, vol. 36, (8), p. 227-228, 2000.

36. U. Keller, D.A.B. Miller, G.D. Boyd, T.H. Chiu, J.F. Ferguson, and M.T. Asom, "Solid-State Low-Loss Intracavity Saturable Absorber for Nd-YLF Lasers - an Antiresonant Semiconductor Fabry-Perot Saturable Absorber", *Optics Letters*, vol. 17, (7), p. 505-507, 1992.

37. L.P. Barry, P.G. Bollond, J.M. Dudley, J.D. Harvey, and R. Leonhardt, "Autocorrelation of ultrashort pulses at 1.5 mu m based on nonlinear response of silicon photodiodes", *Electronics Letters*, vol. 32, (20), p. 1922-1923, 1996.

38. J.A. Armstrong, "Measurement of picosecond laser pulse widths", *Applied Physics Letters*, vol. 10, (1), p. 16-18, 1967.

39. R. Trebino and D.J. Kane, "Using Phase Retrieval to Measure the Intensity and Phase of Ultrashort Pulses - Frequency-Resolved Optical Gating", *Journal of the Optical Society of America a-Optics Image Science and Vision*, vol. 10, (5), p. 1101-1111, 1993.

40. D.T. Reid, W. Sibbett, J.M. Dudley, L.P. Barry, B. Thomsen, and J.D. Harvey, "Commercial semiconductor devices for two photon absorption autocorrelation of ultrashort light pulses", *Applied Optics*, vol. 37, (34), p. 8142-8144, 1998.

Chapter 2 – Femtosecond Laser Systems Operating Around 1300nm

2.1 Introduction

As mentioned in Chapter 1, there are several important applications that require ultrashort pulse lasers operating in the 1300nm spectral region. This has stimulated development of Cr^{4+}:forsterite lasers, which operate in the 1300nm spectral range. In this chapter the subject matter is concentrated on the design and construction of a mode-locked Cr^{4+}:forsterite laser that incorporates a relatively new saturable Bragg reflector (SBR) device as the mode-locking element. Section 2.2 will introduce the reader to Cr^{4+}:forsterite as a suitable laser gain material whereas in section 2.3 there will be some discussion on the SBR mode-locking element and why it has advantages over alternative mode-locking devices. The remainder of the chapter relates to the design, construction, operation and characterisation of both continuous-wave and mode-locked Cr^{4+}:forsterite laser configurations.

2.2 Cr^{4+}:forsterite as a laser gain material

In transition metal vibronic laser gain materials the interactions between the active dopant ion and the host crystal lattice determine the positions and broadening characteristics of the electronic energy levels. The strength of the crystal field at these ion sites can shape the energy levels to afford media that can support large gain bandwidths (>30nm) and long upper state lifetimes (>3μs). The lasing action and precise relationship between the important energy levels of chromium ions depends on the host in which they reside. This next section details the interaction of chromium ions within a forsterite lattice that leads to laser emission at 1300nm. Section 3.2 is concerned with these processes in the Cr^{4+}:YAG laser gain material.

Forsterite [$(FeMg)_2SiO_4$] belongs to a class of crystals called olivines[1]. The magnesium rich member of these olivines occurs naturally as one of the main constituents of the Earth's upper mantle[2]. It is this magnesium rich crystal into which chromium is placed as a dopant. The first Cr:forsterite laser was demonstrated in 1988[3], but there was uncertainty over the charge ion responsible for the laser action given that chromium can be doped into a forsterite crystal with differing charge states. Cr^{3+} ions can be substituted into octahedrally coordinated Mg^{2+} sites and Cr^{4+} ions into tedrahedrally coordinated Si^{4+} sites. Initially it was thought that the Cr^{3+} ion was responsible for lasing action at 1300nm. After further spectroscopic analysis it was confirmed to be the Cr^{4+} ion[4, 5]. Further studies showed that the presence of Cr^{3+} ions in the lattice actually lead to a decrease in lasing efficiency[6].

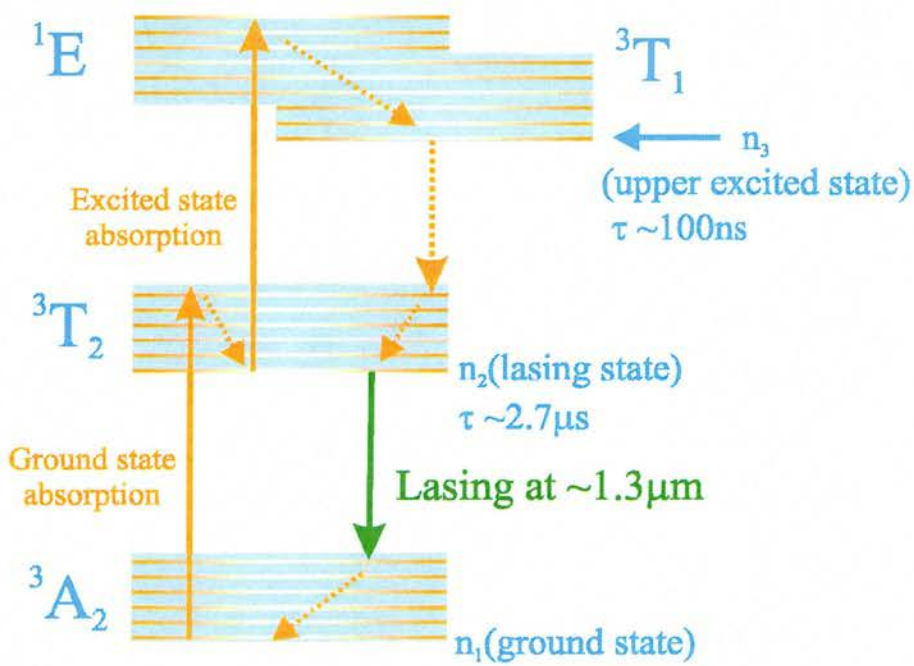

Fig. 2.1 *Simplified energy-level diagram of Cr^{4+} in forsterite.*

Fig. 2.1 shows the simplified energy-level diagram of Cr^{4+} in forsterite[7]. When pumped at 1064nm, Cr^{4+} ions are excited from the ground state of $^3A_2$ to the upper laser

state of $^3T_2$. This 1064nm pump light also excites Cr^{4+} ions from the $^3T_2$ state to the ^1E level as a result of excited-state absorption. This state then relaxes to the upper excited state of $^3T_1$, which then returns to the lasing state $^3T_2$ through non-radiative relaxation.

The ^1E state crosses the $^3T_1$ state, which produces an electronic bottleneck trap. This trap delays the nonradiative decay of the upper excited electron state for ~10ps. The lifetime of the $^3T_1$ state is around a few hundred nanoseconds. At room temperature the lasing state has a well known lifetime of 2.7μs. However, this upper-state lifetime is sensitive to temperature. If the crystal is cooled to liquid nitrogen temperatures then the upper-state lifetime increases to ~20μs. This temperature dependence has implications when pumping a forsterite crystal because the associated thermal load associated with strong pumping can effect adversely the upper-state lifetime. This feature requires suitable attention when selecting the pump intensities within the crystal necessary to obtain an ample population inversion.

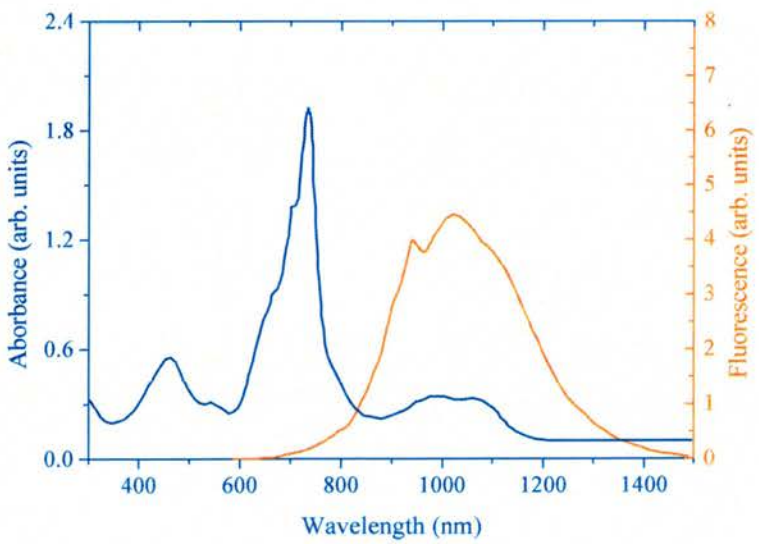

***Fig. 2.2** Absorption and emission spectra of Cr^{4+}:forsterite.*

Fig. 2.2 shows the absorption and emission spectra for Cr^{4+}:forsterite. The $^3A_2 \rightarrow {}^3T_1$ and $^3A_2 \rightarrow {}^3T_2$ transitions give rise to two broad absorption bands. One peaks around 738nm and the other is in the range of 850-1150nm. These absorption bands cover the operating wavelengths of many commercially available pump lasers such as Nd:YAG, Nd:YVO_4 and ytterbium fibre lasers which operate at 1064nm. There have also been Cr^{4+}:forsterite lasers that have been pumped by 980nm master-oscillator-power-amplifier (MOPA) schemes[8] and by AlGaInP laser diodes operating at 680nm[9]. The emission spectra from Cr^{4+}:forsterite extends from 700nm to1400nm.

The interaction between the lasing ion transition and the surrounding lattice dictates the emission spectra of a crystal lattice. For the transition metal ion Cr^{4+}, lasing occurs between the electronic levels $^3T_2 \rightarrow {}^3A_2$ of the 3d electrons. These electrons are not shielded from the surrounding lattice, allowing for strong electron-phonon (vibronic) coupling. This coupling gives rise to a broadly tunable output ranging from 1130nm to 1367nm[6] and allows Cr^{4+}:forsterite to be used for generating ultrafast pulses.

2.3 The GaInNAs mode-locking element

A wide range of passively mode locked near-infrared solid-state lasers operating in the 1200-1600nm region have used saturable Bragg reflectors (SBRs) and semiconductor saturable absorbing mirrors (SESAMs) to initiate the mode-locking process[10-12]. The previously reported saturable absorbers for operation in this wavelength region have been based on InGaAs quantum wells on GaAs based Bragg mirrors or InGaAsP quantum wells on InP based Bragg mirrors, both of which have recognized shortcomings[13]. The indium concentration required for longer wavelength operation (>1μm) of an InGaAs device results in a lattice constant differential that is beyond the

critical level for a coherently strained InGaAs:AlAs/GaAs Bragg mirror structure. Strain relaxation occurs with the inevitability of high non-saturable losses and low damage thresholds, which makes the devices unusable in near-infrared solid state lasers. The alternative scheme of growing an InGaAsP absorber on an InP-based mirror structure offers narrow bandwidth Bragg mirror reflectivity, due to the small refractive index contrast achievable with materials that are lattice matched to InP, but this restricts significantly the pulse durations that can be generated.

Recently, however, a significant new route in the design and development of more suitable SBR devices for ultrashort pulse lasers has been demonstrated[14-16]. Sun *et al.*[14] gave the first demonstration of passive mode locking using a GaInNAs SBR incorporated within a high power picosecond Nd-based laser operating near 1300nm, thus demonstrating the high damage threshold of GaInNAs based saturable devices. The key has been the use of GaAs-based SBRs that incorporate GaInNAs quantum wells for saturable absorption. Inclusion of small percentages of nitrogen not only reduces the strain, but also shifts the absorption edge very effectively into the 1200-1600nm region. The low-loss nature of these GaInNAs SBRs is crucial for the development of efficient and reliable Cr^{4+}:forsterite lasers. The active forsterite medium has relatively low gain so its lasing efficiency suffers when lossy intracavity elements are inserted into the system. This means that Cr^{4+}:forserite lasers that incorporate InGaAs on GaAs SBRs[13, 17, 18] have inferior performance characteristics compared to their cw or Kerr-lens mode locked counterparts.

The GaInNAs SBRs utilised in the laser systems evaluated in this project were provided by the Institute of Photonics at the University of Strathclyde. They were grown by solid-source molecular beam epitaxy and have been reported elsewhere[14]. The structures consisted of 21-layer-pair AlAs (115-nm)/GaAs (97-nm) Bragg stacks.

The final quarter-wave layer of GaAs contained a nominally 7-nm-thick $Ga_{0.65}In_{0.35}N_{0.019}As_{0.981}$ single quantum well, which was grown at 430°C, midway within the layer.

Reflectivity characterisations, carried out at the Institute of Photonics, showed that the stop-band of the Bragg stack was >110nm in bandwidth, and centred around 1320nm. This meant that the Bragg stack was capable of supporting femtosecond pulses with spectral bandwidths >20nm. The excitonic luminescence decay (i.e. the impulse recovery time) was shown to be mono-exponential with a time constant varying between 69ps and 111ps, depending on the pump fluence[19]. These GaInNAs devices were so recently developed that their other characteristics (modulation depth, saturation fluence and non-saturable losses) had not been determined. It was hoped that successful operation of these devices in a Cr^{4+}:forsterite laser system would provide some further characterisation of these new devices.

2.4 The Cr^{4+}:fosterite laser cavity

There are various aspects of a laser cavity that must be considered prior to construction. These include: the design of stable cavity geometries, the pump source and pump geometries, appropriate mirror sets; and the Cr^{4+}:forsterite crystal itself. These issues are detailed below.

2.4.1 Cavity design

Before opting for the generation of femtosecond pulses at 1300nm it was vital that a stable cw source was constructed first. The main requirement for a cw laser based on a low-gain material, such as Cr^{4+}:forsterite, is a good overlap of tightly focused laser and pump beams inside the gain crystal. This can be achieved by using a near-diffraction

limited pump beam (M^2~1). The most suitable cavity design is based around a four-mirror cavity, which allows the laser to operate at the centre of a large stability region and can facilitate the insertion of other intracavity elements such as prisms and SBRs. Fig. 2.3 illustrates a typical four-mirror Z-cavity.

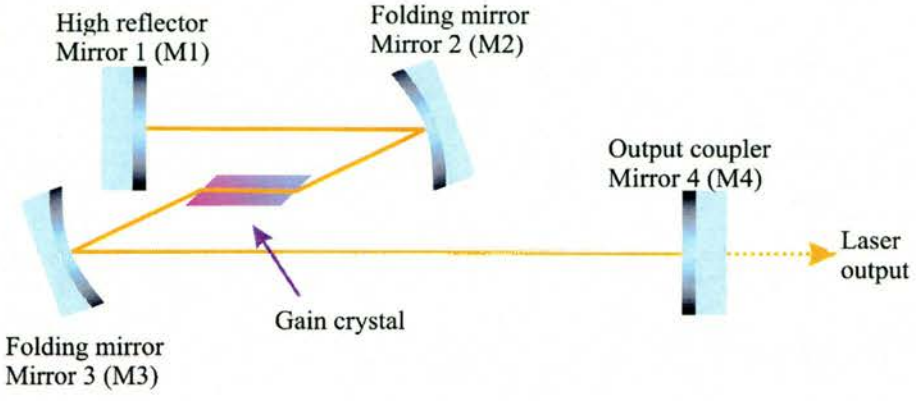

Fig. 2.3 *Schematic of a typical four-mirror, astigmatically compensated laser cavity.*

There are significant benefits associated with the use of a four-mirror cavity. Given that it is usual to Brewster-angle the ends of the laser rod in order to minimise Fresnel losses, it is necessary to compensate for the associated astigmatism from the angled surfaces. This can be achieved by suitable alignment of the curved folding mirrors (M2 and M3) either side of the laser gain material. In an asymmetric arrangement a tight focus exists at the high reflector M1. To initiate mode locked operation the high reflector is replaced by the SBR device where this tight focus is exploited. The long arm of the cavity (M3 to M4) provides a well-collimated beam into which dispersion compensating prisms can be inserted. The output power from the laser can be adjusted through the coupling efficiency of the output coupler M4.

A laser cavity design package was used to calculate the correct positions and angles of the four mirrors and the laser crystal. This package was based on ABCD

matrix multiplication of a Gaussian beam[20, 21] and provided information about the various beam mode sizes throughout the laser system.

2.4.2 Pump source and pump geometry

The pump source that was used for this part of the project was an infrared Nd:YVO_4 IR laser (*Spectra Physics*). This source was capable of producing up to 10W of linearly polarised, near-diffraction limited light at 1064nm. This light was passed through a half waveplate, a simple telescope arrangement and a focusing lens before passing through one of the folding mirrors (M3) and onto the crystal face. Using a simple telescope system in conjunction with a focussing lens it was possible to vary the pump spot size and focus the pump beam to an appropriate size in order to maximise the mode matching of the pump and laser mode beams. The half waveplate was necessary to rotate the linearly polarised output from the pump laser to minimise pump reflection at the Brewster-angled face of the laser crystal. This allowed maximum absorption of the pump light in the crystal rod. A wide range of lenses were available for the construction of the telescope system and focusing lens. A computerised beam profiler was used to verify the pump-mode beam overlap. A schematic of the pump geometry is shown below.

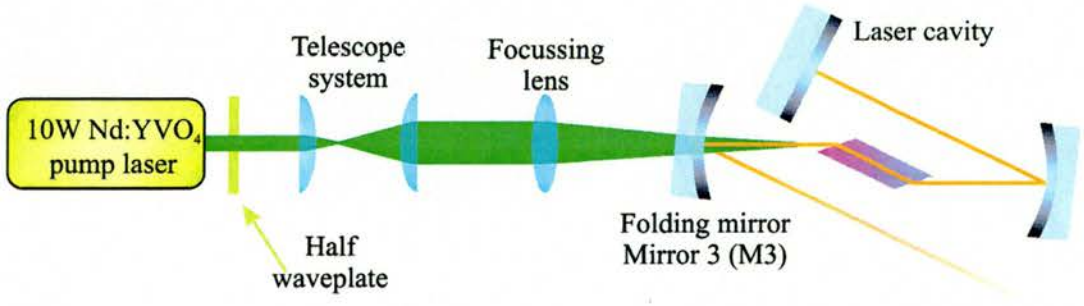

Fig. 2.4 *Schematic of the pump laser and pump geometry used on the Cr^{4+}:forsterite laser system.*

2.4.3 Mirrors and crystals

The cavity mirrors utilised in the Cr^{4+}:Forsterite lasers of this project were designed specifically for operation around 1300nm. In total, nine mirrors were purchased from *LaserOptik GmbH*[22]. Four of them were folding mirrors (two with radii of curvature of -75mm, and two with radii of curvature of -100mm). These mirrors were coated for broadband high reflection (R>99.996%) between 1250-1370nm and high transmission of the pump light at 1064nm. The other five mirrors consisted of two broadband plane-wedged high reflectors and three plane-wedged output couplers with coupling efficiencies of 0.5%, 1% and 2%. This selection of mirrors allowed various cavity configurations to be constructed, depending on the laser mode beam sizes and coupling efficiencies that were required for suitable operation of the laser.

The Brewster-cut Cr^{4+}:forsterite laser crystal had a peak small-signal pump absorption coefficient of $1.3cm^{-1}$ and was 11.6mm in length. The crystal was wrapped in indium foil and tightly clamped in a water-cooled copper mount. This mount was maintained at a temperature of 14°C to aid the removal of heat from the crystal when pumped at high powers.

2.5 Continuous-wave operation of Cr^{4+}:forsterite laser

During the design of the initial Cr^{4+}:forsterite cavity, the decision was taken to construct a pump lensing arrangement that would produce a beam spot size on the laser crystal that was similar in size to the laser mode beam in the crystal. This thus facilitated good mode-matching of the two beams. In this case the cavity design software implied a beam diameter of ~80μm propagating through the Cr^{4+}:forsterite crystal. This was matched with a pump spot size of 82μm by selecting appropriate lenses for the telescope system in Fig. 2.4. Although cw operation was achieved, the lasing threshold

was measured to be 3.7W, which was much higher than expected[23] and raised concern as to the quality of crystal rod. After a further literature survey[1, 2], the cavity and pumping scheme were re-designed to provide a pump spot size and beam mode size of ~45μm through the crystal. As previously mentioned, due to the short upper-state lifetime of Cr^{4+}:forsterite, a high intensity pump beam is needed to provide an ample population inversion for suitable gain. This was not being achieved with the large (~80μm) pump spot size. Significant performance improvements were observed when this new cavity was constructed.

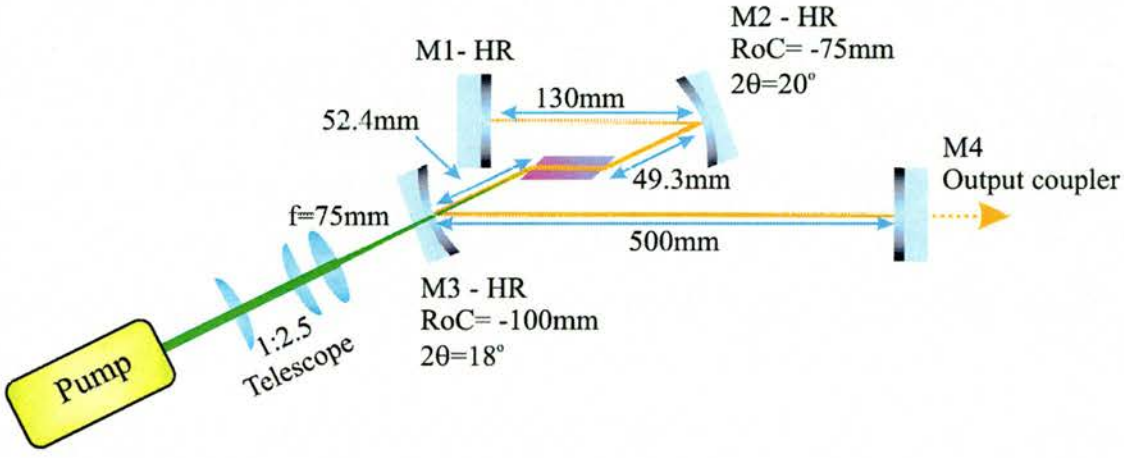

Fig. 2.5 *Schematic of laser cavity that was designed for cw operation.*

The above figure details the cavity configuration that was used such that the laser generated cw laser light at 1300nm. The performance of the laser was evaluated for the three output couplings and the corresponding data is shown in Fig. 2.6.

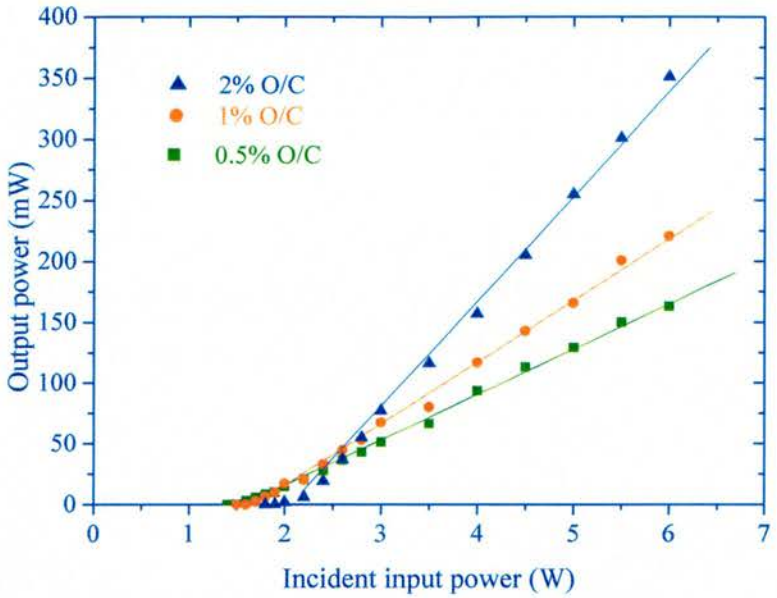

Fig. 2.6 *Cw performance characteristics of Cr:forsterite laser.*

A minimum threshold of 1.4W was achieved with the 0.5% output coupling. This compared well with similar Cr^{4+}:forsterite lasers[23]. The measured slope efficiencies with the 0.5%, 1% and 2% output couplers (O/C) were 2.6%, 3.3% and 4.4% respectively. With the 2% O/C in place, a maximum cw output power of 350mW was achieved at a 6W pump power level. At higher pump powers thermal lensing effects in the Cr^{4+}:forsterite crystal caused the laser cavity to become unstable and the power dropped significantly. The free-running wavelength of the laser was measured to be 1287nm. With an intracavity prism inserted into the long arm of the laser it was possible to tune this wavelength from 1230nm to 1350nm.

This evaluation demonstrated the successful operation of a Cr^{4+}:forsterite laser. The high output powers available and the large spectral bandwidth were then harnessed to generate femtosecond pulses.

2.6 Mode-locked operation of Cr^{4+}:forsterite laser incorporating a GaInNAs SBR

The tight focus at mirror M1 can be used to generate a high incident pump fluence, which can initiate saturable absorber mode locking even in low gain, and low intracavity-power lasers. The size of the focused spot at M1 is determined primarily by the length of the two arms of the cavity, which is one advantage of using a four-mirror asymmetric Z-cavity.

The cavity design was modified slightly from the cw arrangement shown in Fig. 2.5 to provide a spot size of $2.8 \times 10^{-3} mm^2$ incident on the GaInNAs SBR device. This size was deemed sufficient to initiate the mode-locking process. To determine the compatibility of the GaInNAs SBR for the mode locking of this low-gain laser, the power characteristics of the laser with a 0.5% O/C were compared on replacing the HR end mirror M1 with the SBR device. Initial mode-locking regimes were observed at pump powers greater than 5.3W. Fig. 2.7 shows that the SBR exhibited identical performance to the HR-coated end mirror above this threshold, which implied that the SBR device had negligible (<0.1%) non-saturable loss. It should be noted that these results were taken without the dispersion compensating prisms in place, so the pulses had durations of a few picoseconds. This demonstrates that GaInNAs devices have significantly lower parasitic losses when compared against their InGaAs/GaAs counterparts[13]. Below this mode-locking threshold, the loss due to the SBR was a result of the saturable loss alone.

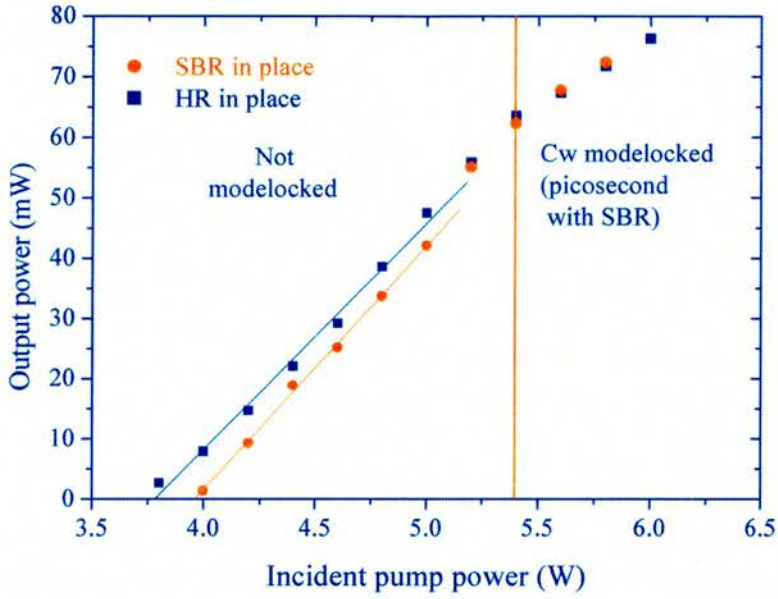

Fig. 2.7 *Power transfer characteristics of the Cr:forsterite laser with a 0.5% O/C, with and without the SBR.*

For operation in the femtosecond regime, two fused silica dispersion-compensating prisms were incorporated in the long arm of the laser resonator with a tip-to-tip separation of 35mm as shown in Fig. 2.8.

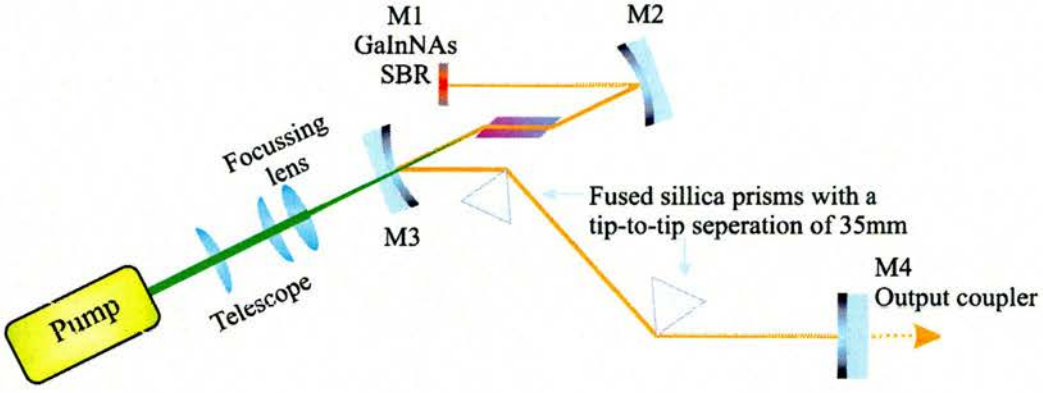

Fig. 2.8 *Schematic of laser cavity incorporating dispersion compensating prisms for femtosecond operation.*

With the 0.5% O/C, mode locking was self-starting when the incident pump power was increased to 3.6W. A representative intensity autocorrelation and spectral profile centred at a wavelength of 1288nm are included as Fig 2.9.

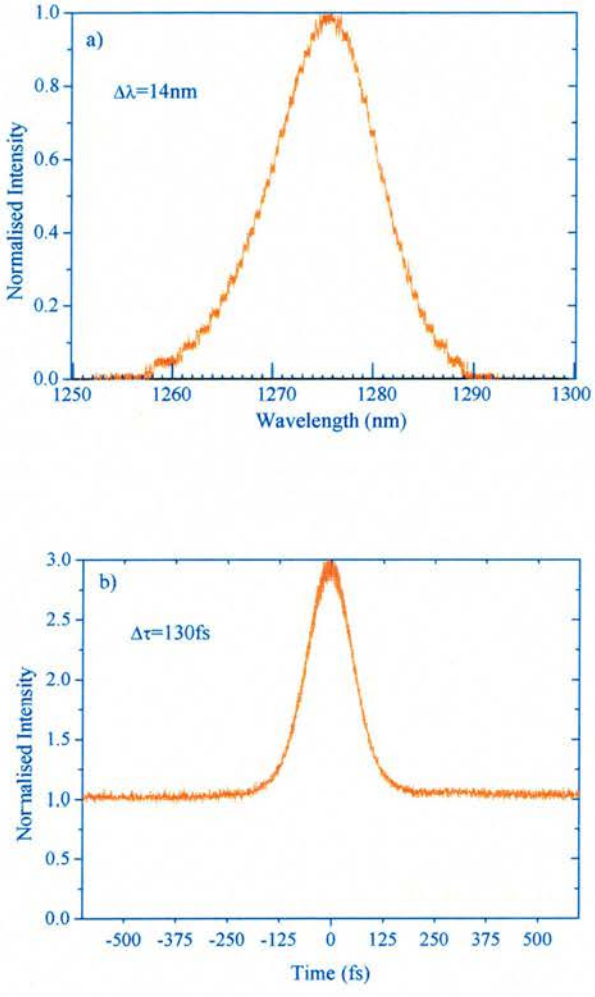

Fig. 2.9 *(a) gives the optical spectrum and (b) the measured intensity autocorrelation of the Cr^{4+}:forsterite laser giving pulse durations of 130fs.*

By assuming a $sech^2$ intensity profile, the pulse duration was determined to be 130fs. With the corresponding spectral width of 14nm, the implied time-bandwidth product of 0.33 indicated that operation was near the transform limit. The pulse repetition rate of the laser in this configuration was 178MHz, which corresponded to a cavity length of ~750cm. Average output powers up to 25mW in stable femtosecond pulse sequences

were obtained with the 0.5% O/C and 35mW with the 1% O/C. The output power was limited because of the relatively high insertion loss of the fused silica prisms. The figure below shows these power characteristics, with the prisms in place.

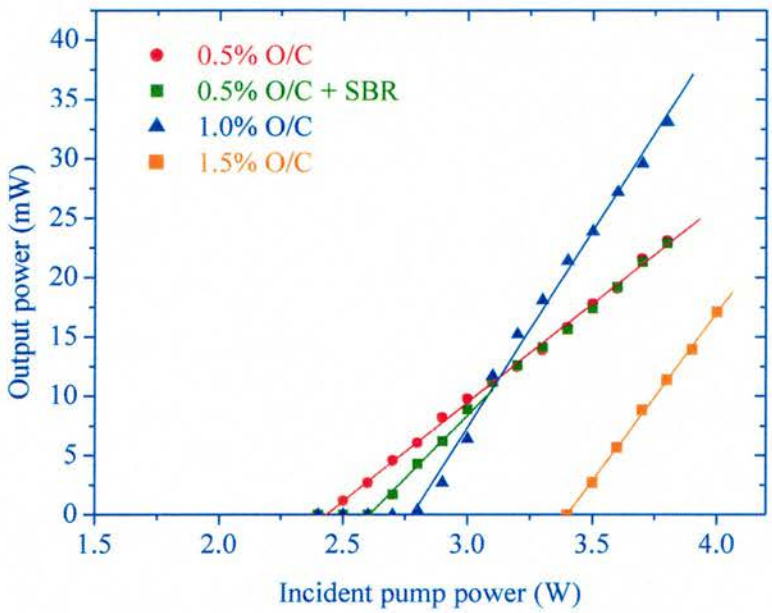

Fig. 2.10 *Power transfer characteristics of Cr^{4+}:forsterite laser with different output couplers.*

The Institute of Photonics at the University of Strathclyde were able to use the above data to provide us with an estimate of the modulation depth of the SBR. Using a Findlay-Clay calculation[24], these collaborators estimated the saturable loss, i.e. the SBR modulation depth, to be 0.24%. The data also provided us with an estimation of the saturation fluence needed to saturate the SBR device. The saturable losses were bleached for mode locked average laser output powers greater than ~12mW with the 0.5% O/C in place. The spot size on the SBR during these measurements was $8\text{x}10^{-6}\text{cm}^2$ hence, for a mode locked repetition rate of 178MHz, the saturation fluence was of the order of $10\mu\text{J/cm}^2$. This value compares well against other SBR devices[17, 25], which have saturation fluences in the range, $100\text{-}800\mu\text{J/cm}^2$.

An intracavity slit was inserted into the long dispersed arm of the laser to assess the tunability of the system when mode locked in the picosecond domain. This was achieved with the 0.5% O/C in place at a pump power of 4.5W. Wavelength tuning of the mode-locked pulses was possible from 1268-1291nm as illustrated in Fig. 2.11.

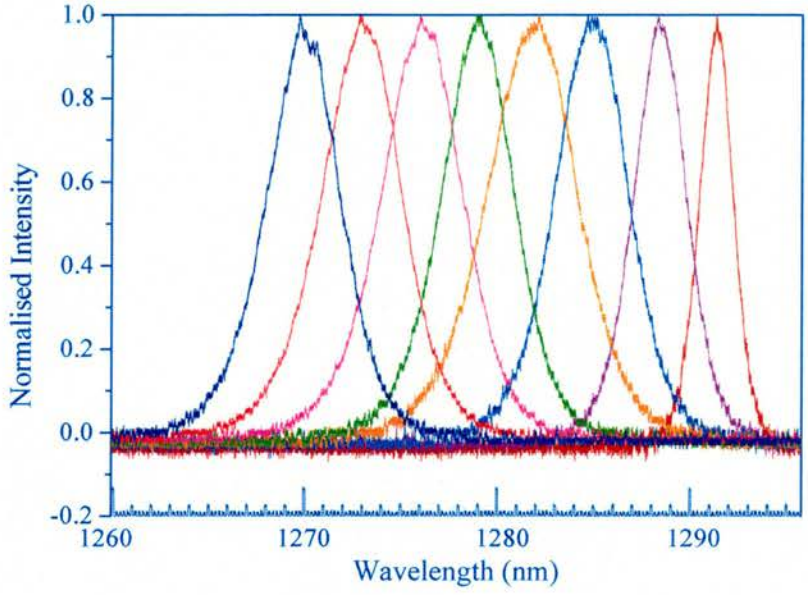

Fig. 2.11 *Spectra from the femtosecond mode locked Cr^{4+}:forsterite laser demonstrating a tuning range of 23nm.*

The maximum output power of 25mW was obtained at wavelengths around 1275nm and pulse durations ranged from 170fs at 1275nm to 350fs at either edge of the tuning range. A maximum output power of 45mW was obtained with the 1% O/C in place but the tuning range in this case was reduced to 1273-1290nm.

2.7 Future work and conclusions

In this chapter the design and construction of a femtosecond Cr^{4+}:forsterite laser system that has used a novel GaInNAs SBR structure has been discussed. This is the first time

that GaInNAs devices have been used in a laser to generate femtosecond pulses in the 1300nmm spectral region. This confirms more generally the potential of low-loss GaInNAs-based SBRs as mode-locking elements in femtosecond solid-state lasers. Further development can now be concentrated on several areas of this particular laser system. These include the replacement of the relatively high loss prism system with dispersion compensating mirrors (in the form of chirped mirrors or GTI mirrors). These would bring about a reduction in the cavity size and therefore an increase of the pulse repetition frequency (prf). It is believed that a prf of at least 1GHz is obtainable. This would make such a laser system very attractive for use in both telecommunication experiments and biophotonics applications. It is also believed that this system could be used in conjunction with frequency doubling crystals to generate femtosecond pulses in the spectral region centred around 750nm. The potential of the GaInNAs devices looks very promising as well. The results obtained from the above experiments have given the Institute of Photonics a greater understanding of how these devices work and how they might be adapted to work at longer wavelengths. Indeed, on the basis of the work described here, it is expected that there may soon be a low-loss GaInNAs mode-locking element that could be incorporated into suitable laser configurations to generate femtosecond pulses in the 1550nm telecommunications window.

2.8 References

1. A. Sennaroglu, "Broadly tunable Cr4+ doped solid-state lasers in the near infrared and visible", *Progress in Quantum Electronics*, vol. 26, (6), p. 287-352, 2002.
2. H.R. Verdun, L.M. Thomas, D.M. Andrauskas, T. McCollum, and A. Pinto, "Chromium-doped forsterite laser pumped with 1.06 μm radiation", *Applied Physics Letters*, vol. 53, (26), p. 2593-2595, 1988.
3. V. Petricevic, S.K. Gayen, R.R. Alfano, K. Yamagishi, H. Anzai, and Y. Yamaguchi, "Laser action in chromium-doped forsterite", *Applied Physics Letters*, vol. 52, (13), p. 1040-1042, 1988.
4. V. Petricevic, S.K. Gayen, and R.R. Alfano, "Laser action in chromium-activated forsterite for near-infrared excitation: Is Cr^{4+} the lasing ion?" *Applied Physics Letters*, vol. 53, (26), p. 2590-2592, 1988.
5. W. Jai, H. Liu, S. Jaffe, and W.M. Yen, "Spectroscopy of Cr^{3+} and Cr^{4+} ions in forsterite", *Physical Review B (Condensed Matter)*, vol. 43, (7), p. 5234-5242, 1991.
6. V.G. Baryshevskii, M.V. Korzhik, A.E. Kimaev, M.G. Livshits, V.B. Pavlenko, M.L. Meil'man, and B.I. Minkov, "Tunable Chromium Forsterite Laser in the Near IR Region", *Journal of applied spectroscopy*, vol. 53, (1), p. 675, 1990.
7. T. Togashi, Y. Nabekawa, T. Sekikawa, and S. Watanabe, "High-peak-power femtosecond Cr:forsterite laser system", *Applied Physics B: Lasers and Optics*, vol. 68, (2), p. 169-175, 1999.
8. J.M. Evans, V. Petricevic, A.B. Bykov, A. Delgado, and R.R. Alfano, "Direct diode-pumped continuous-wave near-infrared tunable laser operation of Cr^{4+}:forsterite and Cr^{4+}:Ca_2GeO_4", *Optics Letters*, vol. 22, (15), p. 1171-1173, 1997.
9. L. Quan, X. Liu, and F. Wise, "Cr:forsterite laser pumped by broad-area laser diodes", *Optics Letters*, vol. 22, (22), p. 1707-1709, 1997.
10. S. Tsuda, W.H. Knox, S.T. Cundiff, W.Y. Jan, and J.E. Cunningham, "Mode-locking ultrafast solid-state lasers with saturable Bragg reflectors", *Ieee Journal of Selected Topics in Quantum Electronics*, vol. 2, (3), p. 454-464, 1996.
11. U. Keller, K.J. Weingarten, F.X. Kartner, D. Kopf, B. Braun, I.D. Jung, R. Fluck, C. Honninger, N. Matuschek, and J.A. der Au, "Semiconductor saturable absorber mirrors (SESAM's) for femtosecond to nanosecond pulse generation in solid-state lasers", *IEEE Journal of Selected Topics in Quantum Electronics*, vol. 2, (3), p. 435-453, 1996.
12. B. Craig and A. Krueger, "Saturable Bragg reflectors simplify modelocking", *Laser Focus World*, vol. 36, (8), p. 227-228, 2000.
13. P.T. Guerreiro, S. Ten, E. Slobodchikov, Y.M. Kim, J.C. Woo, and N. Peyghambarian, "Self-starting mode-locked Cr:forsterite laser with semiconductor saturable Bragg reflector", *Optics Communications*, vol. 136, p. 27-30, 1997.

14. H.D. Sun, G.J. Valentine, R. Macaluso, S. Calvez, D. Burns, M.D. Dawson, T. Jouhti, and M. Pessa, "Low-loss 1.3-μm GaInNAs saturable Bragg reflector for high- power picosecond neodymium lasers", *Optics Letters*, vol. 27, (23), p. 2124-2126, 2002.

15. O.G. Okhotnikov, T. Jouhti, J. Konttinen, S. Karirinne, and M. Pessa, "1.5-mu m monolithic GaInNAs semiconductor saturable-absorber mode locking of an erbium fiber laser", *Optics Letters*, vol. 28, (5), p. 364-366, 2003.

16. V. Liverini, S. Schon, R. Grange, M. Haiml, S.C. Zeller, and U. Keller, "Low-loss GaInNAs saturable absorber mode locking a 1.3 μm solid-state laser", *Applied Physics Letters*, vol. 84, (20), p. 4002-4004, 2004.

17. Z. Zhang, K. Torizuka, T. Itatani, K. Kobayashi, T. Sugaya, and T. Nakagawa, "Self-starting mode-locked femtosecond forsterite laser with a semiconductor saturable-absorber mirror", *Optics Letters*, vol. 22, (13), p. 1006-1008, 1997.

18. Z. Zhang, T. K., T. Itatani, K. Kobayashi, T. Sugaya, T. Nakagawa, and H. Takahashi, "Broadband semiconductor saturable-absorber mirror for a self-starting mode-locked Cr:forsterite laser", *Optics Letters*, vol. 23, (18), p. 1465-1467, 1998.

19. S. Calvez, J.-M. Hopkins, S.A. Smith, A.H. Clark, R. Macaluso, H.D. Sun, M.D. Dawson, T. Jouhti, M. Pessa, K. Gundogdu, K.C. Hall, and T.F. Boggess, "GaInNAs/GaAs Bragg-mirror-based structures for novel 1.3μm device applications", *Journal of Crystal Growth*, vol. 268, p. 457-465, 2004.

20. M.H. Dunn, "Lasers 2", *MSc. Lecture course*, vol., (Lecture 14), 2001.

21. A.E. Siegman, "Lasers", Calafornia: University Science Books, 1986.

22. LaserOptik. http://www.laseroptik.de/,http://www.laseroptik.de/.

23. N. Zhavoronkov, A. Avtukh, and V. Mikhailov, "Chromium-doped forsterite laser with 1.1W of continuous-wave output power at room temperature", *Applied Optics*, vol. 36, (33), p. 8601-8605, 1997.

24. D. Findlay and R.A. Clay, "Measurement of Internal Losses in 4-Level Lasers", *Physics Letters*, vol. 20, p. 277, 1966.

25. G.J. Spuhler, S. Reffert, M. Haiml, M. Moser, and U. Keller, "Output-coupling semiconductor saturable absorber mirror", *Applied Physics Letters*, vol. 78, (18), p. 2733-2736, 2001.

Chapter 3 – Femtosecond Lasers Operating Around 1550nm

3.1 Introduction

Progress in the refinement of Cr^{4+}:YAG lasers has been ongoing since their initial demonstration in 1988[1]. The main motivation for research in this area is attributable to the overlap of the Cr^{4+}:YAG emission spectrum with the optical communication windows centred at 1300nm and 1550nm. Although the broadband nature of the Cr^{4+}:YAG gain material allows operation of these lasers at either of the communication windows, most research undertaken with Cr^{4+}:YAG has focused on its operation around 1550nm.

The established technique of Kerr-lens mode locking is rarely self-starting in Cr^{4+}:YAG lasers and so an external perturbation (such as a mechanical vibration) is required to initiate the process. Although a critical cavity alignment technique[2] can be used to ensure self-starting operation of KLM Cr^{4+}:YAG lasers[3] they have operated with less stability and tolerances in comparison to other systems. Mode-locking methods for Cr^{4+}:YAG lasers which involve semiconductor saturable absorbers based on Bragg reflectors have also been demonstrated[4-6]. This approach relaxes the need for critical cavity alignment and ensures Cr^{4+}:YAG lasers are more reliable for practical applications.

In this chapter the subject matter is focused on the design and construction of a Cr^{4+}:YAG laser that incorporates a saturable Bragg reflector and uses a diode-pumped Yb-fibre laser as the pump source. The chapter will begin with a discussion of the Cr^{4+}:YAG crystal as a laser gain material for the 1550nm spectral region. Section 3.3 provides a description of the saturable Bragg reflector as a mode-locking element. The remainder of the chapter is concerned with the design, construction, operation and

characterisation of the laser system. The achievements described in this chapter represent foundation matter for some topics covered in Chapter 4, where the ideas described in this chapter are developed further to produce a femtosecond laser that has a multi-GHz pulse repetition frequency.

3.2 Cr^{4+}:YAG as a laser gain material

In 1987 yttrium aluminium garnet (YAG) was doped with chromium and oxidised to the tetravalent state[1]. It was first thought that this process formed impurity colour centres within the YAG lattice, but after further spectroscopic investigation[7], it was understood that the chromium ions themselves gave rise to the various spectroscopic characteristics of a Cr^{4+}:YAG crystal[7-12]. Much like the Cr^{4+}:forsterite gain material discussed in section 2.2, Cr^{4+}:YAG is also a vibronically broadened gain medium. However, the position of the Cr^{4+} ions within a YAG lattice is more complicated than in the forsterite lattice, which leads to some interesting polarisation features, which are discussed later.

Yttrium aluminium garnet ($Y_3Al_5O_{12}$) has a cubic crystal lattice structure. Unfortunately, the site symmetry of the active Cr^{4+} ion is less than cubic. In this unusual case, anisotropic centres are created within an isotropic host lattice. This means that the actual sites of the Cr^{4+} ions form elongated tetrahedrons, which give rise to orbital splitting of the exited states and lowers the symmetry of the sites to a D_{2d} configuration, as illustrated in the simplified energy level diagram overleaf.

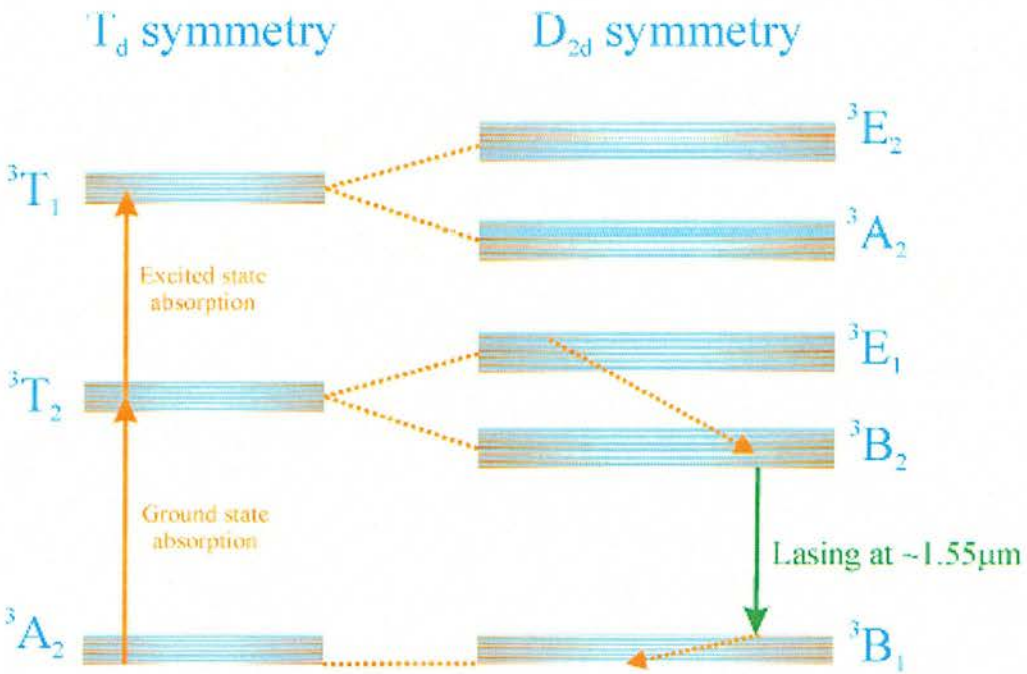

***Fig. 3.1** Energy level diagram of Cr^{4+} in YAG.*

The strong near-infrared absorption band around 1000nm is very broad (>200nm) and gives rise to the $^3A_2 \rightarrow {}^3T_2$ transition illustrated above. Nonradiative decay takes place rapidly to populate the upper laser state $^3B_2$. Excited state absorption also takes place from the $^3T_2$ state to the higher-lying $^3T_1$ state but this relaxes quickly (~50ps) to the $^3T_2$ state. At room temperature the upper-state lifetime ranges between 3.4μs-4.1μs[9, 12, 13]. This is the case because, much like Cr^{4+}:forsterite, the upper-state lifetime (the $^3B_2$ level) of Cr^{4+}:YAG is temperature dependent. For example, the upper-state lifetime has been shown to be an order of magnitude greater when cooled to 77K[13, 14]. This temperature dependence must be considered when designing the pumping scheme for the Cr^{4+}:YAG laser because high thermal loads associated with the pump intensity in the gain material will reduce the upper-state lifetime and therefore reduce the efficiency of the lasing process. Laser action takes place for transitions from the $^3B_2$ state to the top of the $^3B_1$ state. The absorption and fluorescence spectra are as shown in Fig. 3.2.

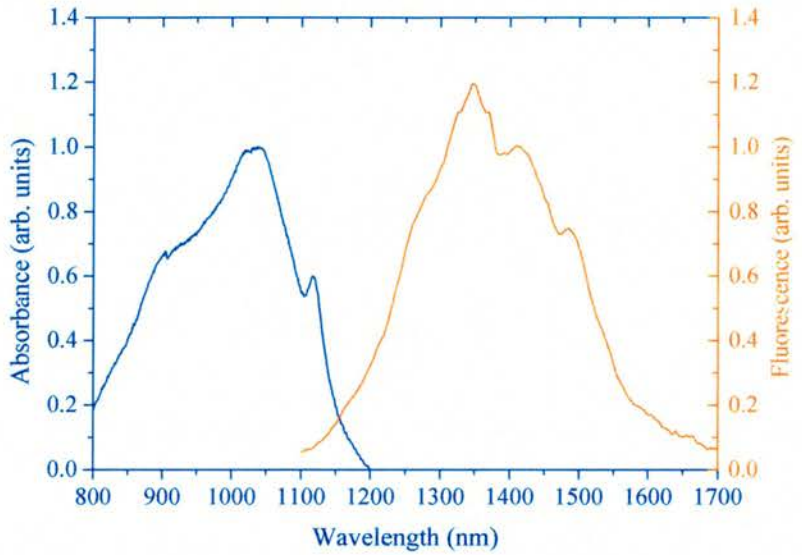

Fig. 3.2 *Absorption and emission spectra of Cr^{4+}:YAG.*

The strong absorption band in Cr^{4+}:YAG peaks between 900-1100nm. This makes Cr^{4+}:YAG particularly attractive for pumping with Nd:YAG or Yb-fibre laser sources, both of which are well developed and operate at 1064nm. There have also been several Cr^{4+}:YAG schemes which have made use of 980nm diode lasers as the pump source[15, 16].

As with its forsterite counterpart, the Cr^{4+}:YAG lattice allows for strong electron-phonon vibronic coupling, giving rise to a broad fluorescence bandwidth that extends over some 400nm[10]. As discussed in Chapter 1, this broad bandwidth feature is essential for the generation of ultrashort pulses. The peak fluorescence emission occurs at 1350nm but absorption of atmospheric water vapour at 1380nm shifts the peak laser emission to 1450nm. Due to the unusual position of the active Cr^{4+} ions within the YAG crystal lattice there is a variation of the emission and absorption features of the lattice depending on the polarisation being observed.

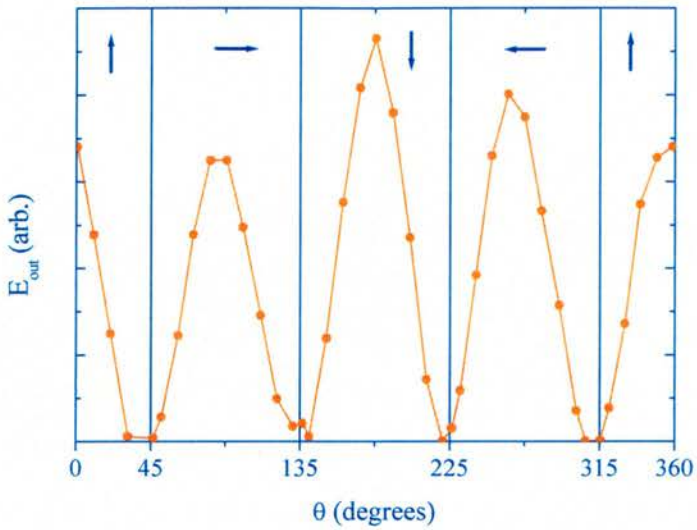

Fig. 3.3 *Dependence of the laser emission on the angle between the pump polarisation and the b-axis of the crystal lattice. The arrows indicate the polarisation of the Cr^{4+}:YAG laser emission.*

Fig. 3.3 shows how a polarised pump beam will selectively excite different active centres within the lattice, as the polarisation is rotated. This causes the polarisation of the laser output to flip as described in greater detail in references 7 and 14. The point to note from this polarisation feature is that efficient absorption of pump light can only be achieved when the crystal has been orientated to the correct angle in order that the most appropriate ions are excited within the lattice. This is achieved by introducing a λ/2 waveplate into the laser system, so that the polarisation state of the pump source can be correctly orientated, and the laser efficiency can thus be optimised.

3.3 The SBR mode-locking element

Section 2.3 discussed the physics of a SBR mode-locking element based on GaInNAs, which was successfully implemented within a Cr^{4+}:forsterite laser operating at

wavelengths around 1300nm. Unfortunately the development of GaInNAs devices has not yet been extended to the 1550nm spectral region. At this wavelength region it is necessary to utilize an earlier design of SBR structure, consisting of an AlAs/GaAs Bragg stack and an InGaAs/InP quantum-well[4, 17, 18]. This device is illustrated in Fig 3.4.

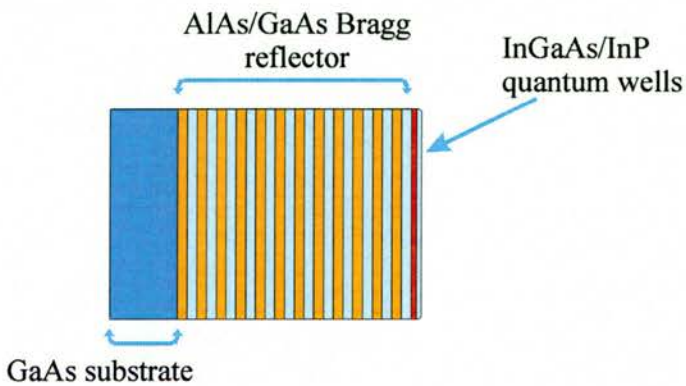

Fig 3.4 *Diagram of the SBR structure used to mode lock the Cr^{4+}:YAG laser.*

As mentioned in section 2.3, this device does have several shortcomings[19]. At wavelengths above 1100nm there is a lattice mismatch between the InGaAs/InP quantum well layer and the Bragg stack. This gives rise to a strain relaxation between the two layers thus increasing the non-saturable losses and lowering the damage threshold of the device. An alternative scheme involves growing InGaAsP absorbers on InP-based mirror structures but the Bragg mirror stack of these devices can only support a limited spectral bandwidth. This is due to the small refractive index contrast achievable with materials that are lattice matched to InP and thus limits their suitability for the generation of femtosecond pulses.

In spite of the above shortcomings these SBR structures are the only available saturable absorber devices that can be used at present to generate femtosecond pulses from Cr^{4+}:YAG laser systems operating at around 1550nm. A device similar to the one illustrated in Fig 3.4 was obtained from the Institute of Optics in Rochester, USA. The

SBR was grown by molecular beam epitaxy and consisted of a 25-layer-pair AlAs/GaAs Bragg stack, which had a broadband reflectivity R>99.4% centred at 1550nm with a bandwidth of 150nm. Two uncoupled 6nm-wide InGaAs/InP quantum wells separated by 7nm and located 15nm from the top of the surface provided the saturable absorption required to initiate mode locking. The modulation depth of the device was estimated to be ~1%. Information about the impulse recovery time of the device was not provided but was assumed to be ~50ps.

3.4 The Cr^{4+}:YAG laser cavity

In Chapter 2 the various aspects that were to be considered before constructing a Cr^{4+}:forsterite laser were discussed. A similar discussion will now be presented for a Cr^{4+}:YAG laser that incorporated an SBR as the mode locking element.

3.4.1 Cavity design

The cavity design requirements for this Cr^{4+}:YAG laser were very similar to those required for the Cr^{4+}:forsterite laser described in Chapter 2. Cr^{4+}:YAG is also a low-gain material and therefore requires good overlap of the tightly focused laser and pump modes within the gain crystal, to ensure low operational thresholds[20]. Due to these requirements the decision was made to construct a highly asymmetric, astigmatically compensated four-mirror Z-fold cavity similar to the one illustrated in Fig 2.3 and again overleaf in Fig 3.5.

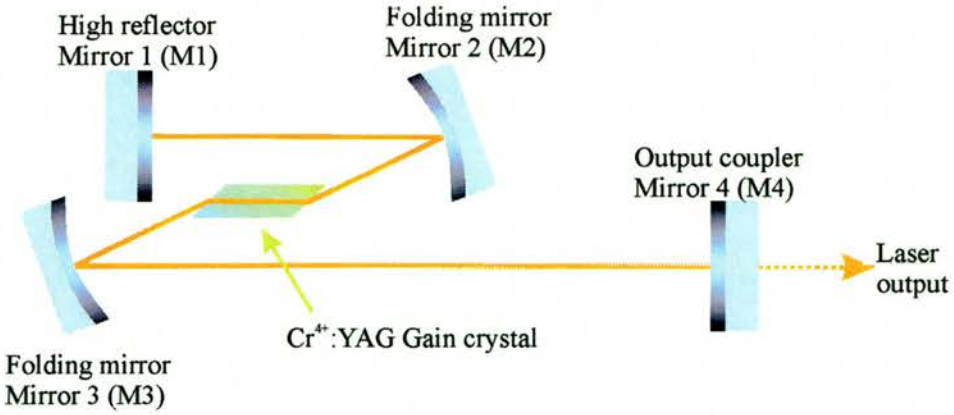

Fig. 3.5 *Schematic of a typical four-mirror, astigmatically compensated laser cavity.*

As discussed earlier in Chapter 2, the angles of the curved folding mirrors compensate for the astigmatism brought about by the Brewster-angled gain element. This type of cavity design also allows for a tight intracavity focused beam to exist within the cavity. There are two minimal beam waists that can be created within the cavity. The cavity is designed so that one of these focal spots exists within the centre of the laser gain crystal (in order to access the required gain), and the other focal spot exists at the front face of mirror M1 (where the SBR will be inserted, in order to initiate mode locking). The sizes of these two focal spots can be adjusted by varying the distances between the four mirrors and the gain element. The same laser cavity design package described in Chapter 2 was used to calculate the necessary positions of the mirrors, the laser crystal and the beam mode sizes within the laser system.

3.4.2 Pump source and pump geometry

The pump source that was used for this Cr^{4+}:YAG laser consisted of a high power diode-pumped cw Yb-doped fibre laser (*IPG laser model PYL-10-LP*). This laser was much more compact than the Nd:YVO_4 laser used in the Cr^{4+}:forsterite laser counterpart. This compact Yb-fibre laser had a footprint of 23 × 18cm^2, was air-cooled

and capable of producing up to 10W of linearly polarised near-diffraction-limited light at 1064nm. Fig. 3.6 illustrates how this pump beam was first passed through a waveplate and simple telescope arrangement before being focused tightly (w_p = 38μm ± 2μm) by a 100mm focal length convex lens into the Cr^{4+}:YAG laser rod.

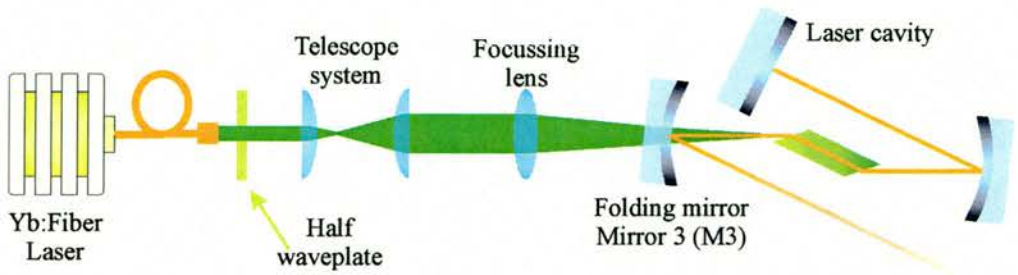

Fig. 3.6 *Schematic of the pump laser and the pump geometry used to excite the Cr^{4+}:YAG laser rod.*

3.4.3 Mirrors and the laser crystal

The Cr^{4+}:YAG laser rod utilised in this work was a 20mm long Brewster-cut crystal that was purchased from *Bicron*[21]. The rod had a diameter of 5mm and a small-signal gain coefficient of 1.2cm^{-1}. To aid the removal of heat from the rod it was wrapped in indium foil and clamped into a copper heatsink, which was water-cooled to 15°C.

The laser mirrors were purchased from *LaserOptik*[22]. The folding mirrors, M2 and M3, were coated for broadband high reflection (R>99.94%) between 1430-1630nm and for high transmission of the pump beam at 1064nm. They had radii of curvature of -100mm and -75mm for the long and the short arms respectively. At one end of the cavity, a flat-wedged output coupler of either 0.5%, 1% or 2% transmission was selected for the results presented in the following sections. A flat-wedged HR mirror (M1) or the SBR device terminated the short arm of the cavity.

3.5 Continuous-wave operation of the 4-mirror Cr^{4+}:YAG laser system

The figure below details the cavity configuration that was designed to operate in the continuous-wave (cw) regime.

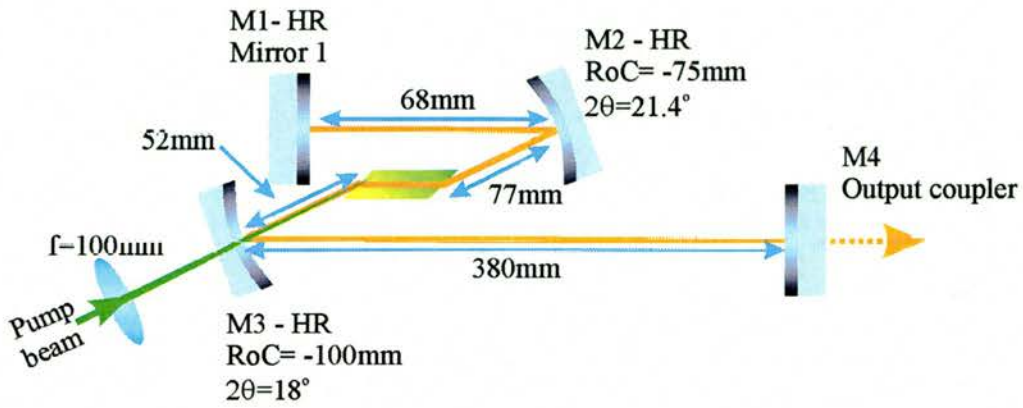

***Fig 3.7** Schematic of a Cr^{4+}:YAG laser cavity designed for cw operation.*

This cavity design produced a laser mode radius of 67μm×40μm in the Cr^{4+}:YAG rod. The pump beam passed through the telescope system and a 100mm focusing lens produced a pump spot on the Cr^{4+}:YAG rod with a beam radius of 40μm ± 2μm, producing the required overlap of the pump and laser modes needed for low threshold operation of the laser system[20].

The cw performance of the laser was evaluated using the three different output couplers. Fig. 3.8 shows the variation of the output power as a function of absorbed pump power (The absorption of the Cr^{4+}:YAG rod during lasing was estimated to be 78%.). The corresponding thresholds for lasing were reached with 0.5W, 0.8W and 1W of absorbed pump power and the measured slope efficiencies were 11%, 18% and 20% with 0.5%, 1% and 2% output couplers, respectively. The laser emission in this free-running regime peaked around 1490nm with a measured linewidth of 0.6nm. Output powers as high as 1W were obtained with the 2% output coupler when pumped at 8W.

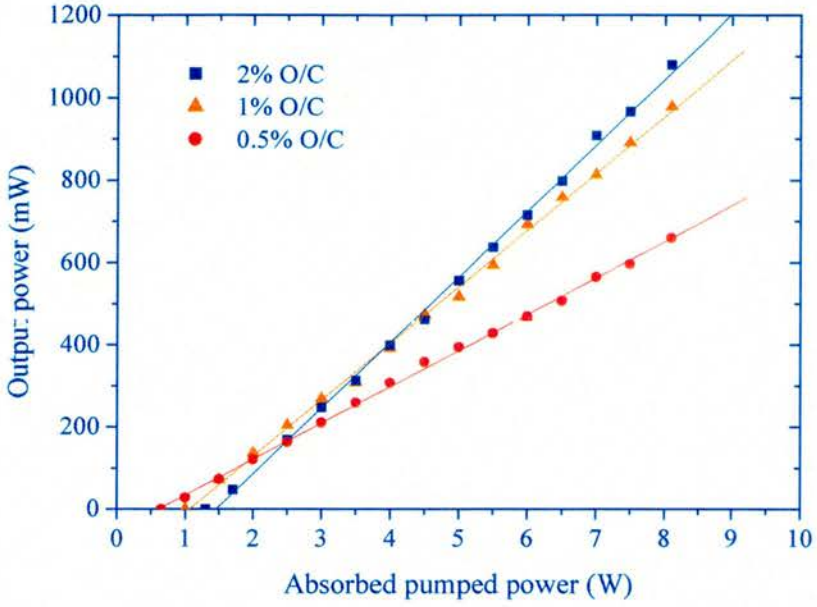

Fig. 3.8 *Cw performance characteristics for the 4-mirror Cr^{4+}:YAG laser.*

Using the data of slope efficiency measurements at different output couplers, the total parasitic round-trip cavity losses were estimated to be approximately 1%. A Brewster-cut IR-grade fused silica prism was employed in the long arm of the cavity for wavelength tuning.

The broadest tuning range of the laser was obtained with a 0.5% output coupler and extended from 1400nm to 1590nm as detailed in Fig. 3.9. Tuning to shorter wavelengths was limited by the reflectivity characteristics of the high-reflectivity mirror set used. The gain-bandwidth of the Cr^{4+}:YAG rod set the tuning limit at the longer wavelengths.

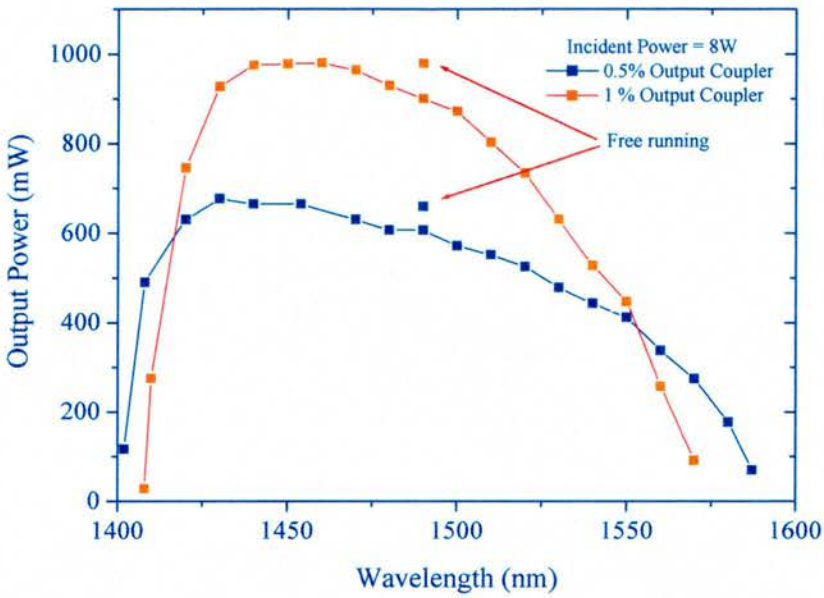

Fig 3.9 *Measured tuning range of laser operating in the cw regime for 0.5% and 1% output couplers.*

As with the cw Cr^{4+}:forsterite laser, this cw laser demonstrated suitably large bandwidths and output powers to imply compatibility with the generation of femtosecond pulses.

3.6 Mode-locked operation of a 4-mirror Cr^{4+}:YAG laser

For operation in the mode-locked regime, the end mirror high reflector (M1) was replaced with the SBR device. The choice of a highly asymmetric cavity design allowed the cavity beam waist on the SBR to be varied easily over a relatively wide range by adjusting the length of the short arm of the resonator. The spot sizes that could be achieved by adjusting the distance of the short arm is presented below.

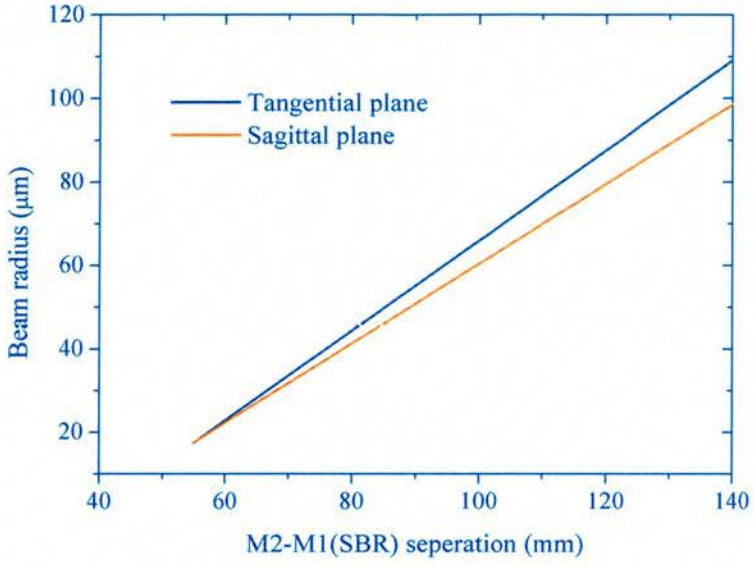

Fig 3.10 *Graph of intracavity focus on the SBR with varying short cavity arm length.*

The excitonic absorption edge in the SBR shifted the cw operation from 1490nm to 1530nm. Using measurements of the laser threshold with different output couplers, it was possible to estimate the small-signal insertion loss of the SBR at 1530nm to be around 3% per round trip, including the 0.5% transmission loss[4]. To obtain stable and efficient mode-locked operation the laser spot radius on the SBR was varied over the range of 15μm to 100μm. Mode locking was not observed when the beam spot size on the SBR was less than 20μm. An increase in the length of short arm of the cavity and careful adjustment of the SBR position then led to self-starting mode-locked operation of the laser. Two fused silica prisms with low OH^- content were inserted into the long arm of the cavity with a tip-to-tip separation of 18cm, which provided suitable group-velocity dispersion compensation to facilitate the generation of femtosecond pulses. The best performance was obtained with a laser spot size on the SBR of approximately 37μm, although mode-locked operation was possible with spot radii up to 80μm. Optimum stability was achieved when the average output power was between 25mW

and 65mW for an output coupling of 0.5% and between 35mW and 95mW for 1% output coupling. This corresponded to a saturation fluence in the range of 0.36-1.3mJ/cm^2. The corresponding range of absorbed pump power was between 2.5W and 4.5W. Mode locking was sustained with excellent day-to-day reproducibility of output power and pulse duration. Fig. 3.11 shows a typical intensity autocorrelation and spectrum centered at 1528nm with an average output power of 95mW.

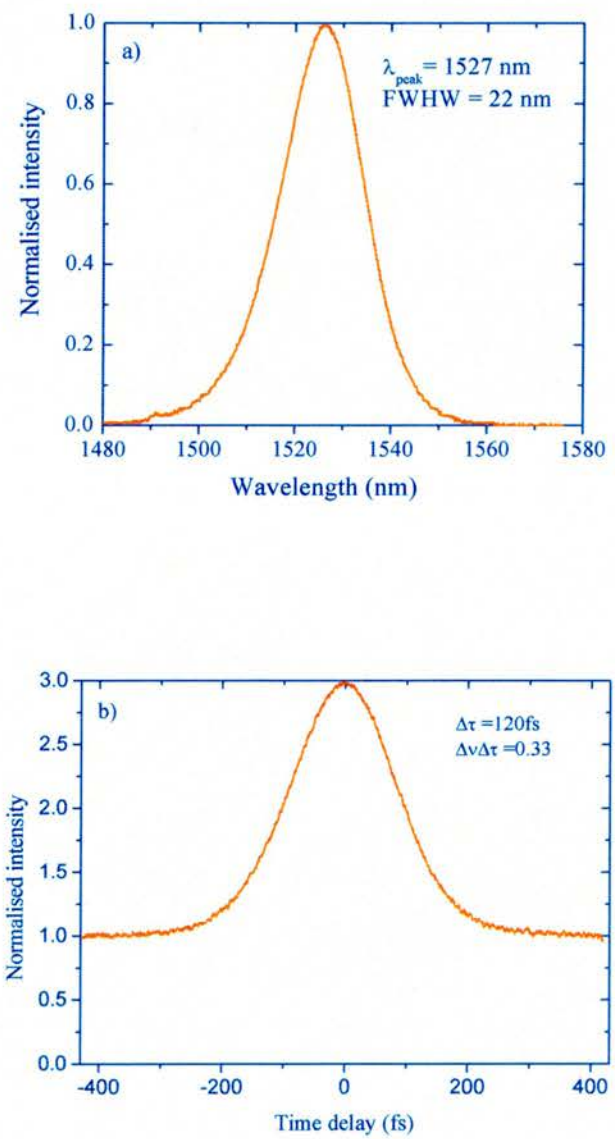

Fig. 3.11 *Measured optical spectrum and corresponding intensity autocorrelation of the mode-locked Cr^{4+}:YAG laser.*

By assuming a $sech^2$ intensity profile, the FWHM pulse duration was determined to be 120fs (Fig. 3.11(a)). The corresponding spectral width was 22nm, as shown in Fig. 3.11(b), which implies a time-bandwidth product of 0.33, which is close to the transform-limit. It was not possible to obtain pulses with duration of less than 120fs because of the restrictions on bandwidth set by the Bragg reflector. By inserting a vertical slit into the cavity between the second prism and the output coupler the laser was tunable from 1520nm to 1545nm. The pulse durations increased from 120fs to 190fs as the laser was tuned away from the free-running wavelength of 1528nm. This can be accounted for by the decrease in the efficiency of saturable absorption at longer wavelengths when tuning selects wavelengths away from the SBR excitonic absorption peak around 1500nm[23].

3.7 Conclusions

In conclusion, a stable self-starting femtosecond Cr^{4+}:YAG laser has been demonstrated. A diode-pumped Yb-fiber laser was used as the pump source and mode-locking operation was initiated and stabilised by a SBR. Using the fibre laser as the pump source allowed the entire laser to be constructed on a $900\times600mm^2$ footprint, making the system relatively compact. With a highly asymmetric, four-mirror cavity that had been designed for adjustable beam spot sizes on the saturable absorber, 120fs pulses with an output average power of 95mW centered at 1528nm were obtained at a prf of 205MHz.

Further development of this system would require SBR devices that have better characteristics (i.e. lower non-saturable losses) than the one that was provided for this work. There are a few devices that have the necessary low-loss characteristics[24, 25],

but they are not widely available. It is hoped that further development of GaInNAs structures may herald high quality mode-locking elements for solid-state sources operating at 1550nm. To reach the high pulse repetition frequency necessary for datacommunications-based experiments another solution must be sought in the form of a Kerr-lens mode locked version of the Cr^{4+}:YAG laser.

3.8 References

1. N. Angert, N.I. Borodin, V. Garmesh, V.A. Zhitnyuk, A. Okhrimchuk, O. Siyuchenko, and A.V. Shestakov, "Lasing due to impurity color centers in yttrium aluminium garnet crystals at wavelengths in the range 1.35-1.45μm", *Soviet Journal of Quantum Electronics*, vol. 18, (1), p. 73-74, 1988.
2. G. Cerullo, S. De Silvestri, and V. Magni, "Self-starting Kerr-lens mode locking of a Ti:sapphire laser", *Optics Letters*, vol. 19, (14), p. 1040-1042, 1994.
3. Y.P. Tong, P.M.W. French, and J.R. Taylor, "All-solid-state Kerr lens mode-locked Cr4+:forsterite laser", *Electronics Letters*, vol. 32, (8), p. 737-738, 1996.
4. B.C. Collings, J.B. Stark, S. Tsuda, W.H. Knox, J.E. Cunningham, W.Y. Jan, R. Pathak, and K. Bergman, "Saturable Bragg reflector self-starting passive mode locking of a Cr4+:YAG laser pumped with a diode-pumped Nd:YVO4 laser", *Optics Letters*, vol. 21, (15), p. 1171-1173, 1996.
5. B.C. Collings, K. Bergman, and W.H. Knox, "True fundamental solitons in a passively mode-locked short- cavity Cr4+:YAG laser", *Optics Letters*, vol. 22, (14), p. 1098-1100, 1997.
6. M.J. Hayduk, S.T. Johns, M.F. Krol, C.R. Pollock, and R.P. Leavitt, "Self-starting passively mode-locked tunable femtosecond Cr4+:YAG laser using a saturable absorber mirror", *Optics Communications*, vol. 137, (1-3), p. 55-58, 1997.
7. H. Eilers, U. Hommerich, S. Jacobsen, W.M. Yen, K. Hoffman, and W. Jai, "Spectroscopy and dynamics of $Cr^{4+}Y_3Al_5O_{12}$", *Physical Review B*, vol. 49, (22), p. 505-513, 1994.
8. S. Kuck, K. Petermann, U. Pohlmann, and G. Huber, "Electronic and vibronic transitions of the Cr4+-doped garnets Lu3Al5O12, Y3Al5O12, Y3Ga5O12 and Gd3Ga5O12", *Journal of Luminescence*, vol. 68, (1), p. 1-14, 1996.
9. S. Kuck, "Laser-related spectroscopy of ion-doped crystals for tunable solid-state laser", *Applied Physics B-Lasers and Optics*, vol. 72, p. 515-562, 2001.
10. A. Sennaroglu, "Broadly tunable Cr4+ doped solid-state lasers in the near infrared and visible", *Progress in Quantum Electronics*, vol. 26, (6), p. 287-352, 2002.
11. B. Henderson, H.G. Gallagher, T.P. Han, and M.A. Scott, "Optical spectroscopy and optimal crystal growth of some Cr^{4+}-doped garnets", *Journal of Physics-Condensed Matter*, vol. 12, p. 1927-1938, 2000.
12. S. Kuck, U. Pohlmann, and G. Huber, "Near-Infrared Emission of Cr4+-Doped Garnets - Lifetimes, Quantum Efficiencies, and Emission Cross-Sections", *Physical Review B*, vol. 51, (24), p. 17323-17331, 1995.
13. A. Sennaroglu, C.R. Pollock, and H. Nathel, "Efficiant continuous-wave chromium-doped YAG laser", *Journal of the Optical Society of America B-Optical Physics*, vol. 12, (5), p. 930-937, 1995.
14. G.J. Valentine, "Development of all-solid-state modelocked laser sorces at 1.55μm", PhD thesis: School of Physics and Astronomy, University of St Andrews: St Andrews, 1998.

15. I.T. Sorokina, S. Naumov, E. Sorokin, E. Wintner, and A.V. Shestakov, "Directly diode-pumped tunable continuous-wave room-temperature Cr4+: YAG laser", *Optics Letters*, vol. 24, (22), p. 1578-1580, 1999.

16. S. Naumov, E. Sorokin, and I.T. Sorokina, "Directly diode-pumped Kerr-lens mode-locked Cr4+: YAG laser", *Optics Letters*, vol. 29, (11), p. 1276-1278, 2004.

17. D.J. Ripin, J.T. Gopinath, H.M. Shen, A.A. Erchak, G.S. Petrich, L.A. Kolodziejski, F.X. Kartner, and E.P. Ippen, "Oxidized GaAs/AlAs mirror with a quantum-well saturable absorber for ultrashort-pulse Cr4+: YAG laser", *Optics Communications*, vol. 214, (1-6), p. 285-289, 2002.

18. A.A. Lagatsky, C.G. Leburn, C.T.A. Brown, W. Sibbett, and W.H. Knox, "Compact self-starting femtosecond Cr4+: YAG laser diode pumped by a Yb-fiber laser", *Optics Communications*, vol. 217, (1-6), p. 363-367, 2003.

19. P.T. Guerreiro, S. Ten, E. Slobodchikov, Y.M. Kim, J.C. Woo, and N. Peyghambarian, "Self-starting mode-locked Cr:forsterite laser with semiconductor saturable Bragg reflector", *Optics Communications*, vol. 136, p. 27-30, 1997.

20. A.J. Alfrey, "Modeling of Longitudinally Pumped CW Ti:Sapphire Laser Oscillators", *IEEE Journal of Selected Topics in Quantum Electronics*, vol. 25, (4), p. 760-766, 1989.

21. Bicron, http://www.bicron.com.

22. LaserOptik. http://www.laseroptik.de/,http://www.laseroptik.de/.

23. J. Theimer, M. Hayduk, M.F. Krol, and J.W. Haus, "Mode-locked Cr4+:YAG laser: model and experiment", *Optics Communications*, vol. 142, (1-3), p. 55-60, 1997.

24. Z. Zhang, T. Nakagawa, K. Torizuka, T. Sugaya, and K. Kobayashi, "Gold-reflector-based semiconductor saturable absorber mirror for femtosecond mode-locked Cr^{4+}:YAG lasers", *Applied Physics B: Lasers and Optics*, vol. 70, (0), p. S59-S62, 2000.

25. Z. Zhang, T. Nakagawa, K. Torizuka, T. Sugaya, and K. Kobayashi, "Self-starting mode-locked Cr4+: YAG laser with a low-loss broadband semiconductor saturable-absorber mirror", *Optics Letters*, vol. 24, (23), p. 1768-1770, 1999.

Chapter 4 – Reaching for Higher Pulse Repetition Frequencies

4.1 Introduction

As discussed in Chapter 3 the fluorescence bandwidth of Cr^{4+}:YAG extends from 1200 nm to 1600 nm. In 2001, Ripin and co-workers accessed around 200 nm of this gain bandwidth and produced pulses with durations shorter than 20 fs[1]. Cr^{4+}:YAG solid-state lasers[2, 3] also have superior performance compared with the conventional sources[4, 5] that are used in a wide variety of datacommunications applications. These solid-state laser sources are becoming attractive for the generation of multi-gigahertz data rates as they generate femtosecond pulses with high power, broad spectral bandwidth and excellent timing-jitter performance. These characteristics underpin the suitability of these lasers to wavelength division multiplexing (WDM), optical time division multiplexing (OTDM) and hybrid OTDM/WDM combinations.

In this chapter the subject matter is focused on the development of high pulse repetition frequency (prf) Cr^{4+}:YAG femtosecond lasers. This goal was achieved through the design of a simple three-element resonator. This configuration is compatible with Kerr-lens mode locking (KLM) and results in reductions in the laser cavity size and a proportionate increase in the pulse-repetition-frequency making it a suitable candidate for use in various datacommunications-based assesments. The success of this three-element resonator design led to an engineered prototype of the laser system and this aspect of the project is also discussed briefly.

4.2 Previous work on high prf all-solid-state lasers

In 1994 Ramaswamy-Paye and Fujimoto[6] introduced a technique for dispersion compensation involving a prismatic end mirror. Using this technique they reported the

generation of femtosecond pulses at a prf of 1 GHz using a Ti:Sapphire laser. Their approach achieved intracavity compensation without the need for prism pairs or dispersion compensating mirrors. This design concept was later adapted for a Cr^{4+}:YAG laser by Mellish et al.[7] who also reported the generation of femtosecond pulses at 1 GHz where their laser cavity comprised of only three elements as illustrated in Fig. 4.1.

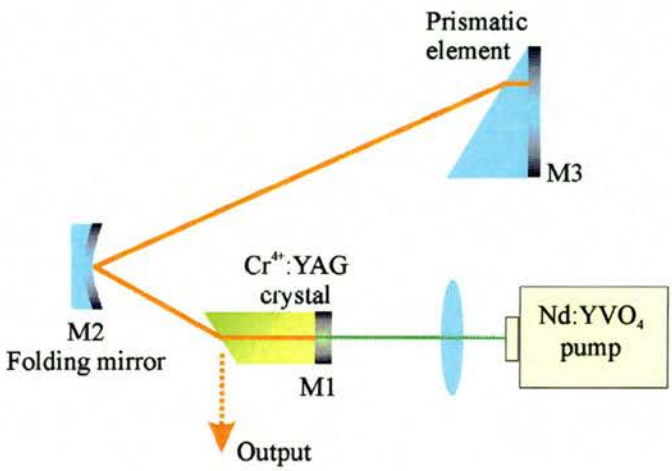

Fig. 4.1 *Schematic diagram of cavity configuration used by Mellish et al. [7] to generate femtosecond pulses at a prf of 1GHz.*

They utilised a 20mm long Cr^{4+}:YAG laser rod that was plane-Brewster cut and coated with a HR mirror on the plane face. The other two elements consisted of a HR folding mirror and a prismatic element which was also HR coated on the normal plane face. The laser output was extracted from the reflection off the surface of the laser crystal, which was not cut at the precise Brewster's angle but gave ~0.4% reflection. KLM operation of this system allowed them to generate 125fs pulses at a prf of 1GHz. The attractive simplicity of this type of cavity geometry allows for easy alignment and contains fewer elements than its 4-mirror counterpart, thus also reducing the losses within the system.

This work was followed by Tomaru *et al.*[3], who designed a similar laser cavity that had a prf up to 1.2GHz with pulse durations of 55fs. This group also built a two-element Cr^{4+}:YAG system (as illustrated in Fig. 4.2) that was capable of generating 115fs pulses at a prf of 2.6GHz, but this setup had a critical drawback that affected its long-term stability.

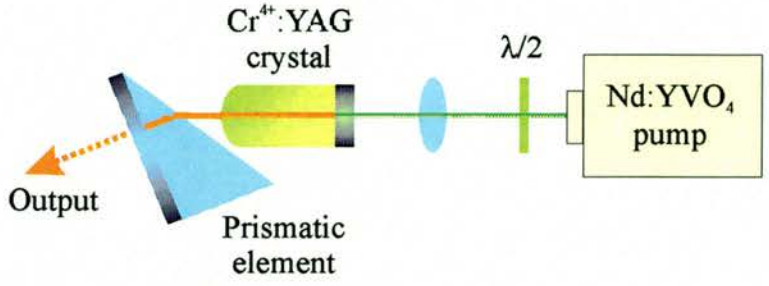

Fig. 4.2 *Schematic of the two-element Cr^{4+}:YAG cavity capable of generating 115fs pulses at a prf of 2.6GHz.*

The astigmatism generated from the Brewster face of the prismatic element could not be corrected in this configuration. The curved nature of the gain crystal did not allow for the compensation of astigmatism arising from the Brewster-cut prismatic element. This meant that there was poor mode matching within the gain crystal, leading to a KLM process that was less efficient than the one generated in the earlier 3-element systems. Mode-locked operation was possible but it was rarely self-starting and the spectrum usually contained an undesired cw component arising from the limited efficiency of the KLM process. If the cw component were to be eliminated then the mode locked operation would last no longer than 10s. These features demonstrate why such a two-element system would not be suitable for operation in a datacommunications system, despite its ability to produce femtosecond pulses with a prf above 2.5GHz.

The work described in the remainder of this chapter involves some of the ideas contained in the references 3, 6-10 but takes them several steps further through the realisation of stable, 1550nm, sub-100fs pulses at prfs greater than 4GHz.

4.3 The single prism idea

In Chapter 1 the prism pair method most commonly used to compensate for positive dispersion generated by the various elements within a laser cavity was outlined as a means of producing favourable conditions for the generation of transform-limited pulses. This method has proved very successful but the prisms have to be separated by a significant distance to provide adequate negative dispersion. This does not allow for the design of compact laser cavities that generate pulses at high prfs (>1GHz). In 1997 Aoshima *et al.*[11] devised a method that used a single prism in each arm of a laser cavity to generate the necessary negative GVD. They constructed a diode-pumped KLM Cr^{3+}:LiSAF laser in the form of a symmetric, 4-mirror z-fold cavity, with a prism in each arm as illustrated in Fig. 4.3.

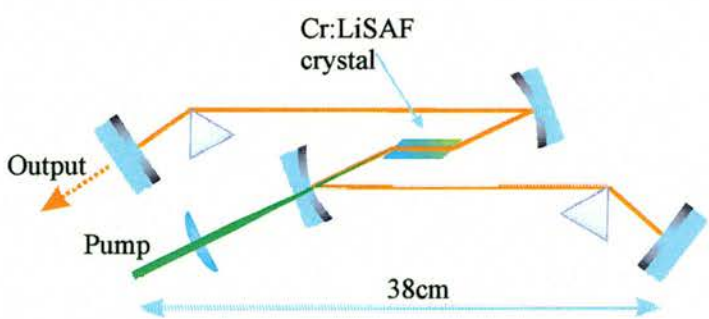

Fig 4.3 *Schematic of compact Cr:LiSAF KLM laser designed by Aoshima et al.[11].*

In this way, the necessary distance between the folding mirrors (for tight focusing) and the required inter-prism path lengths could be combined. This allowed for a

considerable reduction in cavity size and produced 90fs pulses at 874nm with a prf of 235MHz. Hopkins *et al.*[12] carried out a detailed Kostenbauder ray-transfer analysis[13] on the Aoshima-type cavity to understand the role of the prisms and their contributions towards resonator dispersion. This analysis used matrices to describe temporal and spatial beam propagation as well as dispersive effects of the optical system. Kostenbauder used a 1×4 'ray-pulse' vector to describe the spatial displacement x, angle θ, arrival time t, and frequency f, of a propagating monochromatic pulse with respect to a transform-limited midband reference pulse. This reference pulse provided a well-defined spatial and temporal origin at each transverse reference plane within the system so the effect of any optical system on an input ray-pulse vector can be described by

$$\begin{bmatrix} x \\ \theta \\ t \\ f \end{bmatrix}_{out} = T \begin{bmatrix} x \\ \theta \\ t \\ f \end{bmatrix}_{in} \tag{4.1}$$

where x, θ, t, and f, are the elements of each ray-pulse vector and T is a 4×4 transfer matrix that describes the optical system. The transfer matrix is given by

$$T = M_i \cdot M_{i-1} \ldots M_2 \cdot M_1 \tag{4.2}$$

where M_i is the ith optical element of the system that consists of a 4×4 matrix. A summary of the 4×4 element matrices for the most common laser cavity components are given in references 13 and 14. The transfer matrix has the general form

$$T = \begin{bmatrix} \frac{\partial x_{out}}{\partial x_{in}} & \frac{\partial x_{out}}{\partial \theta_{in}} & \frac{\partial x_{out}}{\partial t_{in}} & \frac{\partial x_{out}}{\partial f_{in}} \\ \frac{\partial \theta_{out}}{\partial x_{in}} & \frac{\partial \theta_{out}}{\partial \theta_{in}} & \frac{\partial \theta_{out}}{\partial t_{in}} & \frac{\partial \theta_{out}}{\partial f_{in}} \\ \frac{\partial t_{out}}{\partial x_{in}} & \frac{\partial t_{out}}{\partial \theta_{in}} & \frac{\partial t_{out}}{\partial t_{in}} & \frac{\partial t_{out}}{\partial f_{in}} \\ \frac{\partial f_{out}}{\partial x_{in}} & \frac{\partial f_{out}}{\partial \theta_{in}} & \frac{\partial f_{out}}{\partial t_{in}} & \frac{\partial f_{out}}{\partial f_{in}} \end{bmatrix} \quad 4.3$$

Most of the matrix elements can be put in simpler terms. This provides a transfer matrix of the form

$$T = \begin{bmatrix} A & B & 0 & E \\ C & D & 0 & F \\ G & H & 1 & I \\ 0 & 0 & 0 & 1 \end{bmatrix} \quad 4.4$$

where elements A-D correspond to the changes in output position and slope caused by input changes in position and slope, much like the standard 2×2 matrix solution[15]. Elements E-I represent the spatial chirp, angular dispersion and group velocity dispersion of the system. More information about this mathematical technique can be found in reference 13. Using this method Hopkins and co-workers were able to investigate how the laser mode propagated through an Aoshima-type of cavity.

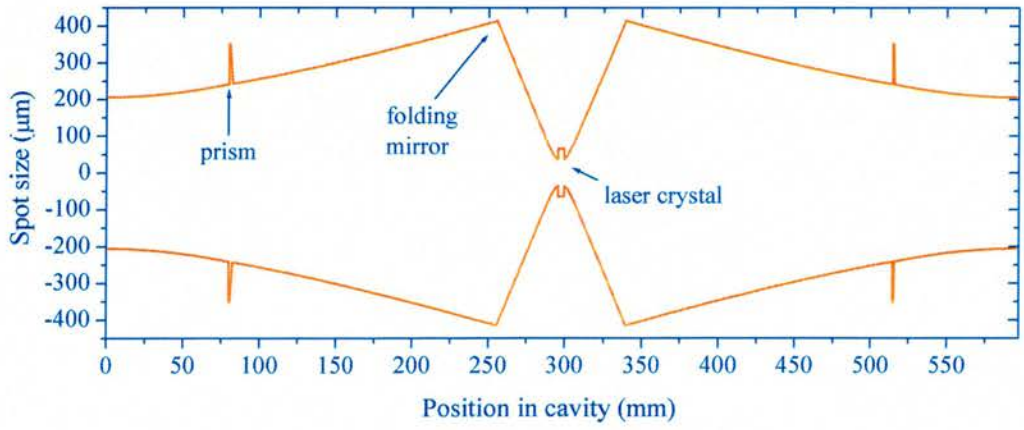

Fig 4.4 *Plot of the tangential transverse beam in the symmetric Aoshima-type cavity[14].*

The figure above illustrates the stable resonator mode Hopkins calculated for the tangential plane of the symmetric cavity at a centre wavelength of 880nm. The positions of the various cavity elements are also marked on the plot. Fig. 4.5 shows how the ray-transfer analysis also allowed Hopkins to plot the displacement of two rays through the cavity that were separated by 20nm relative to the centre wavelength of 880nm.

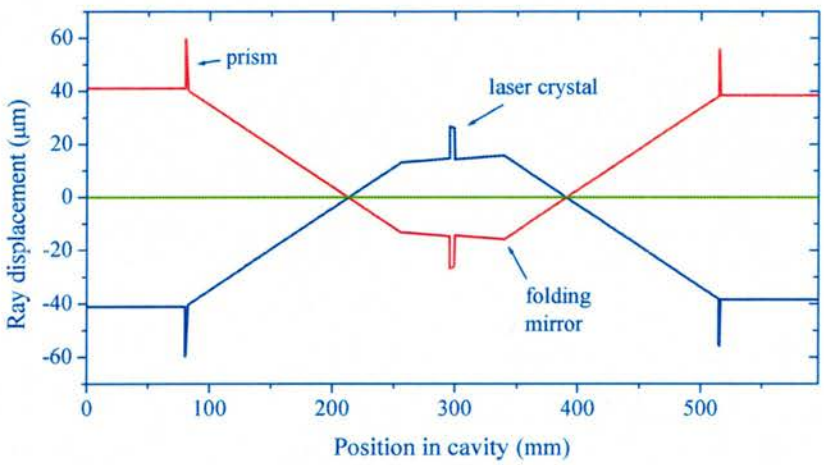

Fig 4.5 *Relative paths traced by two rays through the cavity, separated by 20nm (blue for 870nm and red for 890nm) with respect to the 880nm reference ray (green)[14].*

This plot shows that the rays between the prisms and the end mirrors are spatially dispersed and are also parallel to each other, which establishes the fact that they do not contribute to the dispersion of the cavity. The very slight angular dispersion between the two folding mirror arises from the Brewster-angled gain medium. It is more useful to plot the ray picture on top of the beam mode of the cavity as illustrated in Fig. 4.6.

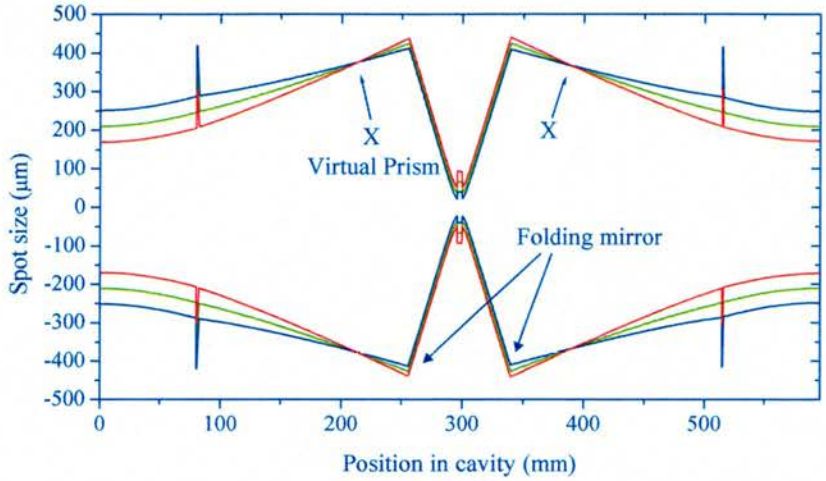

Fig. 4.6 *Plot of Aoshima-type cavity showing the tangential beam superimposed with the rays that are separated by 20nm about the reference ray (green)[14].*

This plot shows that most of the dispersion arises between the prisms and the folding mirrors, where the rays have a large angular displacement. Due to this angular and spatial displacement of the rays, the folding mirrors create 'virtual' prisms at the crossing of the rays (point X). This demonstrated that Aoshima's cavity behaved as though it had two pairs of prisms, one pair in each arm of the cavity.

After investigating these 'virtual' prisms, Hopkins went on to model a Cr^{3+}:LiSAF Aoshima-type *asymmetric* cavity, which had already been constructed in the laboratory environment[12,16] and was producing femtosecond pulses. A schematic of this laser cavity is given in Fig. 4.7.

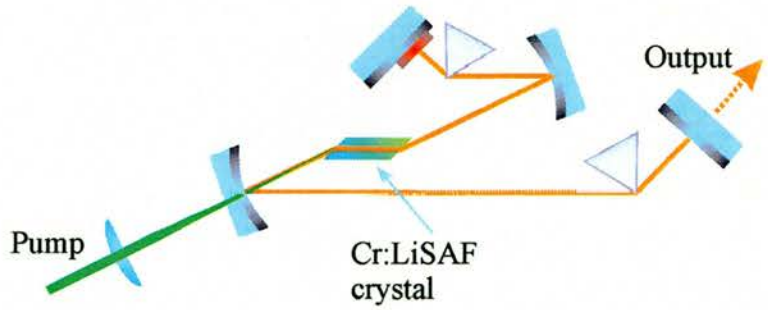

Fig. 4.7 *Schematic of an asymmetric Cr^{3+}:LiSAF cavity that was modelled by Hopkins in order to understand the role of the two prisms within the cavity. This cavity utilised a GaAs SBR to initiate modelocking, which produced pulses as short as 103fs at a peak wavelength of 864nm.*

Again, Hopkins wanted to gain a better understanding of the dispersion properties these 'virtual' prisms had in his laser system. Fig. 4.8 illustrates the ray displacement of two beams through the asymmetric laser cavity and Fig. 4.9 illustrates these rays superimposed with the beam mode running through the cavity.

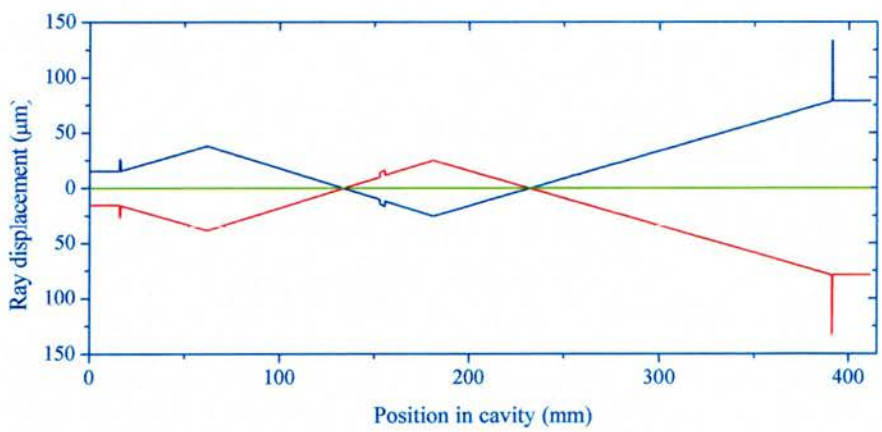

Fig. 4.8 *Relative paths traced by two rays through the cavity, separated by 20nm (blue for 854nm and red for 874nm) with respect to the 864nm reference ray (green) in the asymmetric Aoshima-type cavity.*

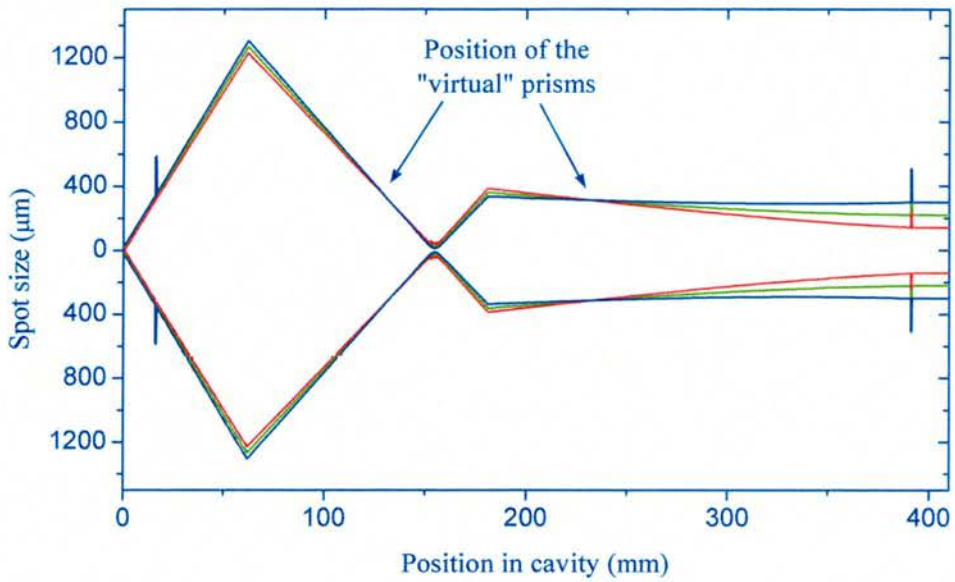

Fig. 4.9 *Plot of Aoshima-type asymmetric cavity showing the tangential beam superimposed with the rays that are separated by 20nm about the reference ray (green).*

Fig. 4.9 clearly illustrates the position of the virtual prisms in this asymmetric system. From the result plotted in Fig. 4.8 Hopkins was able to conclude that the prism in the short arm of the cavity did not contribute a large amount of dispersion to the cavity due to the short distance from the prism to the folding mirror. This implied that the prism in the short arm of the cavity was not necessary as the other physical prism and its virtual partner provided acceptable amounts of negative dispersion for femtosecond operation. This proved to be hugely advantageous, as the removal of one prism from the cavity not only reduced intra-cavity losses, but also made alignment of the cavity an easier task.

Hopkins *et al.* then went on to successfully implement the single prism idea into other Cr^{3+}:LiSAF laser systems[12, 14]. The single prism principles that were investigated by Hopkins in 4-mirror Cr^{3+}:LiSAF laser systems had already been experimentally demonstrated in 4-mirror astigmatically compensated Cr^{4+}:YAG laser systems[9] but

the purpose of my project was to take the ideas and understanding presented by Hopkins and apply them to the compact 3-element Cr^{4+}:YAG design described in section 4.2.

4.4 Prism material properties

As mentioned in Section 1.3.3, in most cases the prism material in a laser system will have positive dispersion properties, which, along with the other positively dispersing elements of the cavity, must be compensated for by providing a suitable separation between the prisms. Fused silica (SiO_2) is one of the few glasses to have negative dispersion properties at 1550nm and is therefore the most popular choice when designing dispersion-compensating schemes for solid-state lasers at this wavelength. Fig. 4.10 gives a plot of the dispersion characteristics over a wide range of wavelengths.

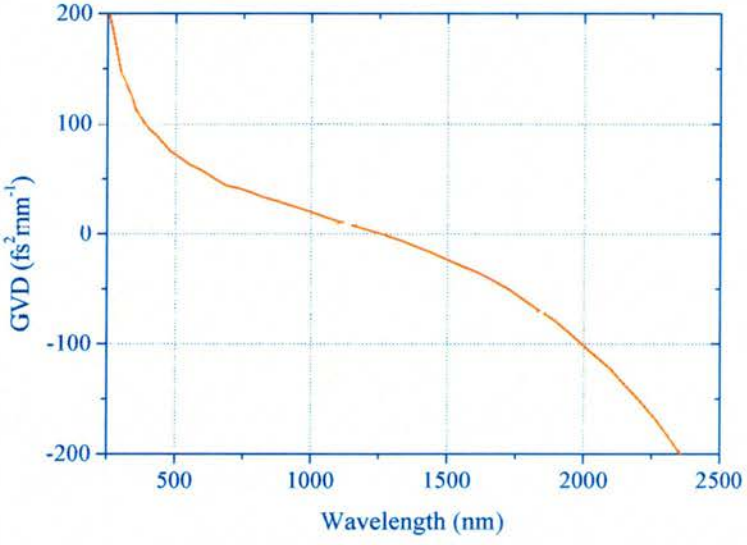

Fig. 4.10 *Group velocity dispersion of fused silica glass[17].*

Due to the negative dispersion properties of fused silica, the optical path length between the prisms can be reduced significantly. This unusual feature is hugely advantageous when designing lasers that need to have relatively short cavity lengths (i.e. high prf). Fused silica is also a material that has a very low insertion loss associated with it. These

were therefore the two main features that dictated the use of a fused silica prismatic element as part of the laser cavities described here.

4.5 Initial design and construction of a 3-element laser system

The laser cavities discussed in Chapters 2 and 3 were both based around well-established and very successful 4-mirror cavity designs[18-22]. These could compensate for astigmatism, allow for the variation of two beam waists within the cavity, incorporate a prism pair and still provide low thresholds. However, the length of cavity needed to meet all of the above requirements was not compatible with the generation of pulses at multi-gigahertz frequencies. Fig. 4.11 illustrates a novel alternative that involved combining the cavity dynamics discussed in sections 4.3 and 4.4 along with the ideas that had already been implemented successfully by the work discussed in section 4.2.

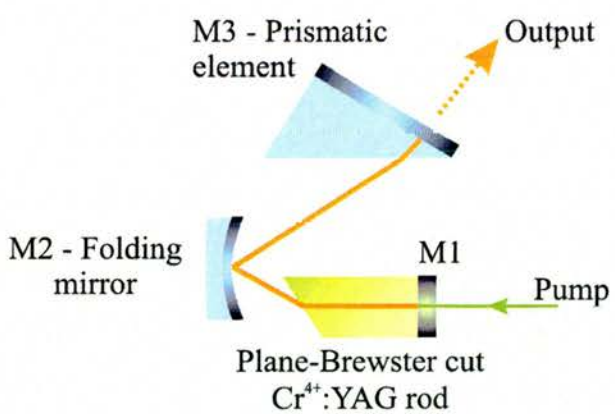

Fig. 4.11 *Schematic diagram of the three-element cavity geometry.*

Again, a laser cavity design package (based on ABCD matrix multiplication of a Gaussian beam[23, 24]) was used to calculate the correct positions and angles of the three elements so that KLM operation of this cavity would yield pulses with a prf ~ 1GHz. A Kostenbauder ray-transfer analysis was also performed to determine if a

virtual prism existed within the cavity. This is plotted in Fig. 4.12 and shows clearly that this is the case.

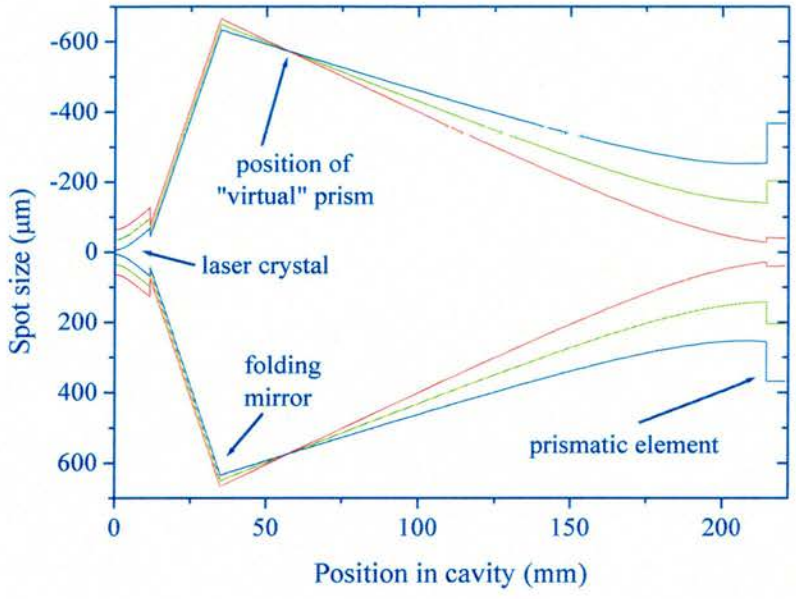

Fig 4.12 *Ray-transfer analysis of three-element cavity showing the existence and position of a virtual prism with in the cavity. The tangential beam is superimposed with rays that are separated by 20nm about the reference ray (green).*

4.5.1 The three elements of the cavity

This initial cavity required a plane-Brewster cut Cr^{4+}:YAG crystal that was ~12mm in length. The decision was made to take an existing good quality Brewster cut 20mm long Cr^{4+}:YAG rod (peak small-signal pump absorption coefficient, $\alpha = 2.2cm^{-1}$) and have it cut and polished into two plane-Brewster rods. One of these rods was specifically designed to be ~12mm in length for the purpose of this project. *LaserOptik GmbH*[25] then coated the plane face of the rod with a dielectric mirror stack that was HR between 1470-1630nm and HT at 1064nm. On its return from being coated, the rod was mounted

in a water-cooled copper mount that was maintained at a temperature of 14°C to handle the thermal loads generated by the relatively high pump intensities.

The design of the cavity necessitated a folding mirror with a radius of curvature (RoC) = -50mm. This folding mirror (with a diameter of 25mm) was designed specifically for operation at ~1550nm, was purchased from *LaserOptik GmbH*, and coated for broadband high reflection (R>99.996%) between 1470-1630nm and high transmission of the pump light at 1064nm.

The third element of the cavity usually consisted of a Littrow prism made of high-grade fused silica but three other elements could also be inserted to allow for a greater characterisation of the cavity. These three elements consisted of a broadband plane-wedged high reflector, a plane-wedged output coupler with a coupling efficiency of 0.5% and a plane-wedged output coupler with a coupling efficiency of 1%. The Littrow prism was purchased from *Crystran Ltd.*[26] and coated with a dielectric mirror on its back face, which provided a coupling efficiency of 0.12% over the 1470-1630nm spectral region.

4.5.2 Pump source and pump geometry

As with some of the other laser systems discussed earlier in this thesis, the pump source consisted of an infrared Nd:YVO_4 IR laser (*Spectra Physics*) that was capable of producing up to 10W of linearly polarised, near-diffraction limited light at 1064nm. The pump light passed through a half waveplate, a 1:1.6 beam expanding telescope arrangement and a f = 220mm focal length lens to focus the pump beam to a spot size of $w_0 \approx 40\mu m$ on the plane face of the Cr^{4+}:YAG crystal. The figure below gives a detailed schematic of the whole laser system that was constructed. The cavity was calculated to have a laser mode radius of 35μm×35μm in the Cr^{4+}:YAG laser rod. This meant that the

~ 40μm pump spot size was suitable for providing the necessary overlap of the pump and laser modes for low threshold operation of the laser system[27].

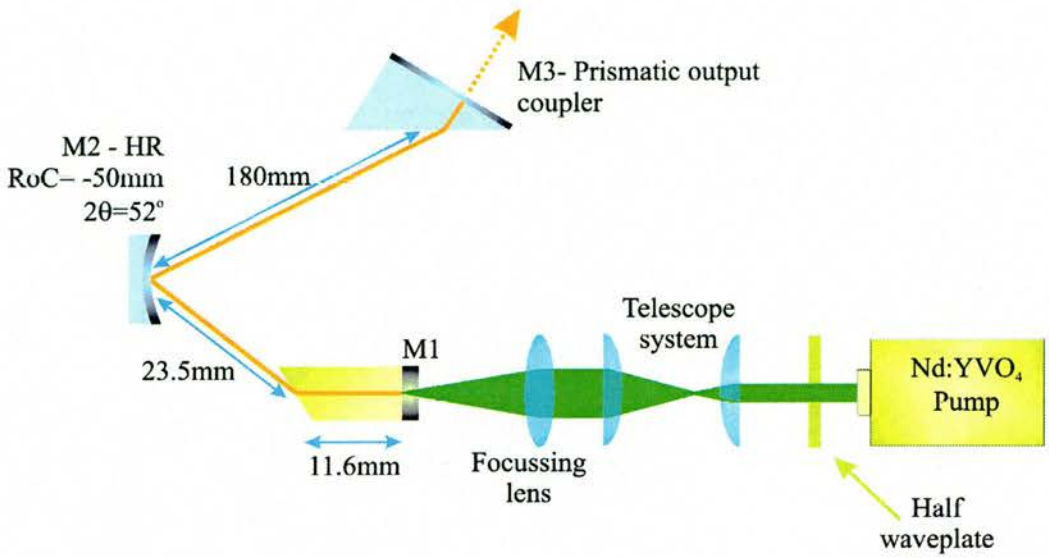

Fig. 4.13 *Schematic diagram of the initial three-element laser system.*

4.6 Initial operation of the 3-element Cr^{4+}:YAG laser system

The results presented in the next two sections relate to the behaviour of the laser cavity initially under cw operation and then under KLM operation. These results show the potential of this system and justify steps discussed in section 4.7, which go on to talk about the improvements needed to obtain sub-100fs, multi-gigahertz operation at 1550nm.

4.6.1 Continuous-wave operation

During cw operation of the system, the plane-wedged HR mirror and output couplers took the place of the Littrow prism. Fig. 4.14 shows the variation of the output power as a function of incident pump power.

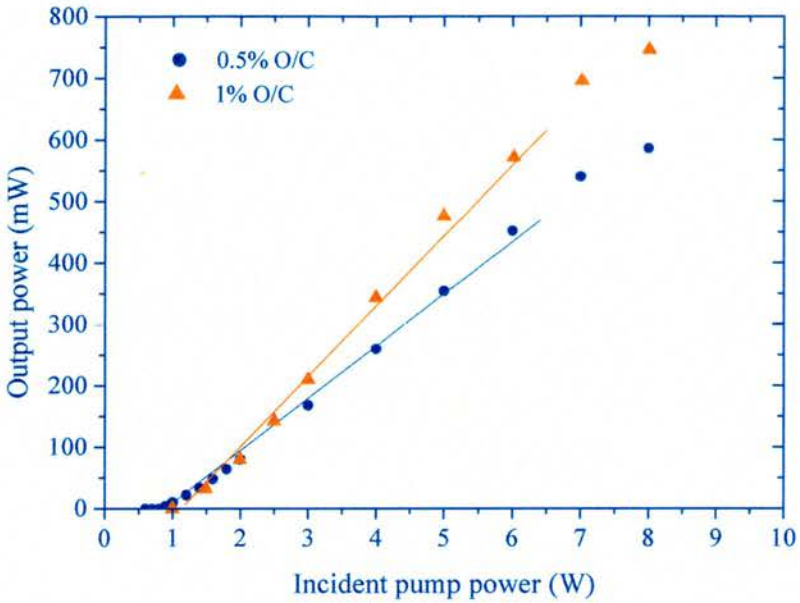

Fig. 4.14 *Cw performance characteristics for the 3-element Cr^{4+}:YAG laser system.*

The thresholds for lasing were reached with 0.9W and 1.2W of incident pump power with 0.5% and 1% output couplers, respectively. The lowest threshold of 0.7W was obtained with the HR mirror in place. The laser emission in this free-running regime peaked at 1490nm with a measured linewidth of ~0.6nm, much like the Cr^{4+}:YAG laser system described in section 3.5. Stable output powers as high as 750mW were achievable with the 1% output coupler when pumped at 8W however thermal effects within the crystal rod, brought about by high pump intensities, caused the output powers to tail off. This can clearly be seen in Fig. 4.14.

The tuning characteristics of the laser were not investigated as this had already been accomplished with the similar laser system described in Chapter 3.

4.6.2 Mode-locked operation

With the Littrow prism in place, Kerr-lens mode locking was achieved by translating the folding mirror, M2, and varying the pump power. The translation of the mirror provided a stability regime that facilitated KLM operation. Variation of the pump power caused thermal lensing effects that often appeared to initiate the build up of pulses within the system. The intracavity dispersion was adjusted by translation of the Littrow prism. It was found experimentally that 5-6mm of fused silica was required to provide an appropriate amount of intracavity negative dispersion for stable mode-locked operation. This corresponded to a round-trip dispersion of $-110fs^2$ at around 1525nm.

The stability of the system at this stage was not yet optimised, as mode locking was only achieved for around a minute or two at a time. It was thought that this instability was due to the pump spot being slightly larger than the beam mode size within the gain crystal. As discussed in Chapter 1, reducing the pump spot to a size that is slightly smaller than the beam mode size favours a more stable mode-locking regime. This was achieved by replacing the f=220mm focusing lens with one that had a focal length of f=200mm. The beam waist, w_0, at the plane face of the crystal was now ~29μm. This adjustment provided much-improved mode-locking stability, with pulsed operation being achieved for hours at a time. Fig. 4.15 shows typical spectral and intensity autocorrelation profiles for the pulses from the mode-locked laser. Assuming $sech^2$ intensity profiles, the pulse duration was determined to be 119fs at a centre wavelength of 1535nm. With the corresponding spectral width of 24nm, the deduced time-bandwidth product was 0.35, indicating that the pulses were fairly close to the transform limit. A pulse repetition frequency of 700MHz was measured using a fast-photodiode (*Newport model D-15 15ps detector*) and a radio-frequency spectrum analyser (*Hewlett-Packard 70000 series*).

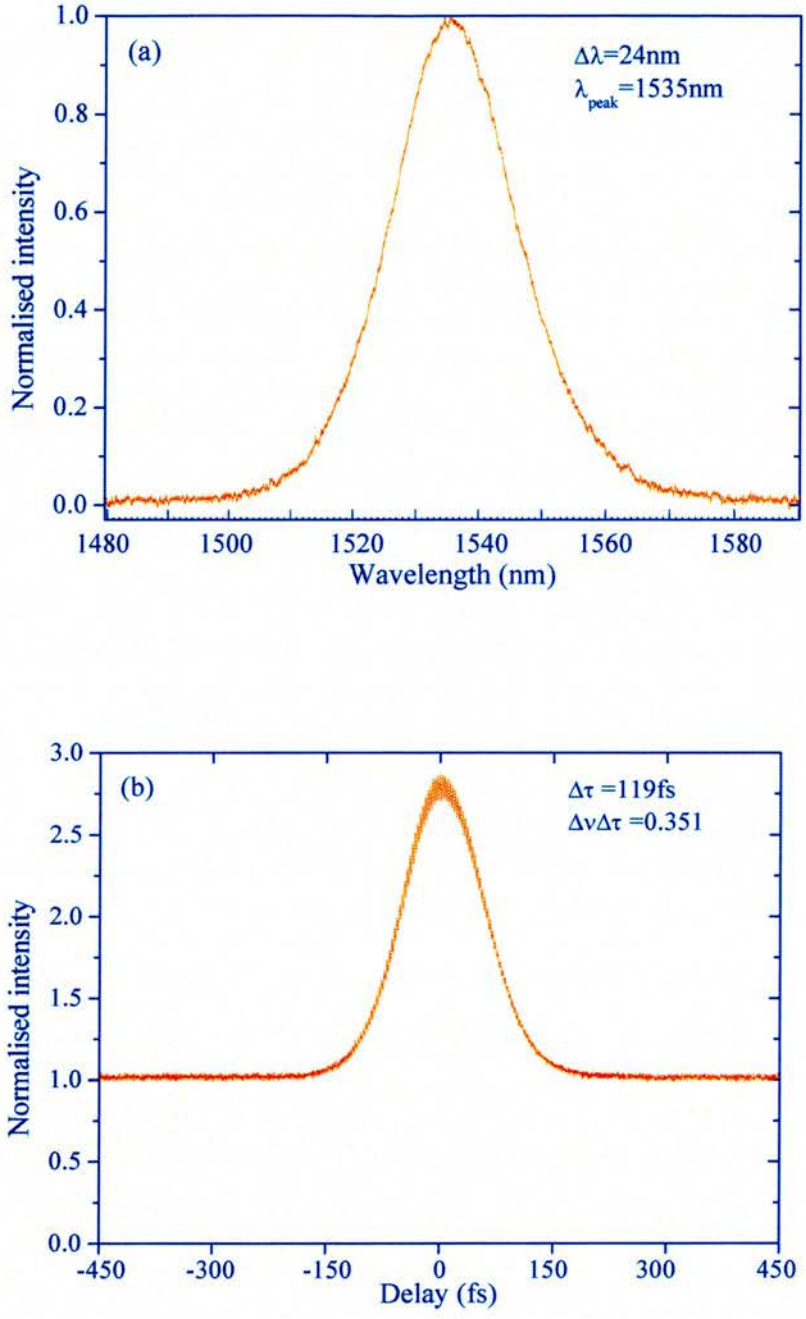

Fig. 4.15 *Measured optical spectrum (a) and corresponding intensity autocorrelation (b) of the mode-locked Cr^{4+}:YAG laser illustrated in Fig. 4.13.*

As discussed earlier, the Littrow prism had an output coupling efficiency of 0.12%, which allowed average output powers of up to 60mW to be generated.

This work was very encouraging as the above results were comparable to those published for Tomaru's three-element laser[3]. Following on from these initial results the length of cavity was then shortened through experimental adjustment of the Littrow prism and the folding mirror positions until stable KLM operation had been achieved at an improved prf of 1.6GHz. However, at these smaller cavity sizes the laser became unstable and was difficult to mode lock. This was due to the folding mirror now having an unoptimised radius of curvature and so to reach higher prfs it was necessary to design a more suitable cavity.

4.7 Updated design and improved results

The Cr^{4+}:YAG rod used by Tomaru had a peak small-signal pump absorption coefficient, $\alpha \leq 1.5cm^{-1}$ and was 18mm in length[3]. The higher quality crystal that I used in the above experiments could achieve similar results with a gain medium that was only ~12mm in length. The use of this shorter crystal allowed for cavity designs that were significantly more compact, and had a higher prf than that demonstrated by Tomaru. The ray-transfer analysis model shown below in Fig 4.16 demonstrates a suitable cavity that would provide a prf > 2.5GHz. This design was the starting point for the next set of experimental assessments, which focused on generating sub-100fs KLM pulses at prfs greater than 3GHz.

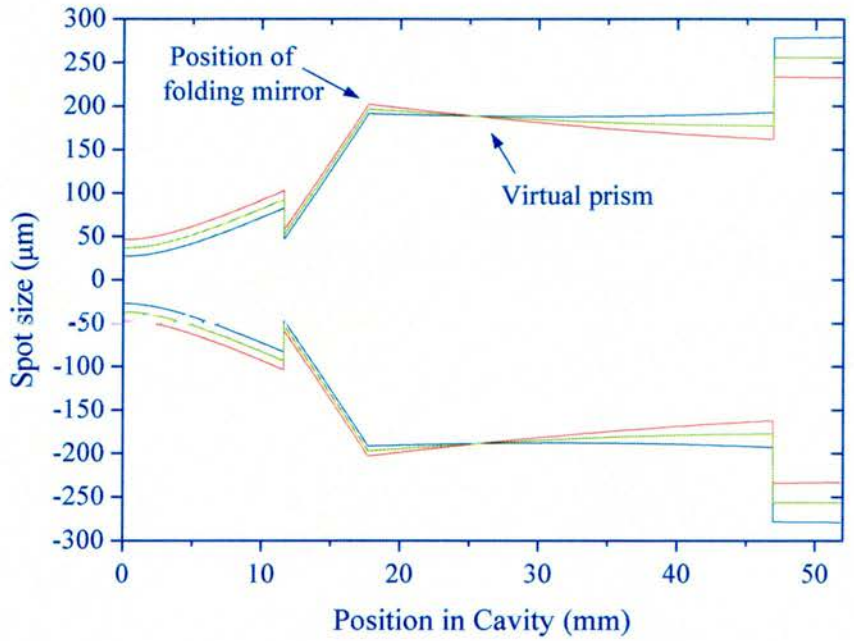

Fig 4.16 *Ray-transfer analysis of an improved three-element cavity. The tangential beam is superimposed with rays that are separated by 20nm about the reference ray (green).*

The length of this cavity was designed to generate pulses with a prf of ~2.5GHz. A schematic of the laser system as a whole is shown below.

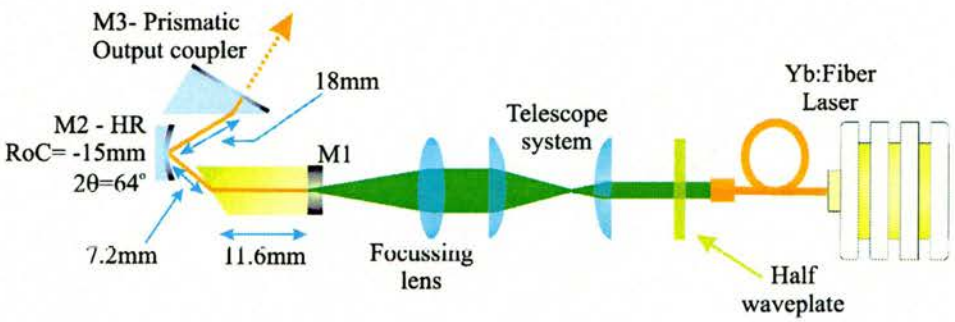

Fig. 4.17 *Schematic diagram of proposed 3-element laser cavity capable of generating femtosecond pulses at a prf ~2.5GHz.*

Although the same Cr^{4+}:YAG gain crystal (from the laser illustrated in Fig. 4.13) was used in this new setup, almost all the other components of the system were improved

upon. The Nd:YVO_4 pump was replaced with a more compact Yb:fibre laser from IPG (identical to the pump source described in Chapter 3) that was capable of producing up to 10W of near diffraction limited cw laser light at 1064nm. This new pump source also had the advantage of providing a more stable power output. The telescope was re-designed so that a f=100mm focusing lens provided a tight $w_0 \approx 30\mu m$ pump spot on the back face of the crystal rod. This was done so that a focusing lens with a longer confocal parameter could be used to provide the correct spot size within the laser rod over a longer distance. The aim of this modification was to increase the area of overlap between the pump and beam modes, thus making the KLM process more stable and efficient.

The new cavity designs required three new, smaller (12.5mm diameter) folding mirrors, which were purchased from *LaserOptik GmbH*[25]. All of these mirrors were highly reflecting between 1470-1630nm but had different radii of curvatures of -18mm, -15mm and -12mm. The use of each folding mirror depended on the size and the stability criterion of the cavity. Initially the RoC=-18mm mirror was employed in the system. Two low loss fused silica Littrow prisms were also purchased and coated with dielectric mirrors on their back faces to improve the coupling efficiency of the laser. One had a coupling efficiency of 0.3% and the other had a coupling efficiency of 0.5%.

4.7.1 Continuous-wave operation

For ease of alignment a plane-wedged 0.5% output coupler was used, instead of a Littrow prism, to achieve initial cw operation of the laser. Fig. 4.18 compares the output powers of this newly designed laser cavity against the powers that were generated by the original laser cavity (Fig. 4.13).

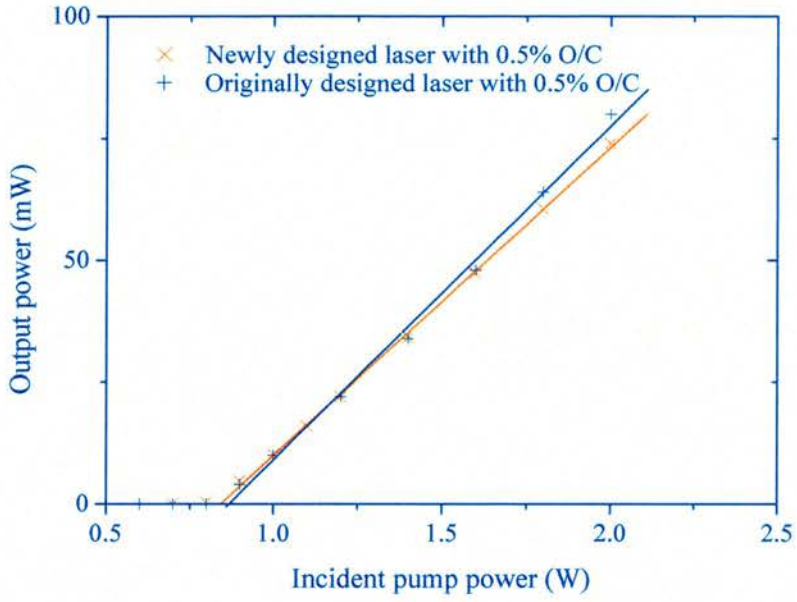

Fig. 4.18 *Output powers from the two 3-element cavities (Fig 4.13 and Fig. 4.17) with a 0.5% output coupler in place.*

It can be seen clearly, and is worth noting, that both systems have the same threshold ($P_{incident}$=0.9W) and produce almost the same output powers. This was a good indication that the new folding mirrors and the cavity design had not compromised the efficiency of the lasing process. With the Littrow prism inserted in place of the plane-wedged O/C it was now possible to attempt KLM operation in this new cavity design.

4.7.2 Mode-locked operation

Again, translating the folding mirror, M2, and varying the pump power initiated Kerr-lens mode locking. Mode locking was established at pump thresholds of approximately 2.6W but the best stability was achieved at pump power levels around 5W. Fig. 4.19 shows the spectral and autocorrelation traces of the new cavity design, with the 0.12% O/C Littrow prism in place.

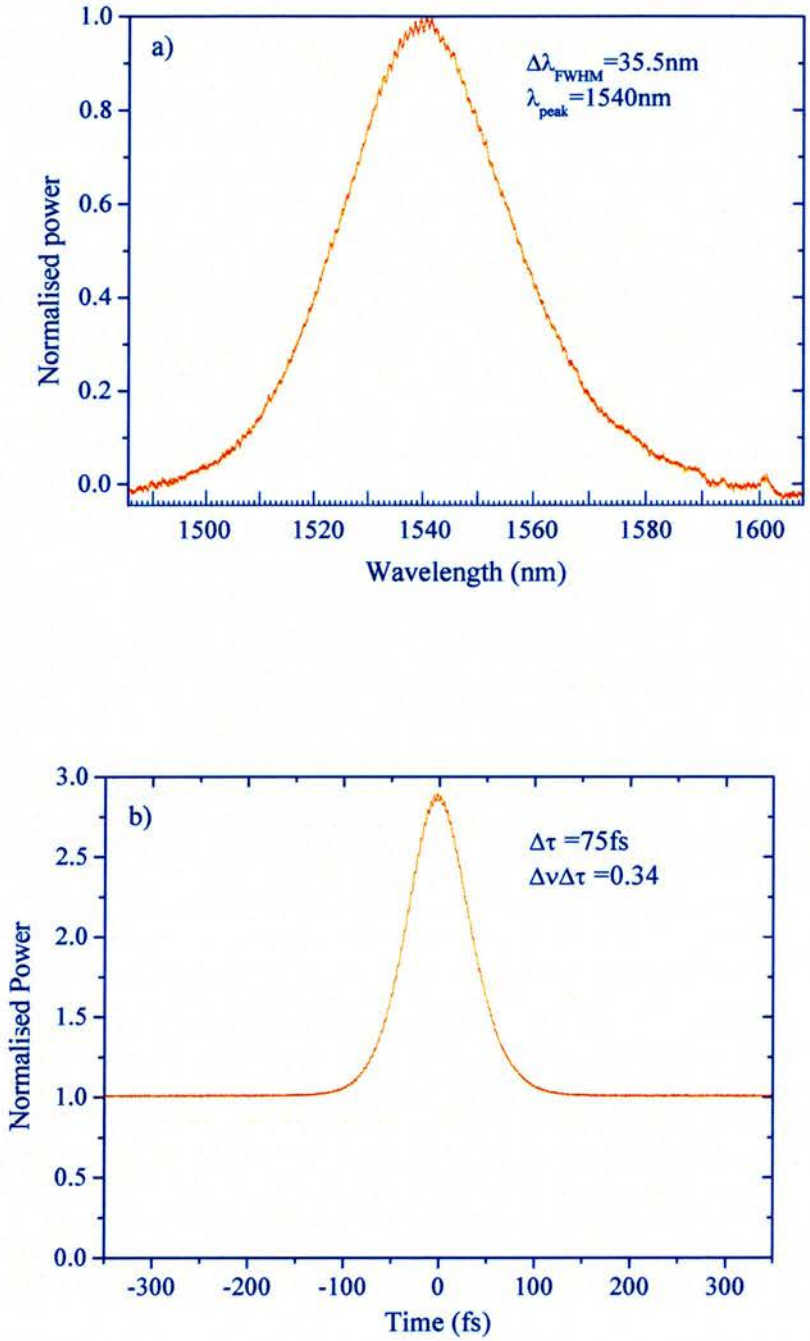

***Fig 4.19** Optical spectrum, (a), and intensity autocorrelation, (b), of KLM 3-element Cr^{4+}:YAG laser operating with a prf of 2.6GHz.*

The peak of the spectral trace was at a wavelength of 1540nm. This spectrum had a full-width half-maximum bandwidth of ~35nm. Again, assuming a $sech^2$ intensity

profile, the pulse duration was determined to be 75fs, giving a time-bandwidth product 0.34, indicating that the pulses were close to the transform limit. The pulses were measured to have an average output power of 31mW at a prf of 2.6GHz. This was a most encouraging result that exceeded the expectations for this cavity design. This was the first time a laser of this type had exceeded the groundbreaking prf of 2.5GHz. With this configuration the laser could sustain KLM operation for several hours at a time, thus confirming its future as a useful tool in a range of datacommunications experiments that could utilize the ~2.5GHz pulse train (as discussed in Chapter 5).

Further developments to the laser were made. These included the replacement of the 0.12% O/C prismatic element with the 0.5% and 1% output coupling prismatic elements and the employment of the other two folding mirrors. Stable mode locking of the laser at different prfs was found experimentally by adjusting the position of the folding mirror, M2, and the distance between the folding mirror and the Littrow prism so that cw operation became unstable and KLM operation was favoured. The change of position of M2 also meant that the pump power had to be adjusted appropriately. These constraints led to some variation of the average output power when the RoC of the cavity fold mirror was varied. Fig. 4.20 gives a summary of the various performance characteristics that were obtained from this three-element Cr^{4+}:YAG laser.

M2 RoC (mm)	O/C (%)	$\Delta\lambda$ (nm)	$\Delta\tau$ (fs)	P_{OUT} (mW)	P.R.F. (GHz)
-18	0.3	37	77	60	2.4
	0.5	34	79	167	2.3
-15	0.3	32	78	60	3.05
	0.5	25	99	104	3.02
-12	0.3	35	83	41	3.71
	0.5	32	82	85	4.02

Fig. 4.20 *Performance features of 3-element laser configurations.*

The highest prf of 4.02GHz was achieved with the RoC=-12mm folding mirror and the 0.5% O/C in place. Fig 4.21 shows the spectrum autocorrelation and RF trace of the system running at a prf of 4.02GHz.

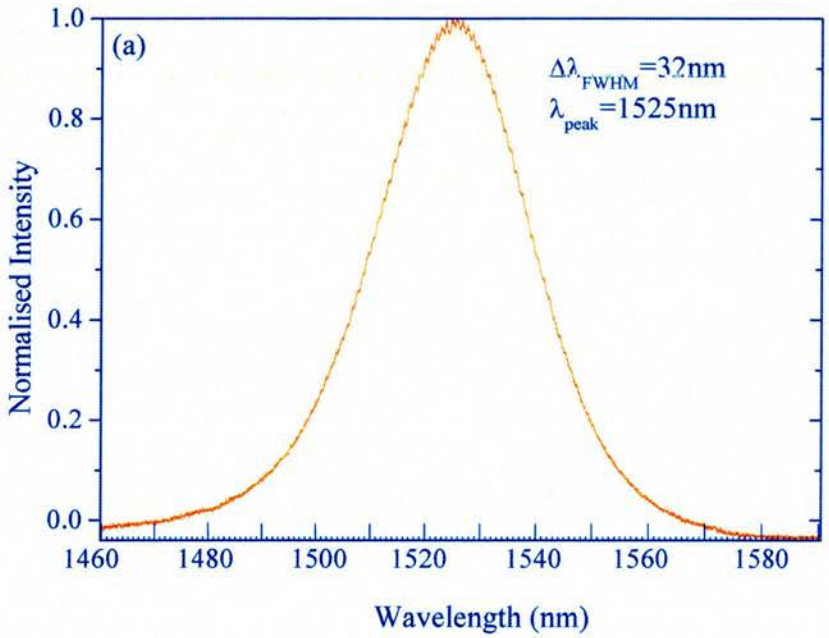

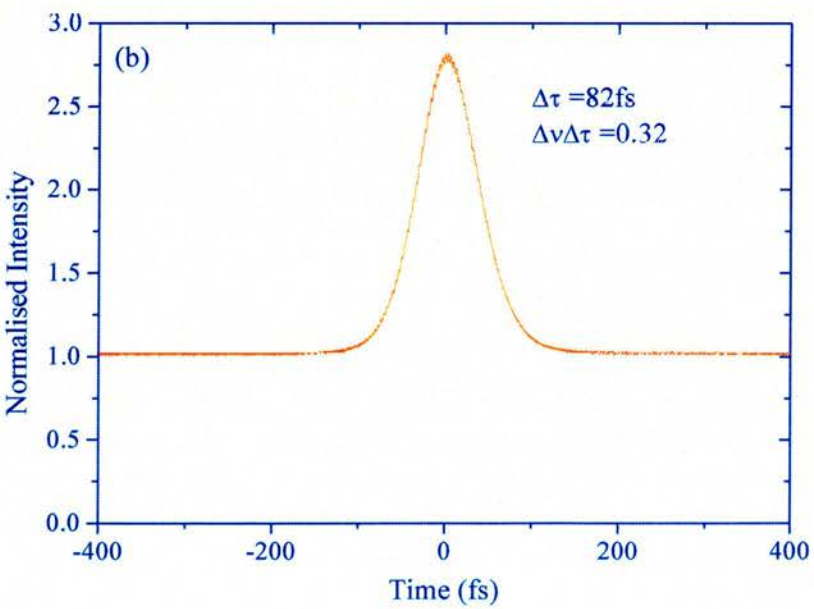

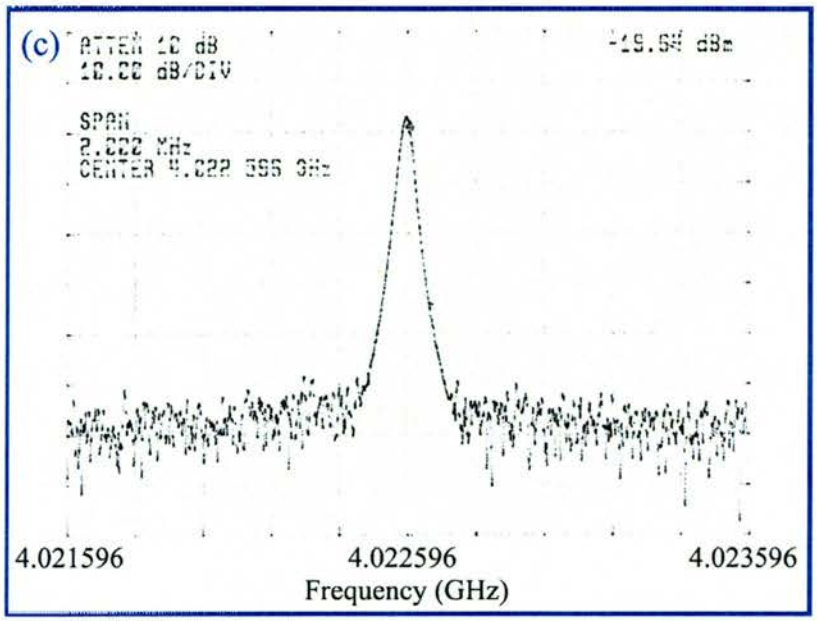

Fig 4.21 *Spectrum (a), autocorrelation (b) and RF spectrum (c) of the 4GHz prf laser.*

These pulses were generated with a spectral bandwidth of 32nm. The pulses had a duration of 82fs, demonstrating a transform limit of 0.32. In this configuration (with the 0.5% O/C in place) the laser was capable of producing as much as 85mW of average power when mode locked.

4.7.3 Future development

The 4GHz prf results described here were possible due to the development of a cavity that was only ~32mm in length. This required the three elements to be physically close one another. Over a third of the cavity length was taken up by the Cr^{4+}:YAG crystal rod and around a quarter was taken up by the Littrow prism. To reach higher pulse repetition frequencies would require a gain crystal that was shorter in length. I would expect the quality of Cr^{4+}:YAG laser crystals to allow the generation of cavities of up to ~5GHz. However, any laser crystal shorter than ~5mm would not have a sufficiently high pump absorption coefficient to support laser action, let alone KLM operation.

In terms of stability, there are several improvements that can still be made. The system that I have designed was constructed on large opto-mechanical mounts that had a certain amount of mechanical drift associated with them. Due to the sensitive nature of the KLM process this often caused the system to become unstable. Also, having a water-cooled system introduced unwanted vibrations into the system, which occasionally contributed to the instability of the KLM operation. To improve the stability of the system, I took the step of developing a more rugged and compact laser package by having an engineered prototype constructed.

4.8 Engineered Prototype

In the past, the ultrashort pulse laser research group in St Andrews has taken successful laser systems based in the laboratory environment and improved on some aspect of the laser design in order to demonstrate its suitability in the real world for real applications. There is no better illustration of this than a Cr:LiSAF laser that we developed to produce 100fs pulses from a power source comprising of just 6 AA batteries[16]. This system had a footprint no larger than the size of an A4 piece of paper, and showed that solid-state lasers need not be confined to the laboratory environment.

After the successful demonstration of the Cr^{4+}:YAG laser at a prf greater than 1GHz there was an obvious drive to establish if an engineered prototype could be demonstrated at the all important 1550nm wavelength region. If successful, the system would start to cement its future as a viable laser source for datacommunications experiments and applications. It is worth noting that this type of laser system is compatible with present day telecommunications systems, some of which run at 2.5GHz.

To help in the development and delivery of a commercial prototype I enlisted the know-how of the St Andrews based *Photonics Innovation Centre* (PIC). One of the key aims of the PIC is to assist various academic groups in commercialising their research, by developing prototype devices through in-house or industry collaborative projects. For the development of my laser system the PIC enlisted some further specialist help from a new company called *PhotoSynergy*.

PhotoSynergy Limited is a joint venture company that was formed in March 2002 by the University of St Andrews and *Ferranti Photonics Limited* and has the benefit of being able to draw design and manufacturing expertise from a company that has had over 30 years of experience in the photonics industry.

Several meetings were held to allow the PIC and *PhotoSynergy* to understand what we were looking for and also to give us an idea of what they could achieve. Our brief was to take a laser system similar to the one illustrated in Fig. 4.22 and engineer it into a simple, robust and compact unit. The figure below gives some idea of the scale of the system in the laboratory environment. The pump source on the right hand side would generate light at 1064nm, which would pass through the half-wave plate, telescope system and focusing lens. The three-element laser cavity is pictured on the left-hand side of the photograph. The laser crystal can be seen in its water-cooled copper jacket. The large water pump needed to cool the copper jacket would sit under the bench. Fig 4.22 also shows how the whole system sat on the 900mm×600mm black breadboard.

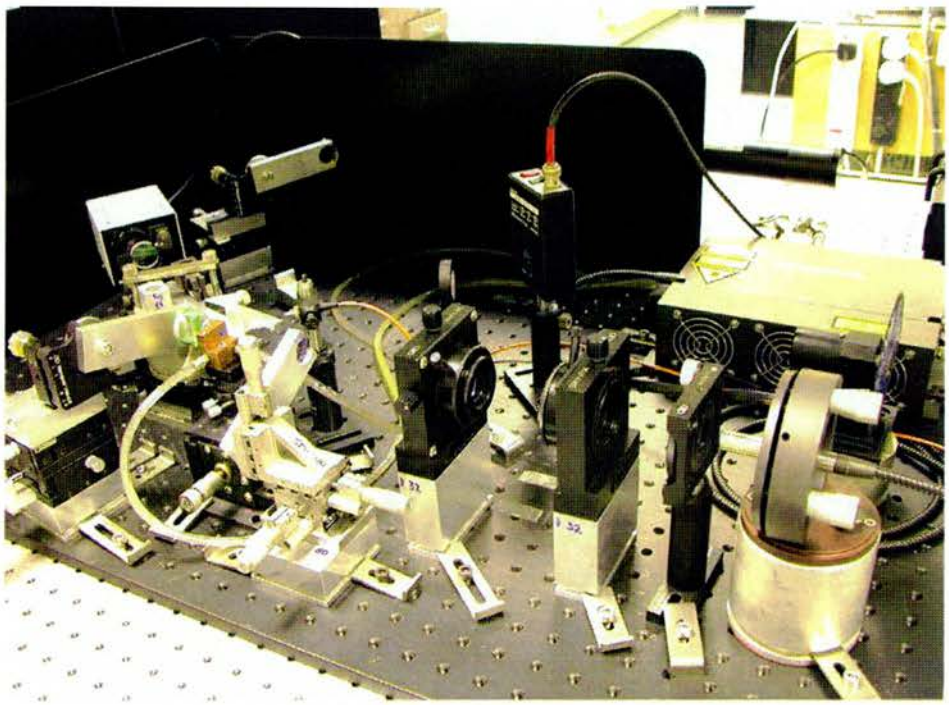

Fig. 4.22 *Photograph of the laboratory-based Cr^{4+}:YAG laser.*

There were two specific improvements of the laboratory-based laser that I wanted re-designed into the new prototype. The main improvement involved controlling the temperature of the laser crystal in the absence of water-cooling. The stability of the KLM process was being affected by vibrations caused by the flow of water passing through the water jacket around the laser crystal. I wanted the new laser system to incorporate a thermo-electric cooling element that would remove heat from the laser crystal without introducing unwanted vibration within the cavity. The other suggested improvement involved placing all three elements of the cavity on a single plate in order to improve mechanical and thermal stability of the laser cavity, which would lead to even greater KLM stability.

For *PhotoSynergy* to design a suitable laser system I provided them with a cavity geometry that would bring about KLM operation at a prf of ~2.5GHz. PhotoSynergy presented a design that they believed they could implement and this design is illustrated in Fig. 4.23.

Due to the thermal load that needed to be extracted out of the system, *PhotoSynergy* decided upon a two-stage cooling system. The first stage removed heat from the copper jacket surrounding the laser crystal into the plate underneath the three elements of the cavity. The second stage removed heat from the plate into a large heatsink underneath the laser cavity.

For a quick delivery time, *PhotoSynergy* were provided with the three appropriate laser cavity elements that would sit in the system. These were the 11.6mm long Cr^{4+}:YAG laser rod, the HR folding mirror that had a –18mm RoC and the 0.3% O/C Littrow prism. It took *PhotoSynergy* 10 weeks to construct and deliver the new laser system, once the design had been finalised. This new commercial prototype is illustrated in the Fig. 4.24.

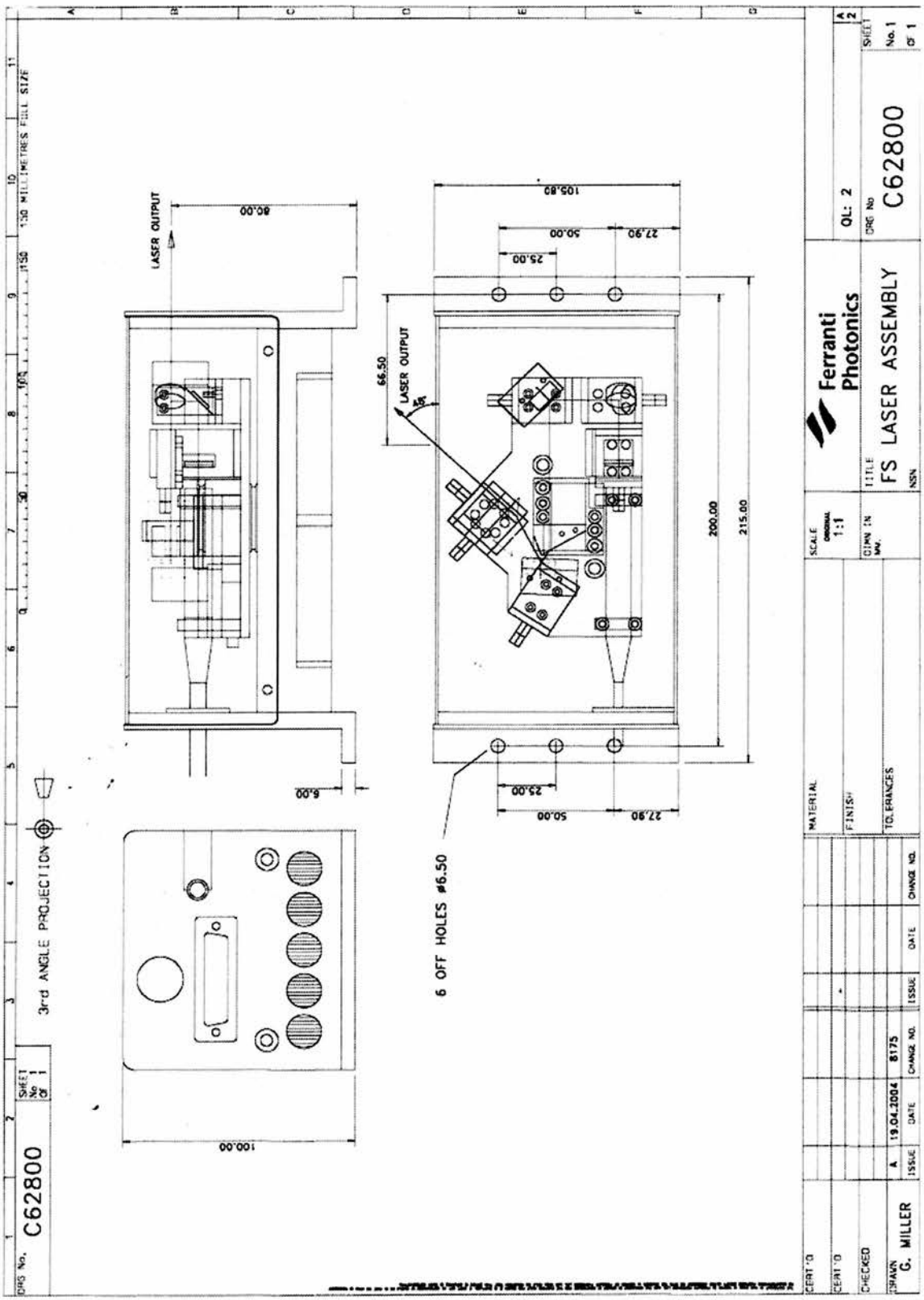

Fig. 4.23 *The PhotoSynergy design plans for the new compact Cr^{4+}:YAG laser system.*

Fig. 4.24(a) and 4.24(b) show the side views of the laser system, while Fig. 4.24(c) and 4.24(d) give an impression of the scale of the cavity. The last photograph in this collection shows the whole laser system with the fibre laser and the TEC control box attached.

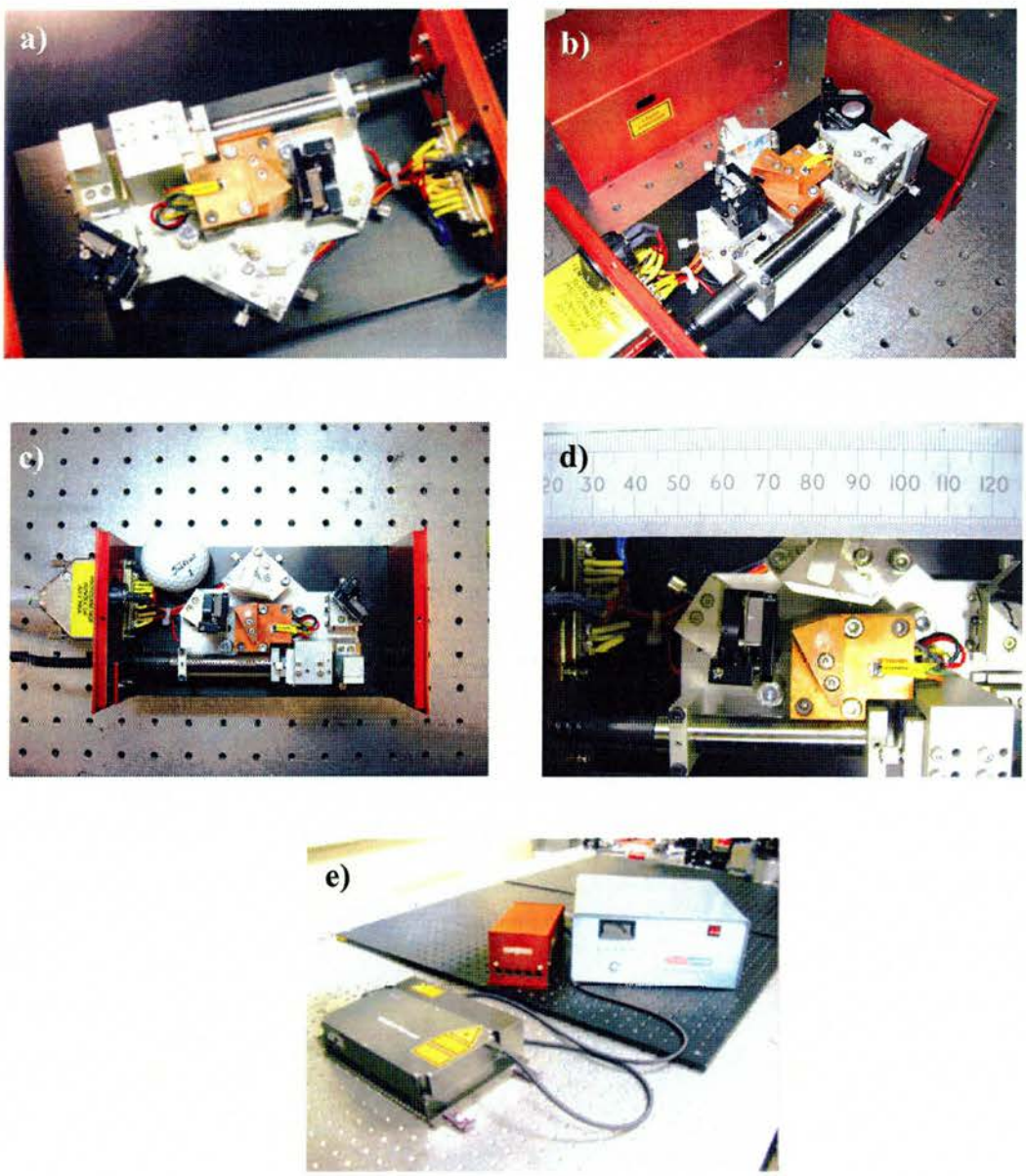

Fig. 4.24 *Commercial prototype of the Cr^{4+}:YAG laser produced by PhotoSynergy.*

Continuous-wave operation of this new laser system proved to be similar to its laboratory-based counterpart, with a lasing threshold of ~1.3W. Mode locked operation took place successfully at a prf of 2.53GHz. Early results revealed that, by placing the whole cavity in a sealed box, limiting the amount of mechanical movement within the cavity and removing the water-cooling system significantly improved the long-term stability of the KLM process. This gave rise to KLM operation over periods of many hours. The laser was capable of generating sub-100fs pulses with an average power of 44mW.

The early success of this laser system meant that it was quickly integrated into a variety of systems based assessments (see Chapter 5). Owing to this fact, a more thorough evaluation of the laser system was not carried out.

4.9 Conclusions

In this chapter the design and operation of a 3-element KLM Cr^{4+}:YAG laser cavity has been described in some detail. The laser system was based around the implementation of a cavity design that only needed one dispersion-compensating prism. Using this feature allowed the initial generation of 119fs pulses with average powers of up to 60mW at a pulse repetition frequency of 700MHz. Further development of the laser system soon yielded 75fs pulses with an average power of 31mW at a vastly improved pulse repetition frequency of 2.6GHz. Another version of this cavity design eventually reached a pulse repetition frequency of 4GHz, which is the highest known value for a Cr^{4+}:YAG laser, and certainly higher than any commercially available solid state laser system.

The last section of this chapter talks about how the success of this laboratory-based laser system was taken through the early stages of an engineering design process

through the realisation of a prototype laser system that generates sub-100fs pulses at a pulse repetition frequency of 2.5GHz, making it a viable candidate for a range of datacommunications experiments.

4.10 References

1. D.J. Ripin, C. Chudoba, J.T. Gopinath, J.G. Fujimoto, E.P. Ippen, U. Morgner, F.X. Kartner, V. Scheuer, G. Angelow, and T. Tschudi, "Generation of 20-fs pulses by a prismless Cr4+: YAG laser", *Optics Letters*, vol. 27, (1), p. 61-63, 2002.
2. C.G. Leburn, A.A. Lagatsky, C.T.A. Brown, and W. Sibbett, "Femtosecond Cr^{4+}:YAG laser with a 4GHz pulse repetition rate", *Electronics Letters*, vol. 40, (13), p. 805-807, 2004.
3. T. Tomaru and H. Petek, "Femtosecond Cr4+: YAG laser with an L-fold cavity operating at a 1.2-GHz repetition rate", *Optics Letters*, vol. 25, (8), p. 584-586, 2000.
4. W.T. Holloway, A.J. Keating, and D.D. Sampson, "Multiwavelength source for spectrum-sliced WDM access networks and LAN's", *IEEE Photonics Technology Letters*, vol. 9, (7), p. 1014-1016, 1997.
5. L. Boivin and B.C. Collings, "Spectrum slicing of coherent sources in optical communications", *Optical Fiber Technology*, vol. 7, (1), p. 1-20, 2001.
6. M. Ramaswamypaye and J.G. Fujimoto, "Compact Dispersion-Compensating Geometry for Kerr-Lens Mode- Locked Femtosecond Lasers", *Optics Letters*, vol. 19, (21), p. 1756-1758, 1994.
7. R. Mellish, S.V. Chernikov, P.M.W. French, and J.R. Taylor, "All-solid-state compact high repetition rate modelocked Cr4+: YAG laser", *Electronics Letters*, vol. 34, (6), p. 552-553, 1998.
8. F. Jager, N. Zhavoronkov, and F. Noack, "Femtosecond all-solid-state Cr : forsterite laser designed in compact three-element layout", *Electronics Letters*, vol. 35, (25), p. 2206-2207, 1999.
9. Y.M. Chang, R. Maciejko, R. Leonelli, and A.S. Thorpe, "Self-starting passively mode-locked tunable Cr4+: yttrium- aluminum-garnet laser with a single prism for dispersion compensation", *Applied Physics Letters*, vol. 73, (15), p. 2098-2100, 1998.
10. D. Kopf, G.J. Spuhler, K.J. Weingarten, and U. Keller, "Mode-locked laser cavities with a single prism for dispersion compensation", *Applied Optics*, vol. 35, (6), p. 912-915, 1996.
11. S. Aoshima, H. Itoh, and Y. Tsuchiya, "Compact Geometry ofr Doide-Pumped Cr:LiSAF Femtosecond Laser", *IEEE Journal of Selected Topics in Quantum Electronics*, vol. 3, (1), p. 95-99, 1997.
12. J.M. Hopkins, G.J. Valentine, B. Agate, A.J. Kemp, U. Keller, and W. Sibbett, "Highly compact and efficient femtosecond Cr : LiSAF lasers", *IEEE Journal of Quantum Electronics*, vol. 38, (4), p. 360-368, 2002.
13. A.G. Kostenbauder, "Ray-Pulse Matrices: A Rational Treatment for Dispersive Optical Systems", *IEEE Journal of Quantum Electronics*, vol. 26, (6), p. 1148-1157, 1990.
14. J.M. Hopkins, "Compact, Low-threshold Femtosecond Lasers", PhD thesis: School of Physics and Astronomy, University of St Andrews: St Andrews, 1999.

15. M.H. Dunn, "Lasers 2", in *MSc. Lecture course*. 2001, School of Physics and Astronomy, University of St Andrews,2001.

16. B. Agate, B. Stormont, A.J. Kemp, C.T.A. Brown, U. Keller, and W. Sibbett, "Simplified cavity designs for efficient and compact femtosecond Cr : LiSAF lasers", *Optics Communications*, vol. 205, (1-3), p. 207-213, 2002.

17. J. Wilson and J. Hawkes, "Optelectronics - An introduction", 3rd ed. London: Prentice Hall, 1998.

18. J.M. Evans, V. Petricevic, A.B. Bykov, A. Delgado, and R.R. Alfano, "Direct diode-pumped continuous-wave near-infrared tunable laser operation of Cr^{4+}:forsterite and Cr^{4+}:Ca_2GeO_4", *Optics Letters*, vol. 22, (15), p. 1171-1173, 1997.

19. P.T. Guerreiro, S. Ten, E. Slobodchikov, Y.M. Kim, J.C. Woo, and N. Peyghambarian, "Self-starting mode-locked Cr:forsterite laser with semiconductor saturable Bragg reflector", *Optics Communications*, vol. 136, p. 27-30, 1997.

20. A.A. Lagatsky, C.G. Leburn, C.T.A. Brown, W. Sibbett, and W.H. Knox, "Compact self-starting femtosecond Cr4+: YAG laser diode pumped by a Yb-fiber laser", *Optics Communications*, vol. 217, (1-6), p. 363-367, 2003.

21. D.E. Spence, P.N. Kean, and W. Sibbett, "60-Fsec Pulse Generation from a Self-Mode-Locked Ti-Sapphire Laser", *Optics Letters*, vol. 16, (1), p. 42-44, 1991.

22. D.J. Ripin, J.T. Gopinath, H.M. Shen, A.A. Erchak, G.S. Petrich, L.A. Kolodziejski, F.X. Kartner, and E.P. Ippen, "Oxidized GaAs/AlAs mirror with a quantum-well saturable absorber for ultrashort-pulse Cr4+: YAG laser", *Optics Communications*, vol. 214, (1-6), p. 285-289, 2002.

23. M.H. Dunn, "Lasers 2", *MSc. Lecture course*, vol., (Lecture 14), 2001.

24. A.E. Siegman, "Lasers". Calafornia: University Science Books, 1986.

25. LaserOptik. http://www.laseroptik.de/,http://www.laseroptik.de/.

26. Crystran, http://www.crystran.co.uk/.

27. A.J. Alfrey, "Modeling of Longitudinally Pumped CW Ti:Sapphire Laser Oscillators", *IEEE Journal of Selected Topics in Quantum Electronics*, vol. 25, (4), p. 760-766, 1989.

Chapter 5 – Incorporation of a Multi-gigahertz, Femtosecond Source into Systems Based Assessments

5.1 Introduction

During the course of designing and constructing the multi-GHz Cr^{4+}:YAG laser that was described in the previous chapter, there was an opportunity to forge a collaboration (through the UPC program) with the researchers in the Centre for Photonic Systems at the University of Cambridge. They are involved in research in several areas including high-speed optical communication systems, local area networks using optical links, optical amplifiers, optical nonlinearities for switching and routing applications, as well as multi-wavelength communication sources and systems.

The purpose of our collaboration was to bring about the successful integration of a solid-state laser source within a systems environment. This chapter will contain discussions of the two systems-based experiments undertaken during the duration of this project.

The first experimental assessment involved the integration of the laboratory-based Cr^{4+}:YAG laser into a spectral slicing experiment to determine the capacity of information that could be generated form a single source. The second assessment involved a brief investigation into the capability of creating ultrashort switching windows using the engineered prototype laser system described in the last section of Chapter 4.

5.2 Spectral slicing based on a multi-gigahertz Cr^{4+}:YAG femtosecond laser

Broadband transmitters will be key components for future terabit communication systems. During the past ten years or so, dense-wavelength-division-multiplexing

(DWDM) systems have enabled the transmission capacity of single-mode fibres to increase from 2.5Gb/s to more than 10Tb/s[1]. This growth has been achieved mainly by simultaneously increasing the number of wavelength channels as well as the transmission rate per wavelength channel. As the number of channels has increased, the use of numerous single-wavelength transmitter lasers operating at different wavelengths has become more challenging, complex and costly. Multi-wavelength optical-time-division multiplexing (OTDM) is becoming an attractive approach because it can remove the need for many transmitters within a system. For this reason, a practical and robust multi-wavelength ultrashort pulse source would be desirable for high capacity OTDM/wavelength-division multiplexing (WDM) systems.

In this section a description is given for the integration of a femtosecond Cr^{4+}:YAG laser source into a novel OTDM/WDM system using a process known as spectral slicing.

Spectral slicing offers the most promising approach for multi-wavelength operation from a single source. In this scheme an ultrashort-pulse laser source having a broad optical spectrum is filtered using a component known as an arrayed-waveguide grating (AWG). The AWG is a device that splits a broadband signal and slices it up into individual wavelength segments to generate a number of closely spaced wavelength channels. The channel spacing depends on the AWG that is employed. Given that the optical source provides light simultaneously for all the channels, the number of active components in the transmitter is reduced by one or two orders of magnitude. This represents a more practical and cost-effective transmitter for WDM systems. However, for large channel numbers, a high quality broadband source is required with gigahertz repetition rates to make use of OTDM technology simultaneously.

Early work on spectrum slicing focused on using broadband incoherent sources such as erbium-doped fibre amplifiers[2] and light emitting diodes followed by a modulator[3]. Although such sources were more widely available and less expensive, making them potentially suitable for low cost access and other network applications, these techniques suffered from a fundamental problem known as spontaneous-spontaneous beat noise[2]. This is negligible when dealing with large bandwidths but becomes the dominant noise feature when dealing with the bandwidths generated in the channels of these WDM systems. This noise feature limits the achievable bit-error rate for a given sliced bandwidth and can only be overcome at the expense of system capacity through a reduction of the bit rate or an increase of the optical bandwidth.

Compared with incoherent sources, mode locked lasers[4] and supercontinuum sources[5] are highly coherent and exhibit negligible spontaneous-spontaneous beat noise. The spectral efficiency of this type of source can therefore be as high as systems based on a number of distinct individual laser sources, offering a much wider range of applications.

Vibronic femtosecond lasers[6, 7] offer superior performance in terms of pulse quality compared with conventional spectral slicing sources. They can generate broadband, chirp-free femtosecond pulses with high power. Cr^{4+}:YAG lasers have shown potential as optical pulse sources but they have not been previously employed in telecommunication or datacommunication applications. It was therefore deemed necessary to investigate the performance of a Cr^{4+}:YAG laser with data modulation and more importantly as a potentially high-capacity multi-wavelength spectral-slicing source. This justified the integration of the multi-gigahertz, femtosecond Cr^{4+}:YAG laser, discussed in Chapter 4, into a spectrum slicing systems evaluation.

5.2.1 The laser source

The laser that was designed and constructed in Chapter 4, (see section 4.7), was used in the following assessments and is illustrated in Fig. 5.1. The folding mirror, M2, had a radius of curvature of –18mm. An average mode locked output power of 15mW was achieved with the 0.12% O/C Littrow prism in place. The laser operated at a centre wavelength of 1560nm. The pulse duration and spectral width of the laser were 70fs and 40nm, respectively, yielding a near-transform-limited time-bandwidth product of 0.33.

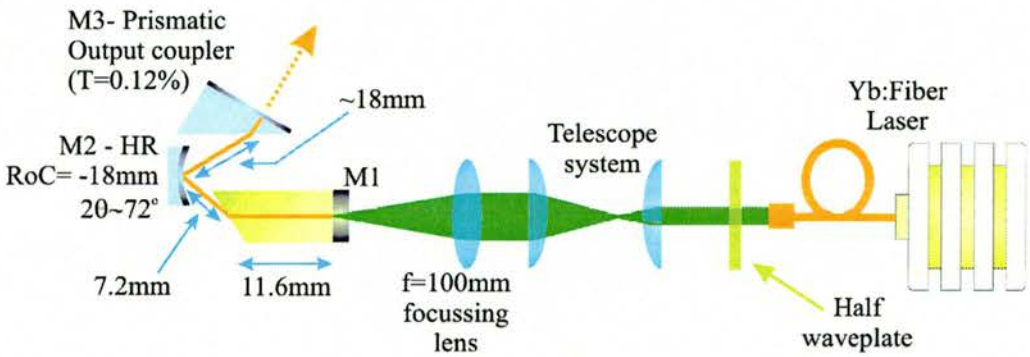

Fig. 5.1 *Schematic diagram of the three-element laser used to generate 70fs pulses at a prf of 2.67GHz.*

A pulse train of ~10GHz was required in order to provide a suitable clock speed for the spectral slicing experiment. This was achieved by running the laser at a prf of 2.67GHz and using a free-space interleaver to increase the pulse train to 10.66GHz.

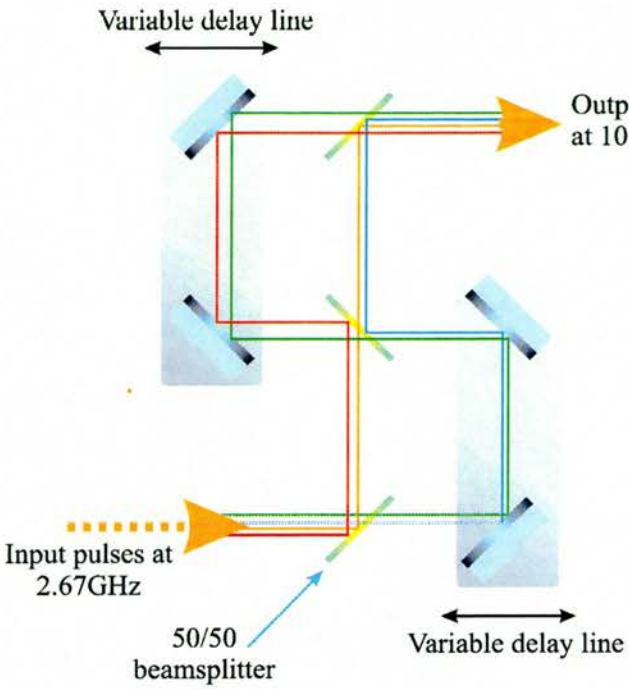

Fig. 5.2 *Diagram of the free-space interleaver used to step up the prf from 2.67GHz to 10.66GHz. Each possible path through the device is shown in a separate colour.*

The free-space interleaver, illustrated in Fig 5.2, consisted of three 50/50 beamsplitters and four dielectric HR mirrors designed for optimal operation at an angle of 45° and a wavelength of 1550nm. The mirrors were mounted on two translation stages so that the delay lines of each arm of the interleaver could be suitably adjusted to provide an accurate 10GHz pulse train.

5.2.2 Systems setup for the spectral slicing experiment

Figure 5.3 illustrates a schematic of the system setup.

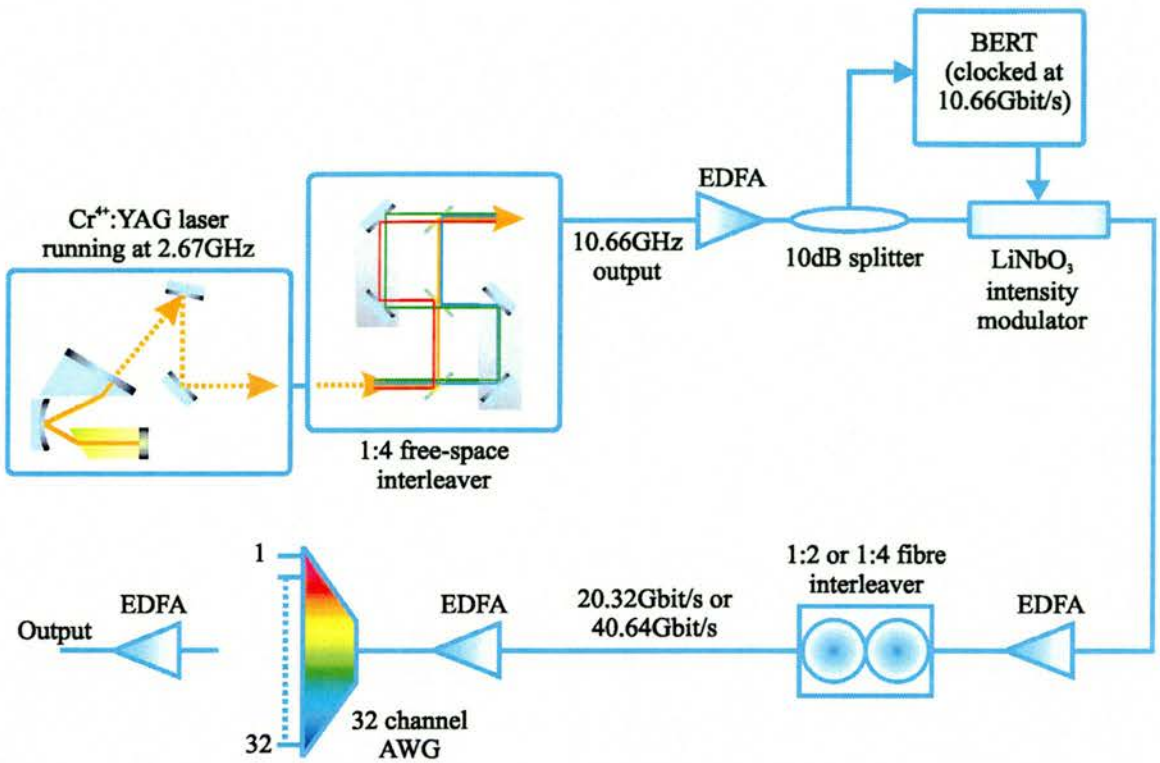

Fig. 5.3 *Experimental setup of the spectral-slicing source based on the Cr^{4+}:YAG laser.*

The output pulses from the interleaver were coupled into a single mode fibre before being amplified by an erbium-doped amplifier (EDFA). These amplified pulses were then transmitted through a 10dB splitter. The 10% output port from this splitter was used to clock a bit-error-rate tester (BERT) at 10.66GHz, while the other 90% of the signal was modulated with data at 10.66Gb/s in a $LiNbO_3$ intensity modulator. The data streams were then amplified again and passively interleaved further in a two-stage fibre interleaver. By blocking or unblocking one of the arms of this interleaver, data streams at 20.32Gb/s or 40.64Gb/s were generated. These interleaved bit streams were amplified by another EDFA before being spectrally sliced in a 32-channel AWG device. The AWG used was a commercially available product from *Lightwave Microsystems*[8] with 32 output channels ranging from 1535.8nm to 1560.6nm with a channel spacing of 100GHz (0.8nm). The insertion loss of the AWG was between 3.2dB and 3.5dB per

channel. The output data streams were further amplified and measured using an *Agilent 86113-A 53GHz* optical receiver.

5.2.3 Results and discussion

Spectral slicing resulted in total capacities of 682Gb/s and 1.36Tb/s with input data streams at 20.32Gb/s and 40.64Gb/s, respectively. As discussed earlier the broad optical spectrum of the laser was 40nm wide.

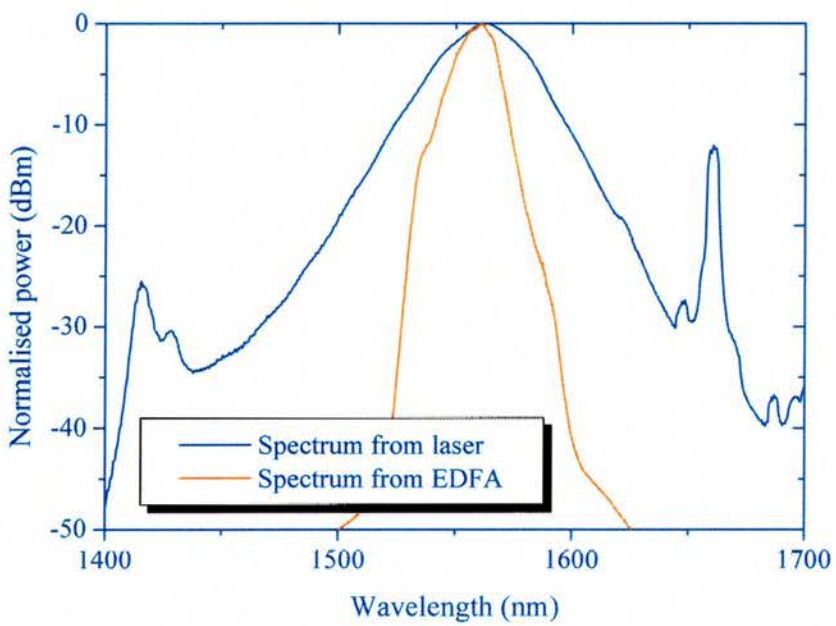

Fig 5.4 *Output spectra of the laser and the EDFA.*

Fig. 5.4 shows that although this spectrum was relatively broad, only the spectral components lying under the EDFA gain region were amplified and transmitted. Fig. 5.5 shows the spectra of the 32 channels from the AWG. The output power of each channel was highly dependent on the input, which was influenced by the shape of the EDFA gain spectrum and varied between –12dBm and –2dBm. This could be improved in the future if a gain-flattening filter was to be employed after the EDFA.

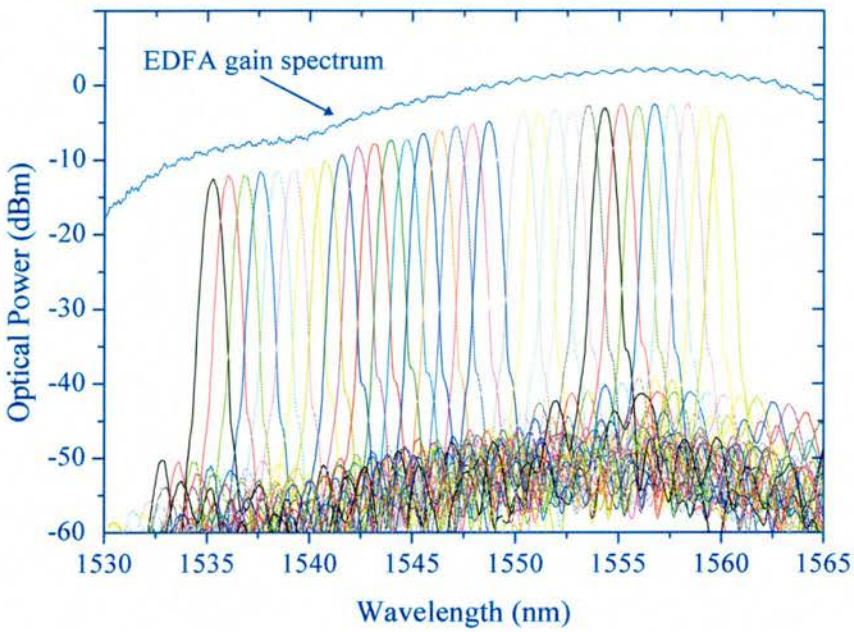

Fig 5.5 *Spectra of the 32 output channels of the AWG underneath the EDFA gain spectrum.*

Since the AWG that was used for this work was not specifically designed for spectral slicing, the cross-talk between neighbouring channels was around 5dB, which restricted the potential of the system for long-haul transmission. However, with the use of orthogonal polarisation multiplexing (in which odd channels and even channels are multiplexed in orthogonal polarisation states to reduce interference to better than 20dB) all 32 channels could be transmitted simultaneously.

The number of wavelength channels demonstrated here was limited by the bandwidth of the EDFAs and the channel number of the AWG. The use of ultra-broadband optical amplifiers covering the EDFA *C* and *L* bands along with higher capacity AWGs would allow access to more of the gain generated by the laser and enable capacities of up to 3Tb/s.

The Q factors measured after spectral slicing for all 32 channels at both 20.32Gb/s and 40.64Gb/s are shown in Fig. 5.6. The Q factor is a parameter that directly reflects the quality of an optical communications signal and is determined by monitoring the amplitude and phase of the signal[9]. The Q factor can be determined by

$$Q = \left. \frac{U_1 - U_0}{\sigma_1 + \sigma_2} \right|_{\varphi=\pi} \qquad 5.1$$

The eye-diagrams that were used to calculate the Q factor are shown as Fig. 5.7. The higher the value of the Q factor the lower the bit error rate (BER). The Q factors for this experiment ranged from 11.4 to 15.5 for the 32x20.32Gb/s source and 8 to 13 for the 32x40.64Gb/s source. The spectral efficiencies of the 682Gb/s and 1.36Tb/s were very good with values of 0.2b/s/Hz and 0.4b/s/Hz respectively. It can be seen that all channels were considered to be error free (Q>6), albeit with considerable variation in channel performance, which arises from the variation in signal-to-noise ratio caused by the spectral gain variation of the EDFA. Again, this could be eliminated by incorporating a gain-flattening filter. Due to the stability of the laser source, the Q factors were stable over a time scale of several hours.

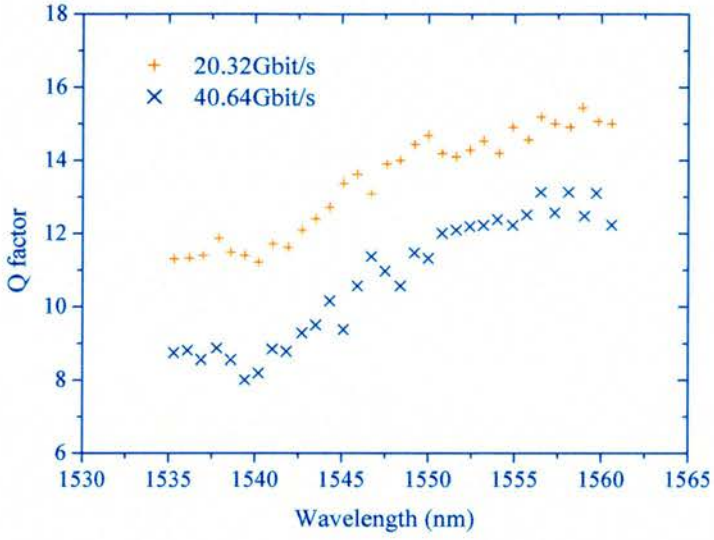

Fig. 5.6 *Q factor measurements after spectral slicing for 32 output channels of AWG.*

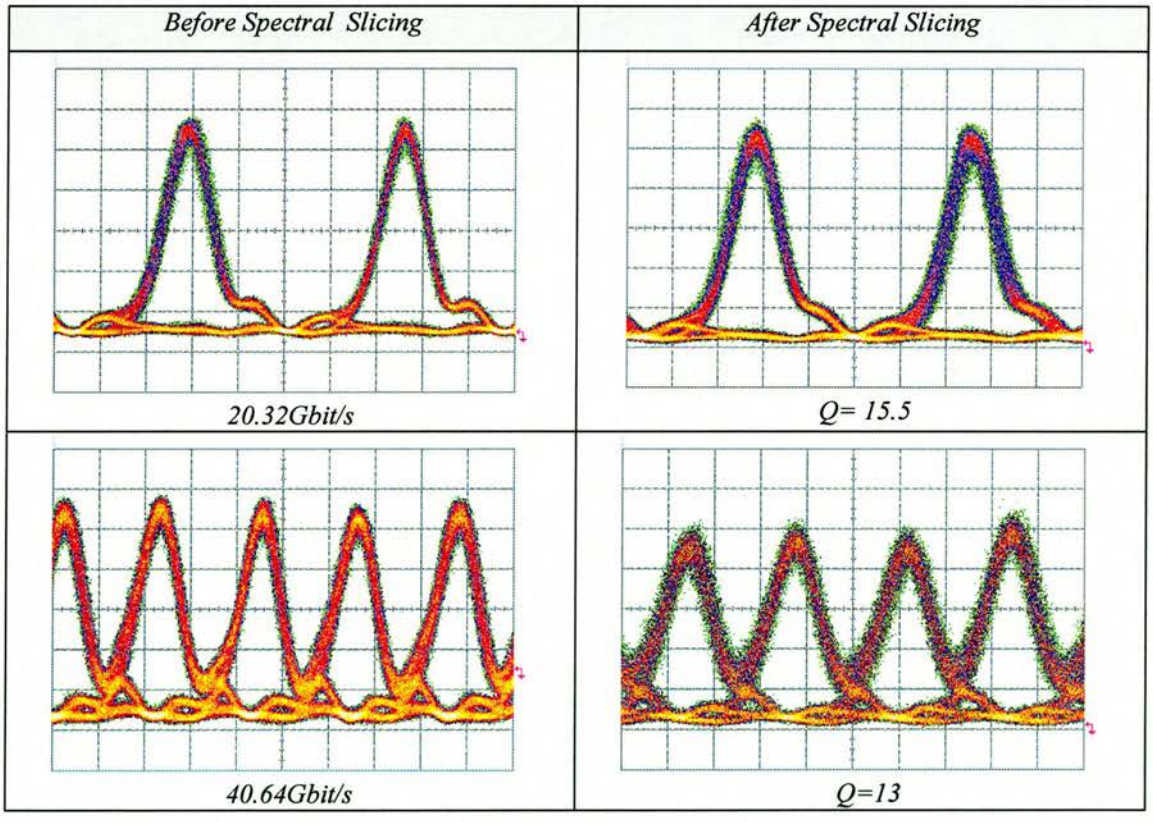

Fig.5.7 *Return-to-zero eye diagrams measured before and after spectral slicing at 20.32Gbit/s, 40.64Gbit/s (x-axis = 5ps/div).*

The data-encoding scheme used in this setup was motivated by the need to use a single modulator at a position where the optical polarisation field was optimised. In a practical OTDM/WDM system, each channel would require a separate modulator, in which case data encoding could take place after spectral slicing.

5.2.4 Final remarks

For the first time, an ultra-high-capacity spectral slicing source has been demonstrated using a practical and stable femtosecond Cr^{4+}:YAG laser. Investigations of the performance were achieved at up to 1.36Tb/s confirming the laser has sufficient capacity and quality to be employed in OTDM/WDM systems[10].

5.3 Demonstration of femtosecond switching of an all-optical switch

Next generation high-speed all-optical communication systems will necessitate the use of ultrashort optical pulses to achieve > 1Tb/s capacity. Therefore, optical pulse sources capable of generating femtosecond pulses and ultrafast switching devices permitting their manipulation are essential components. Sub-picosecond pulse sources suitable for datacommunications applications have already been demonstrated[11, 12]. With respect to ultrafast switching, semiconductor-based interferometric all-optical switches have shown the highest potential due to their low switching power requirement and integrability. Integration is important, as it offers not only reduction in terms of device dimensions but also a high level of stability and volume assembly.

We investigated experimentally the switching speed of a fully packaged hybrid-integrated Mach-Zehnder interferometer (HMZI) switch, supplied by *Corning*[13], for pulses that reached into the femtosecond regime. To achieve fast switching the switch

was operated under push-pull conditions. In these conditions, a push pulse is used to induce a nonlinear phase shift within the semiconductor optical amplifier (SOA) of one arm of the HMZI, thus opening a switching window. A delayed pull pulse is subsequently used to offset the differential phase effect by inducing similar nonlinearities within the SOA of the other arm, thereby closing the switching window. The switching time is thus nominally determined by the delay time between the push and pull switching pulses. Nevertheless, to attain an ultrashort switching window, ultrashort switching pulses are required, especially when considering decreasing the switching window width into the femtosecond regime, as they play a key role in influencing the rise and fall times of the switch output[14, 15].

The laser system designed by *PhotoSynergy* (discussed in Chapter 4) was employed to generate sub-100fs pulses for use as push-pull switching pulses[7, 12]. Orthogonal polarisation switching allowed discrimination of the switching windows from the switching pulses at the output of the HMZI.

5.3.1 Laser source

The laser source comprised the 3-element KLM Cr^{4+}:YAG prototype laser that was produced by *PhotoSynergy* (discussed at the end of Chapter 4). The system operated at a prf of 2.67GHz, generating pulses with durations of ~80fs. These pulses were coupled into a single mode fibre, which connected to the rest of the systems arrangement.

5.3.2 Systems setup

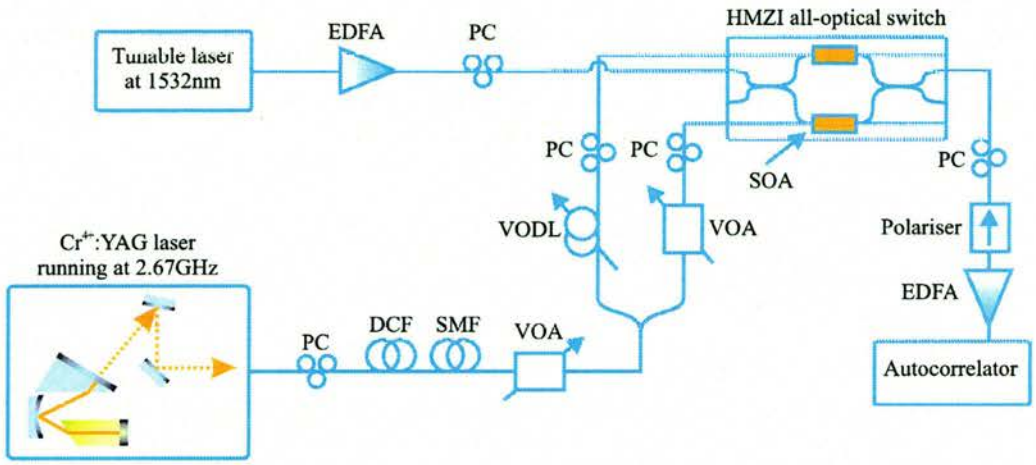

Key

VODL	– Variable optical delay line	EDFA	– Erbium doped amplifier
VOA	– Variable optical atenuator	PC	– Polarisation controller
DCA	– Dispersion compensating fibre	SMF	– Single mode fiber

Fig. 5.8 *System setup used to achieve femtosecond switching windows.*

The pulses were passed through a series of dispersion compensation stages to ensure that the duration of the pulses was at a sub-picosecond timescale upon entering the HMZI (T_{FWHM} =270fs). The pulses were then split into two, to form the push-pull switching pulses, with a variable optical delay line (VODL) used to adjust the time delay between them. The push-pull switching powers were approximately 0dBm. The intended switched out cw light was amplified prior to entering the HMZI and was set at a wavelength of 1532nm corresponding to the gain peak of the EDFAs. The average power of the cw light was 7.5dBm. Input polarisation controllers were used to maintain orthogonality between the cw light and the switching pulses. At the output of the HMZI, an additional polarisation controller was used to linearise the output polarisation state before sending the output to a polariser for switching pulse suppression. The output was detected by an autocorrelator and the switching windows were derived through standard curve fitting.

5.3.3 Results and discussion

Fig. 5.9a) shows the evolution of the measured autocorrelation traces, while Fig. 5.9b) illustrates the corresponding derived switching windows for push-pull pulse delay times that ranged between 7.34ps and 680fs. The experimental autocorrelation traces at large push-pull delay times were approximately triangular in shape thereby yielding quasi-rectangular-like switching windows. With reduced push-pull delay time, the autocorrelation traces gradually become increasingly semi-sec*h*-like in shape thereby indicating triangular-like switching windows.

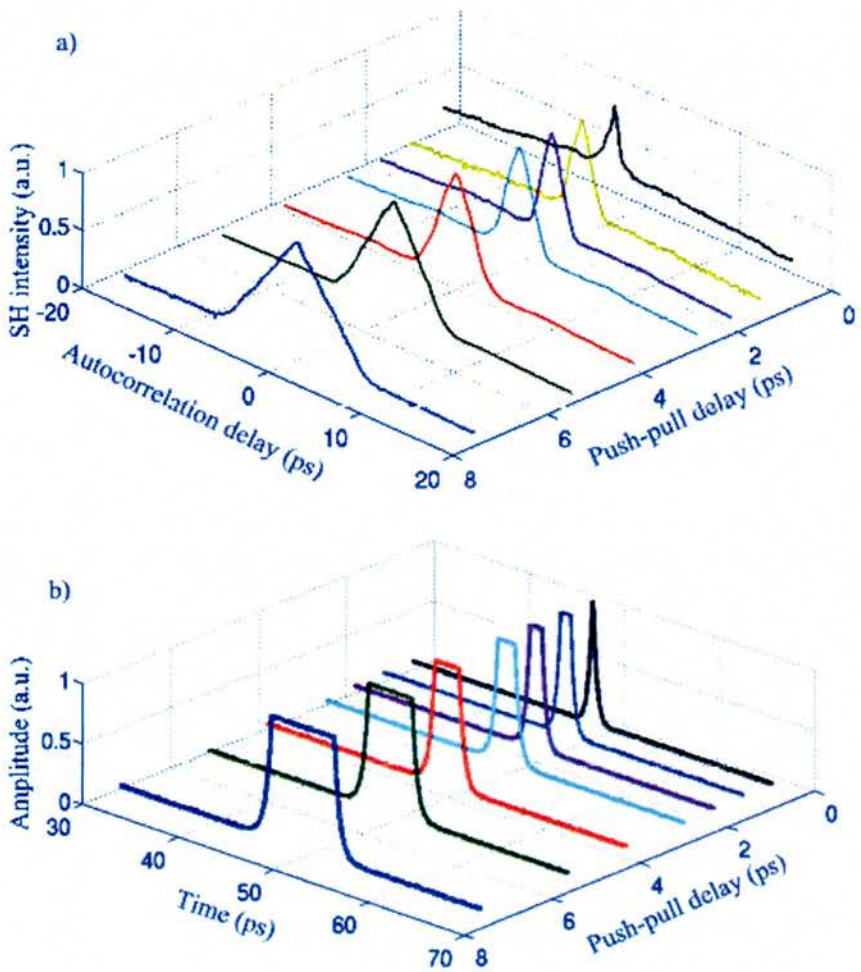

Fig. 5.9 *(a) Evolution of autocorrelation traces of the switching windows against push-pull pulse delay time, (b) corresponding curve fitted switching windows, obtained from the autocorrelation traces, against push-pull pulse delay time.*

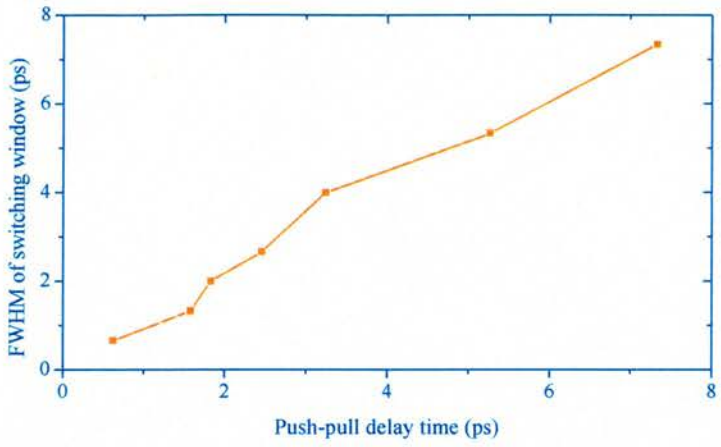

Fig. 5.10 *Switching window width against push-pull pulse delay time.*

The durations of the switching windows were approximately equal to their respective push-pull pulse delay times, as shown in Fig. 5.10. The deduced rise and fall times of the switching windows exhibited an average value of 1ps, which was larger than the widths of the switching pulses used. As the push-pull delay time reduced, there was a decrease of the output amplitude due to reduction of the output energy as a result of narrower switching windows. At a push-pull pulse delay time of 680fs, a switching window width of 623fs was measured, which constituted, the shortest switching window so far reported using a fully packaged all-optical switch.

5.3.4 Final remarks

This short experiment demonstrated femtosecond all-optical switching using a HMZI switch. Employing ultrashort pulses from the Cr^{4+}:YAG laser source, a record switching window of 620fs from a fully-packaged all-optical switch was obtained. The results therefore confirm the feasibility of employing hybrid-integrated platforms in achieving high speed, high performance optical systems.

5.4 Conclusions

This chapter provided a description of the successful integration of a 2.67GHz Cr^{4+}:YAG laser into two very different datacommunications assessments. The first involved interleaving the pulses up to a frequency of 40GHz and spectrally slicing the broad spectral bandwidth of the laser into 32 individual channels via an AWG device. This produced a system that was capable of generating up to 1.36Tb/s, and remains the only system capable of achieving such a high capacity from a single source. The second demonstration involved using the femtosecond laser system to induce switching windows within a fully integrated Mach-Zehnder interferometer device. Such was the quality of the pulses that were generated by the laser that record switching windows as short as 630fs were realised.

These ground-breaking results that have be produced through this collaborative work have made it clear to me that solid-state laser systems have a key role to play within the realm of datacommunications and systems experiments. The future of this type of collaboration (involving the integration of systems-based work and solid-state laser development) can be expected to grow stronger from the preliminary results presented here.

5.6 References

1. K. Fukuchi. "Wideband and ultra-dense WDM transmission technolojy toward over 10-Tb/s capacity", in *Proceedings of Optical Fiber Communication Conf. (OFC)*, 2002.
2. J.S. Lee, Y.C. Chung, and D.J. Digiovanni, "Spectrum-Sliced Fiber Amplifier Light-Source for Multichannel Wdm Applications", *Ieee Photonics Technology Letters*, vol. 5, (12), p. 1458-1461, 1993.
3. S.S. Wagner, H. Kobrinski, T.J. Robe, H.L. Lemberg, and L.S. Smoot, "Experimental Demonstration of a Passive Optical Subscriber Loop Architecture", *Electronics Letters*, vol. 24, (6), p. 344-346, 1988.
4. E.A. De Souza, M.C. Nuss, W.H. Knox, and D.A.B. Miller, "Wavelength-division multiplexing with femtosecond pulses", *Optics Letters*, vol. 20, (10), p. 1166-1168, 1995.
5. L. Boivin and B.C. Collings, "Spectrum slicing of coherent sources in optical communications", *Optical Fiber Technology*, vol. 7, (1), p. 1-20, 2001.
6. T. Tomaru and H. Petek, "Femtosecond Cr4+: YAG laser with an L-fold cavity operating at a 1.2-GHz repetition rate", *Optics Letters*, vol. 25, (8), p. 584-586, 2000.
7. C.G. Leburn, A.A. Lagatsky, C.T.A. Brown, and W. Sibbett. "Three-element modelocked femtosecond Cr^{4+}:YAG laser operating up to 3.6-GHz repetition rate", in *Conference on Lasers and Electro Optics*, 2003.
8. Lightwave-Microsystems, http://www.lightwavemicro.com/.
9. R. Bach and W. Monch, "Optical Q-Factor Measurement", in *The Emerging Optical Network Comprehensive Report*. 2001, International Engineering Consortium,2001.
10. Y.J. Chai, C.G. Leburn, A.A. Lagatsky, C.T.A. Brown, R.V. Penty, I.H. White, and W. Sibbett, "1.36-Tb/s Spectral Slicing Source Based on a Cr^{4+}:YAG Femtosecond Laser", *Journal of Lightwave Technology*, vol. 23, (3), p. 1319-1324, 2005.
11. D.J. Ripin, C. Chudoba, J.T. Gopinath, J.G. Fujimoto, E.P. Ippen, U. Morgner, F.X. Kartner, V. Scheuer, G. Angelow, and T. Tschudi, "Generation of 20-fs pulses by a prismless Cr4+: YAG laser", *Optics Letters*, vol. 27, (1), p. 61-63, 2002.
12. C.G. Leburn, A.A. Lagatsky, C.T.A. Brown, and W. Sibbett. "4GHz-prf femtosecond Cr4+:YAG laser as an OTDM/WDM source", in *Advanced Solid State Photonics - TOPS*, Santa Fe, New Mexico, 2004.
13. G. Maxwell, R.J. Manning, M. Nield, M. Harlow, C. Ford, M. Clements, S. Lucus, P. Townley, R. McDougall, S. Oliver, I. Reid, and S. D. "Very low coupling loss, hybrid-intergrated all-optical regenerator with passive assembly", in *ECOC*, 2002.
14. K. Tajima, S. Nakamura, and Y. Ueno, "Femtosecond all-optical switching using efficient incoherent nonlinearity with slow relaxation", *Materials Science and Engineering B*, vol. 48, p. 88-93, 1997.

15. K.I. Kang, T.G. Chang, I. Glesk, and P.R. Prucnal, "Comparison of Sagnac and Mach-Zehnder ultrafast all-optical interferometric switches based on a semiconductor resonant optical nonlinearity", *Applied Optics*, vol. 35, (3), p. 417-426, 1996.

Chapter 6 – Concluding Remarks

6.1 Summary

The focus behind the development of the laser sources detailed in this work was born out of the Ultrafast Photonics Collaboration (UPC) through which research is being pursued into the development of next-generation ultrafast datacommunications. My project has been concerned with the design, construction and characterisation of all-solid-state laser sources, as well as the integration of these laser sources into datacommunications based assessments, at the all important wavelengths of 1550nm. Fig. 6.1 summarises the most significant results and features of the laser systems that have been constructed throughout the duration of this project.

6.2 Future work

There still remains room for further improvement and development of all the laser systems that have been discussed in this work. This final section outlines some of the improvements that I believe are required for each laser system to move forwards both in terms of source development and potential applications.

As has already been discussed, the success of the Cr^{4+}:forsteite laser incorporating the low-loss GaInNAs SBR mode-locking element has produced an ultrafast source that has potential for a wide range of applications. Lasers operating around 1300nm fit very comfortably into biophotonics applications due to the deep penetration of 1300nm optical radiation into biological tissue. The laser that was discussed in Chapter 2 has already been used to investigate the amount of penetration that is possible in chicken breast tissue[1].

Laser	Cw threshold	Average output power	Prf	Pulse duration	Notable features
4-mirror Cr^{4+}:forsterite operating ~1300nm	1.4W	350mW	178MHz	130fs	• Mode locked by a novel GaInNAs SBR structure • First ever demonstration of a GaInNAs SBR for the generation of femtosecond pulses
4-mirror Cr^{4+}:YAG operating ~1550nm	0.5W	95mW	205MHz	120fs	• Mode locked by a AlAs/GaAs quantum well SBR structure • Stability of system allowed for mode-locked operation for days at a time • Use of compact fibre pump source allowed the whole laser system to be constructed on a 900×600mm^2 footprint
Initial 3-element Cr^{4+}:YAG operating ~1550nm	0.9W	60mW	1.6GHz	119fs	• Successful demonstration of a KLM 3-element cavity capable of generating femtosecond pulses at a prf >1.5GHz
Improved 3-element Cr^{4+}:YAG operating ~1550nm	0.9W	167mW	2.3GHz	79fs	• First ever demonstration of an all-solid-state laser capable of generating sub-100fs pulses at a prf ≥4GHz[2] • The laser incorporated the compact Yb:fibre laser source as the pump for the system • Capable of sustaining KLM operation for several hours at a time • Length of cavity ~19mm (4GHz)
	0.9W	85mW	4.02GHz	82fs	
Cr^{4+}:YAG engineered prototype operating ~1550nm	1.3W	44mW	2.53GHz	Sub-100fs	• Development of 2.5GHz laser system into a commercial prototype • Final laser package had a footprint of 215×106mm^2 • Removed the need for water cooling through the use of a two stage TEC system

Fig. 6.1 *Summary of performance obtained from the various laser systems described in this thesis.*

Work at St Andrews is commencing on other areas that can benefit from the Cr^{4+}:forsterite laser system. These will include optical tweezing[3, 4], two-photon cutting of chromosomes and photoporation[5]. In terms of laser development, I believe it is necessary to investigate the incorporation of dispersion compensating Gires-Tournois interferometer mirrors (GTI) into the cavity, which will allow the cavity size to be reduced. This will, in turn, provide an increased prf. Stable Ti:sapphire systems that have been constructed with GTI mirrors have produced femtosecond pulses at prfs of up to 2.5GHz[6], and the same performance can be achieved from the Cr^{4+}:forsterite systems discussed in Chapter 2. This will make them more suitable for incorporation in to datacommunications applications operating around 1300nm.

Due to the success of the research presented in Chapter 5, the 2.5GHz Cr^{4+}:YAG prototype source continues to be used in a range of datacommunications experiments. Ongoing research has utilised the laser in a novel analogue-to-digital conversion (ADC) system that has recently demonstrated ADC at 80 Giga-samples/second[7]. This experiment, along with those discussed in Chapter 5, illustrate the relevance of this laser to datacommunications and advanced photonics applications. There is scope to improve on the spectral-slicing experiment in terms of the capacity that is achievable. There are plans to use C-band and L-band EDFAs to access a larger proportion of the bandwidth generated by the laser, thus allowing more wavelengths to be spectrally sliced out and a much higher data rate to be achieved.

Development of more robust and reliable 1550nm solid-state laser systems will be achieved through the development of suitable low-loss SBR devices that can be used to initiate the mode-locking process. Throughout this project I have found that SBR mode-locked operation of a laser has been more stable than its purely KLM counterpart, and achieving stable KLM operation at high prfs has proved difficult in some

circumstances. I believe that the development of low-loss GaInNAs structures for operation at 1550nm will be the key for more stable, tuneable, high prf, femtosecond pulses at 1550nm and it is only a matter of time before these structures are realised. In saying that, there is research currently going on that is attempting to realise KLM operation of a Cr^{4+}:YAG laser at a prf of 5GHz, which if successful may become the next useful femtosecond laser source that can be used in datacommunications applications.

6.3 Final remarks

Over the coming years the laser sources that will be required for datacommunications applications will need to have outstanding performance characteristics over a range of differing criteria, in order to cope with the predicted capacity of future communications systems. These criteria will require laser sources that will be more broadband, more compact, more reliable, more efficient, have higher pulse repetition frequencies and be lower in cost than their present day incarnations.

The development of various solid-state laser systems over that last 20 years has shown how continued research is bound to bring improvements to some aspect of laser physics and the applications that they are used in. It should be noted that progress in the field of semiconductor lasers[8, 9] is also furthering the cause for a laser source that will be integrated into datacommunications applications of the future.

The evolution of both solid-state lasers and semiconductor lasers capable of generating femtosecond pulses at suitably high prfs has been steadily improving over the years. There is now also an increasing shift of these lasers from laboratory configurations to more practical and integrated packages that are proving to be successfully compatible with a wide range of technologies. Further progress will

involve greater understanding of the fundamental science as well as the technical innovations that will bring about the future development of femtosecond lasers for datacommunications applications.

6.4 References

1. P. Fischer, A. McWilliam, C.T.A. Brown, K. Wood, M.P. MacDonald, W. Sibbett, and K. Dholakia. "Deep Tissue Penetration of Radiation: 3D Modelling and Experiments - Submitted", in *European Conference of Lasers and Electro-Optics*, Munich, 2005.
2. C.G. Leburn, A.A. Lagatsky, C.T.A. Brown, and W. Sibbett. "4GHz-prf femtosecond Cr4+:YAG laser as an OTDM/WDM source", in *Advanced Solid State Photonics - TOPS*, Santa Fe, New Mexico, 2004.
3. B. Agate, C.T.A. Brown, W. Sibbett, and K. Dholakia, "Femtosecond optical tweezers for in-situ control of two-photon fluorescence", *Optics Express*, vol. 12, (13), p. 3011-3017, 2004.
4. L. Paterson, M.P. MacDonald, J. Arlt, W. Sibbett, P.E. Bryant, and K. Dholakia, "Controlled rotation of optically trapped microscopic particles", *Science*, vol. 292, p. 912-914, 2001.
5. L. Paterson, B. Agate, M. Comrie, R. Ferguson, T.K. Lake, J.E. Morris, A.E. Carruthers, C.T.A. Brown, W. Sibbett, P.E. Bryant, F. Gunn-Moore, A.C. Riches, and K. Dholakia, "Photoporation and cell transfection using a violet diode laser", *Optics Express*, vol. 13, (2), p. 595-600, 2005.
6. B. Stormont, I.G. Cormack, M. Mazilu, C.T.A. Brown, D. Burns, and W. Sibbett, "Low-threshold, multi-gigahertz repetition-rate femtosecond Ti : sapphire laser", *Electronics Letters*, vol. 39, (25), p. 1820-1822, 2003.
7. P. Jiang, Y.J. Chai, I.H. White, R.V. Penty, J. Heaton, A. Kuver, S. Clements, C.G. Leburn, A. McWilliam, A.A. Lagatsky, C.T.A. Brown, and W. Sibbett. "Photonic Analogue to Digital Conversion System Using Broadband Mode Locked Laser with 20GHz Bandwidth - Submitted", in *ECOC*, 2005.
8. C.T.A. Brown, M.A. Cataluna, A.A. Lagatsky, E.U. Rafailov, B. Agate, C.G. Leburn, and W. Sibbett, "Compact laser-diode-based femtosecond sources", *New Journal of Physics*, vol. 6, (175), p. 1-21, 2004.
9. K.A. Williams, M.G. Thompson, and I.H. White, "Long-wavelength monolithic mode-locked diode lasers", *New Journal of Physics*, vol. 6, (179), p. 1-30, 2004.

Publications, Proceedings and Conference Presentations

1. **80 GSPS Photonic Analogue to Digital Conversion**
   P. Jiang, Y. J. Chai, C. G. Leburn, A. McWilliam, I. H. White, R. V. Penty, J. Heaton, A. Kuver, S. Clements, A. A. Lagatsky, C. T. Brown, W. Sibbett
   Conference on Lasers and Electro-Optics, Baltimore, USA, paper CTuN4, May 2005.

2. **1.36Tb/s Spectral Slicing Source Based on a Cr^{4+}:YAG Femtosecond Laser**
   Y. J. Chai, C. G. Leburn, A. A. Lagatsky, C. T. A. Brown, R.V. Penty, I.H. White, W. Sibbett
   Journal of Lightwave Technology Vol 23, 3, 2004.

3. **Experimental demonstration of femtosecond switching of a fully packaged all-optical switch**
   C. K. Yow, Y. J. Chai, C. G. Leburn, A. McWilliam D. Reading-Picopoulos, A. A. Lagatsky, G. Maxwell, R. McDougall, C. T. A. Brown, W. Sibbett, R. V. Penty, I. H, White
   Optical Fibre Communications, Anaheim, USA, paper OThE4 March, 2005.

4. **Femtosecond Cr:forsterite laser modelocked with a GaInNAs saturable Bragg reflector**
   A. McWilliam, C. G. Leburn, A. A. Lagatsky, C. T. A. Brown, W. Sibbett, G. J. Valentine, A. J. Kemp, S. Calvez, D. Burns, M. D. Dawson, J. Kontinnen, T. Jouhti, M. Pessa
   Advanced Solid State Photonics (Twentieth Topical Meeting and Tabletop Exhibit), Vienna, (The Optical Society of America, Washington, DC, 2005), Technical Digest TuB1, 2005.

5. **Compact laser-diode-based femtosecond sources**
   C. T. A. Brown, M. A. Cataluna, A. A. Lagatsky, B. Agate, C. G. Leburn, W. Sibbett
   New Journal of Physics, Vol 6, 175, 2004.

6. **Passive mode locking of a Cr4+:YAG laser by PbS quantum-dot-doped glass saturable absorber**
   A.A. Lagatsky, C.G. Leburn, C.T.A. Brown, W. Sibbett, A.M. Malyarevich, V.G. Savitsky, K.V. Yumashev, E.L. Raaben, A.A. Zhilin
   Optics Communications, Vol. 241, pp 449-454, 2004.

7. **Femtosecond Cr4+:YAG laser with a 4GHz pulse repetition rate**
   C. G. Leburn, A. A. Lagatsky, C. T. A. Brown, W. Sibbett
   Electronics Letters, Vol. 40, No. 13, pp 805-807, 2004.

8. **4GHz-prf femtosecond Cr4+:YAG laser as an OTDM/WDM source**
   C.G. Leburn, Y.J. Chai, A.A. Lagatsky, C.T.A. Brown, R.V. Penty, I.H. White, W. Sibbett
   Trends in Optics and Photonics, Vol. 94, p72-77, G. Quarles Ed., The Optical Society of America, Washington, DC, 2004.

9. **Femtosecond Yb : KYW laser pumped by a single narrow-stripe laser diode**
   A.A. Lagatsky, E.U. Rafailov, C.G. Leburn, C.T.A. Brown, N. Xiang, O.G. Okhotnikov, W. Sibbett
   Laser Optics 2003: Solid State Lasers and Nonlinear Frequency Conversion, edited by Vladimir I. Ustugov, Proceedings of SPIE Vol. 5478 (SPIE, Bellingham, WA, 2004) 15-18, 2004.

10. **Diode-pumped femtosecond Yb:KYW laser with compact three-element cavity**
    A.A. Lagatsky, C.G. Leburn, C.T.A. Brown, W. Sibbett
    Solid State Lasers and Amplifiers, edited by Alphan Sennaroglu, James G. Fujimoto, Clifford R. Pollock, Proceedings of SPIE Vol. 5460 (SPIE, Bellingham, WA, 2004) 255-260, 2004.

11. **Femtosecond Cr4+:YAG laser with a 4GHz pulse repetition rate**
    C. G. Leburn, A. A. Lagatsky, C. T. A. Brown, W. Sibbett
    Advanced Solid State Photonics (Nineteenth Topical Meeting and Tabletop Exhibit), Santa Fe, USA, (The Optical Society of America, Washington, DC, 2004), paper WE4, 2004.

12. **Compact Femtosecond Oscillators (invited)**
    W. Sibbett, B. Agate, C. T. A. Brown, A. A. Lagatsky, C. G. Leburn, B. Stormont, E. U. Rafailov
    Ultrafast Optics IV, F. Krausz Ed, Springer Verlag, 2004.

13. **Highly efficient femtosecond Yb:KYW laser pumped by single narrow-stripe laser diode**
    A. A. Lagatsky, E. U. Rafailov, C. G. Leburn, C. T. A. Brown, N. Xiang, O.G. Okhotnikov,W. Sibbett
    Electronics Letters Vol. 39, No. 15, pp 1108-1110.

14. **Ultrahigh Capacity Source using Spectral Slicing of a Femtosecond Cr4+:YAG Laser.**
    Y. J. Chai, C. G. Leburn, A. A. Lagatsky, C. T. A. Brown, R. V. Penty, I. H. White, W. Sibbett
    LEOS Annual Meeting, Tucson, Arizona, USA, October 2003

15. **Compact self-starting femtoseocnd Cr4+:YAG laser diode pumped by a Yb-fiber laser**
    A. A. Lagatsky, C. G. Leburn, C. T. A. Brown, W. Sibbett, W. H. Knox
    Optics Communications, Vol. 217, pp 363-367, 2003.

16. **Three-element modelocked femtosecond Cr4+:YAG laser operating up to 3.6-GHz repetition rate**
C. G. Leburn, A. A. Lagatsky, C. T. A. Brown, W. Sibbett
Conference on Lasers and Electro-Optics, Baltimore, USA, June 2003.

17. **Diode-pumped lasing of stoichiometric crystal $KYb(WO_4)^2$**
A. A. Lagatsky, C. G. Leburn, C. T. A. Brown, W. Sibbett
European Conference on Lasers and Electro-Optics, Munich, Germany, June 2003.

18. **PbS quantum-dot-doped glass as saturable absorber for passive mode-locking of a Cr4+:YAG laser.**
A. A. Lagatsky, C. G. Leburn, C. T. A. Brown, W. Sibbett, A. M. Malyarevich, V. G. Savitski, K. V. Yumashev, E. L. Raaben, A. A. Zhilin
European Conference on Lasers and Electro-Optics, Munich, Germany, June 2003.

Acknowledgements

I think it is fair to say that I have had the most wonderful time over the last three and a half years. Much of this has been due to the people I have been lucky enough to get to know and work with. There are so many people I would like to thank and I know that I'm bound to forget someone!

I'd like to thank Professor Wilson Sibbett for allowing me to undertake a PhD degree in his group - thank you for your trust, support and kind words over the last few years. Your inspiration and enthusiasm has made this a wonderful experience.

To Alexander Lagatsky– Большое спасибо за то, что ты был отличным учителем. Я все еще благоговею перед твоими знаниями. Я всегда получал огромное удовольствие беседуя и обсуждая наши дела с тобой. Я не смог бы и пожелать себе лучшего преподователя. Спасибо тебе!

Special thanks must go to my friends Tom Brown and Ben Agate, who not only proof read this collection of words and pictures but also "gave as good as they got" – WUMF!

My thanks also goes to past and present members of W-squad including Iain Cormack, Barry Stormont, Edik Rafailov, Helen Little, Alan McWilliam, Pascal Fischer, William Whelan-Curtin, Maria Ana Cataluna, Douglas McRobbie and Abdul Sarmani – Thank you for letting me borrow various bit of equipment throughout the years and for providing the happiest working environment in the world. Hats off! – All the time!

A special mention must go to Alan Kemp, Gareth Valentine and John-Mark Hopkins, who all helped me get my head round *that* MathCad model. We got there in the end! Cheers.

Members of the Centre for Photonic Systems at Cambridge University, including Yew Jun Chai, Chee Kim Yow, Pisu Jiang, Adrian Wonfor, Emmanuel Moll, Richard Penty and Ian White, must be thanked for being most welcoming and allowing me be part of some wonderfully exciting experiments.

Thanks also to Lesley Aitken, Lee Staniforth and Mary Rodger for all the car hires they organised for me – always with a smile.

I'd also like to give a mention to Phil Dyer and Gerry Young whose enthusiasm for physics started me off down this path – cheers ☺

Finally, I would also like to give a *BIG* thank you to my beloved family and wife-to-be (hooray!) for their never-ending love and support – I couldn't be luckier.

Chrisp